TRIBOLOGICAL STUDY OF ELECTROLESS NICKEL COATINGS INCORPORATED WITH NANOPARTICLES

Thesis submitted by

DEVIPRASANNA MOHANTY

Doctor of Philosophy

(Engineering)

DEPARTMENT OF MECHANICAL ENGINEERING

FACULTY COUNCIL OF ENGINEERING &TECHNOLOGY

JADAVPUR UNIVERSITY

KOLKATA, INDIA

2023

JADAVPUR UNIVERSITY

KOLKATA-700032, INDIA

INDEX No. 259/18/E

1. Title of the Thesis:

TRIBOLOGICAL STUDY OF ELECTROLESS NICKEL COATINGS INCORPORATED WITH NANOPARTICLES

2. Name, Designation & Institution of the Supervisor(s):

i. Dr. Tapan Kumar Barman

Professor, Department of Mechanical Engineering,

Jadavpur University, Kolkata-700032

ii. Dr. Prasanta Sahoo

Professor, Department of Mechanical Engineering,

Jadavpur University, Kolkata-700032

3. List of Publications (Referred Journals):

i. Mohanty, D., Barman, T.K. and Sahoo, P. (2023) "Tribo-mechanical properties and corrosion study of nano zirconia reinforced electroless Ni-B coatings", Biointerface Research in Applied Chemistry, **in press. [Scopus]**

ii. Mohanty, D., Barman, T.K. and Sahoo, P. (2023) "Tribological Behavior, Mechanical Properties and Electrochemical Corrosion Response of Ultrasonically Assisted TiO_2 Reinforced Electroless Ni–B Coatings". Journal of Institution Engineers (India) Series D, https://doi.org/10.1007/s40033-023-00508-4. **[Scopus]**

iii. Mohanty, D., Bhowmick, A.K., Barman, T.K. and Sahoo, P (2023). "Scratch and corrosion behaviour study of electroless Ni-B reinforced with ultrasonicated nano TiO_2". Materials Today: Proceedings, 2023, https://doi.org/10.1016/j.matpr.2023.03.353. **[Scopus]**

iv. Mohanty, D., Barman, T.K. and Sahoo, P. (2021) “Effect of incorporation of nano-alumina on tribo-mechanical behavior of electroless Ni-B coatings”. Jurnal Tribology, 30, pp 24-43. **[Scopus]**

v. Mohanty, D., Barman, T.K. and Sahoo, P. (2019) “Characterisation and corrosion study of electroless Nickel-Boron coating reinforced with alumina nanoparticles”. Materials Today: Proceedings, 19(2), pp 317-321, https://doi.org/10.1016/j.matpr.2019.07.216. **[Scopus]**

4. List of Patents: Nil

5. List of presentations in National/International Conferences:

i. Mohanty, D., Bhowmick, A.K., Barman, T.K. and Sahoo, P (2022). “Scratch and corrosion behaviour study of electroless Ni-B reinforced with ultrasonicated nano TiO_2”. International conference on Advances in Materials, Sensors and Microelectornic Devices (ICAMSMD 2022), hosted by GLA University, Mathura, Uttar Pradesh, 9^{th}-10^{th} December, 2022, Paper ID: 8252

ii. Mohanty, D., Barman, T. K. and Sahoo, P. (2020) “Characterisation and Tribo Behavior of Nano Alumina Incorporated Electroless Ni-P Coatings”. International Conference on Advancements in Mechanical Engineering (ICAME 2020), hosted by Aliah University, Kolkata, West Bengal, 16^{th}-18^{th} January, 2020, Paper ID: ICAME_00064

iii. Mohanty, D., Barman, T.K. and Sahoo, P. (2019) “Characterisation and corrosion study of electroless Nickel-Boron coating reinforced with alumina nanoparticles”. International Conference on Manufacturing, Material & Engineering (ICMMSE-2019), hosted by CMR Institute of Technology, Hyderabad, Telengana, 16^{th} -18^{th} August 2019, Paper ID: ICMMSE-254

6. List of Book Chapters:

i. Mohanty, D., Barman, T. K. and Sahoo, P. (2022) "Effect of Nano Alumina Reinforcements on the Tribological Behavior of Electroless Nickel-Phosphorus Coatings". In Recent Advancements in Mechanical Engineering: Select Proceedings of ICRAME 2021, pp. 211-221.

STATEMENT OF ORIGINALITY

I, DEVIPRASANNA MOHANTY registered on 07.05.2018 do hereby declare that this thesis entitled **"TRIBOLOGICAL STUDY OF ELECTROLESS NICKEL COATINGS INCORPORATED WITH NANOPARTICLES"** *contains literature survey and original research work done me as part of Doctoral studies.*

All information in this thesis have been obtained and presented in accordance with existing academic rules and ethical conduct. I declare that, as required by these rules and conduct, I have fully cited and referred all materials and results that are not original to this work.

I also declare that I have checked this thesis as per the "Policy on Anti Plagiarism, Jadavpur University, 2019", and the level of similarity as checked by iThenticate software is **3** *%.*

Signature of Candidate: Deviprasanna Mohanty

(Deviprasanna Mohanty)

Date: 19/07/2023

Certified by Supervisors:

(Signatures with date, seal)

1. Tapan Kr. Barman

(Dr. Tapan Kumar Barman)

Professor
Dept. of Mechanical Engineering
Jadavpur University, Kolkata-32

2. Prasanta Sahoo 19/07/2023

(Dr. Prasanta Sahoo)

Professor
Dept. of Mechanical Engineering
Jadavpur University, Kolkata-32

CERTIFICATE FROM THE SUPERVISORS

This is to certify that the thesis entitled **"TRIBOLOGICAL STUDY OF ELECTROLESS NICKEL COATINGS INCORPORATED WITH NANOPARTICLES"** *submitted by Shri DEVIPRASANNA MOHANTY, who got his name registered on 07.05.2018 for the award of Ph.D. (Engineering) degree of Jadavpur University is absolutely based upon his own work under our supervision and that neither his thesis nor any part of the thesis has been submitted for any degree/diploma or any other academic award anywhere before.*

1. Tapan kr. Barman

(Dr. Tapan Kumar Barman)

Signature of the supervisor

Professor
Dept. of Mechanical Engineering
Jadavpur University, Kolkata-32

2. Prasanta Sahoo 19/07/2023

(Dr. Prasanta Sahoo)

Signature of the supervisor

Professor
Dept. of Mechanical Engineering
Jadavpur University, Kolkata-32

Abstract

Electroless coatings are based on a process known as autocatalytic deposition, wherein a reducing agent triggers a chemical reaction between metal ions and a metal surface, resulting in the formation of a continuous and uniform metal coating. Unlike traditional electroplating methods that rely on electrical current, electroless coatings utilize chemical reactions to deposit a uniform and adherent layer of material onto the substrate.

Electroless coatings offer numerous advantages over traditional electroplating methods, making them suitable for a wide range of applications. Some of the key advantages include: Uniformity, good adhesion, high corrosion resistance and high wear resistance versatility. The unique properties of electroless coatings make them highly sought after in numerous industrial applications. Some prominent applications include: electronics and electrical components, the automotive industry, aerospace and defence, chemical processing, etc.

The present thesis work involves the deposition of binary Ni-B, binary Ni-P and composite Ni-B and Ni-P coatings reinforced with nanoparticles, and investigation into their characteristics and their properties. Three different nanoparticles (viz. nano-Alumina, nano-Titania and nano-Zirconia) are incorporated into Ni-B coatings. Morphology, hardness and elastic modulus, friction and wear behaviour, scratch resistance and corrosion characteristics of these coatings are evaluated experimentally. Finally, an attempt is made to compare the properties of the coatings produced by incorporating nano-Alumina in Ni-B and Ni-P coatings. It is believed that the present results will serve both academic and industrial interests.

This page is left blank intentionally

Acknowledgement

I would like to express my deepest gratitude and appreciation to all those who have supported and contributed to the completion of my PhD thesis. Their guidance, encouragement, and assistance have been invaluable throughout this journey.

First and foremost, I am indebted to my supervisors, Dr. Tapan Kumar Barman and Dr. Prasanta Sahoo, for their exceptional mentorship and unwavering support. Their expertise, insightful feedback, and dedication to my academic development have been instrumental in shaping this research. I am truly grateful for their patience, guidance, and the countless hours invested in supervising and refining this thesis.

I am deeply thankful to my lab mates and fellow researchers who have provided valuable discussions, technical support, and camaraderie. Their intellectual contributions and friendship have made this academic journey more enjoyable and meaningful.

My deepest appreciation goes to my family for their unconditional love, encouragement, and understanding throughout this challenging process. Their unwavering support, patience, and belief in my abilities have been the cornerstone of my success. I am truly grateful for their sacrifices and constant motivation.

Finally, I would like to express my heartfelt gratitude to all the participants who volunteered their time and expertise for this study. Without their willingness to contribute to my research, this work would not have been possible.

In conclusion, I extend my sincere appreciation to all those mentioned above, as well as anyone else who has been involved in my academic journey, directly or indirectly. Your support and contributions have played a pivotal role in the completion of this thesis, and I am forever grateful.

Thank you all.

DEVIPRASANNA MOHANTY

This page is left blank intentionally

Table of Contents

List of Figures

This page is left blank intentionally

List of Tables

This page is intentionally left blank

Chapter 1: Introduction

Outline: *1.1 Background of work, 1.1.1 Surface modification, 1.2 Electroless plating process, 1.3 Notable works in the field of electroless plating, 1.4 Bath chemistry of electroless Ni-P and Ni-B coatings, 1.5 Parameters affecting the deposition rate of EN plating, 1.6 Structure and properties of EN coatings, 1.7 Physical and mechanical properties, 1.7.1 Porosity, density and melting point , 1.7.2 Hardness, 1.7.3 Residual stress, 1.7.4 Ductility and tensile strength, 1.7.5 Surface roughness, 1.8 Tribo-behaviour of EN coatings, 1.9 Corrosion, 1.10 Nanoparticle reinforced coatings, 1.11 Summary of literature review, 1.12 Research plan, 1.12.1 Objectives, 1.12.2 Outline of the work, 1.13 Closure*

1.1 Background of work

Egyptians were the first to use coatings for protection against environmental decay. Prior to them, coatings were primarily used for decorative purposes. During the initial years, coating materials were limited to resin and polymers primarily known as paint. With the requirement for harder and more environment resistant materials metallic and composite coatings came into existence. To meet the industrial requirements the coatings kept on improving and a variety of coatings emerged. The present study involves one such coating method known as Electroless coating.

1.1.1 Surface modification

Surface alteration techniques generate surfaces which have properties different from that of the substrate material. These techniques have been developed to meet the challenge of ever-degrading materials. Materials degrade primarily by the component-to-component interaction and component-to-environment interaction, with time. This degradation generally starts with the surface; hence surface modification is required. Surfaces are modified not only to improve the life of these materials but also to impart

necessary property enhancement, not inherent in the base material. Fig. 1.1 shows some surface modification technologies employed in various industries.

While diffusion and surface hardening processes are used to alter the surface properties of the base metal, plating, thin coatings, hard facing and thermal spraying are used to deposit new materials on top of the base metal. The coating requires the shielding of the base material by a foreign material (coating material), which results in the enhancement of the property of the overall material (base material and coating). Coating addresses specific property requirements of the concerned base material and even enhances the aesthetics of the components. Electroless plating is one such surface modification process.

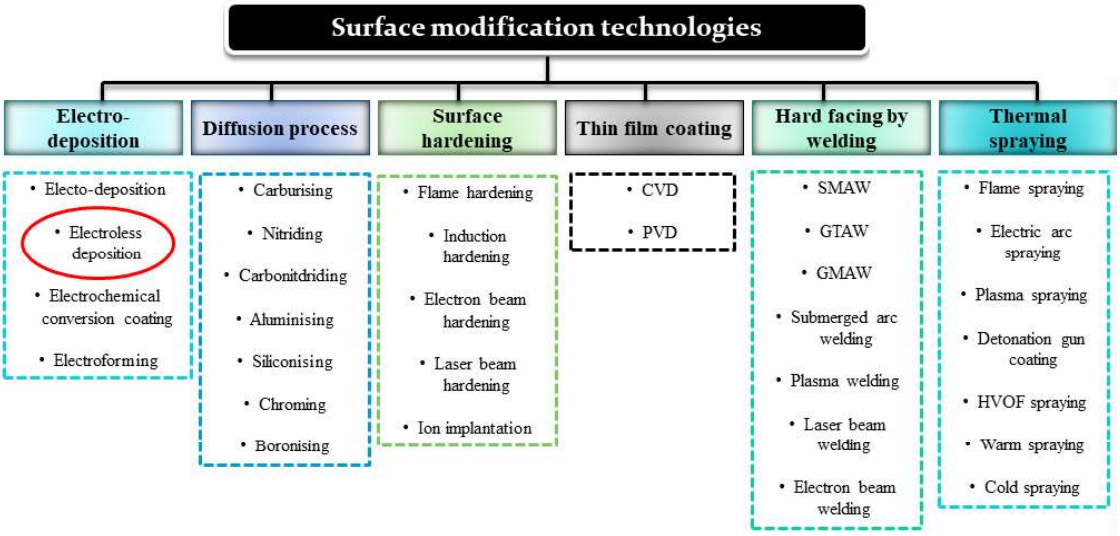

Fig. 1.1: Some surface modification techniques used in industries (Budinski, 1988).

1.2 Electroless plating process

Electroless plating is a versatile coating process which improves the wear and corrosion properties of engineering components (Delaunois and Lienard, 2002; Narayanan and Seshadri, 2004; Gilley et al., 2012; Sudagar et al., 2013; Gadhari and Sahoo, 2016; Ghaderi et al., 2016; Loto, 2016). In this plating process, a reducing agent reacts with a metallic salt in a liquid solution which results in a uniform coating of metal atoms onto the substrate. In contrast to electroplating, electroless plating can generate uniform coating

even on intricate shapes and non-conducting surfaces. One such case is electroless copper deposition to manufacture printed circuit boards (PCB), which are made up of glass fibre-reinforced epoxy resin, a nonconducting substrate. The electroless process is autocatalytic. Many uses of electroless plating process include VLSI (Very large scale integrated) technology, electromagnetic shielding, decorative platings, functional coatings for oil and gas, automotive, chemical and aerospace industries (Das and Sahoo, 2011; Sahoo and Das, 2011; Sha et al., 2011; Bülbül et al., 2012; Domínguez-Ríos et al., 2012; Çelik et al., 2016). Additionally, the electroless coatings also provide very low surface roughness without any effective pitting (Krishnan et al., 2006). A necessary condition for a sound coating is the optimal transfer rate of metal ions onto the substrate from the chemical bath. A very slow reaction rate results in a low coating thickness whereas a fast rate of reaction causes the precipitation of the metal ions. Thus, in order to optimise the reaction kinetics, a catalyst is applied to the substrate surface (Szunerits and Thouin, 2007). This catalyst hastens the reduction rate at the substrate surface and concentrates the deposition of metal ions on it, thus, avoiding the formation of precipitate in the solution.

With the intention of further improving the mechanical properties such as hardness, Young's modulus along with tribological characteristics, electroless nickel coatings are being reinforced with nanoparticles. TiO_2, ZrO_2, Al_2O_3 are some examples of metallic oxides being used as reinforcement in these coatings. Besides these, SiC and other carbon-based nanoparticles such as carbon nanotubes (CNT) and graphenes are being used by present researchers as reinforcements.

Although this plating process was discovered as a result of a chemical accident observed by Wurtz in 1844, its application as a coating method was established by Brener and Riddell (1946). A number of authors have reported various aspects of these coatings namely wear resistance, corrosion resistance, high hardness as well as the decorative uses (Wang et al., 2014; Fetohi et al., 2015; Wang et al., 2016; Domínguez et al., 2017; Kundu et al., 2018; Lee and Lee, 2018). In recent times, the properties of these coatings have been further improved by the co-deposition of nanoparticles. These nano-structured particles are often deposited as an additional layer beyond the primary layer of EN coatings although

they may also be deposited along with the primary coating layer. A typical electroless plating setup is shown in Fig. 1.2.

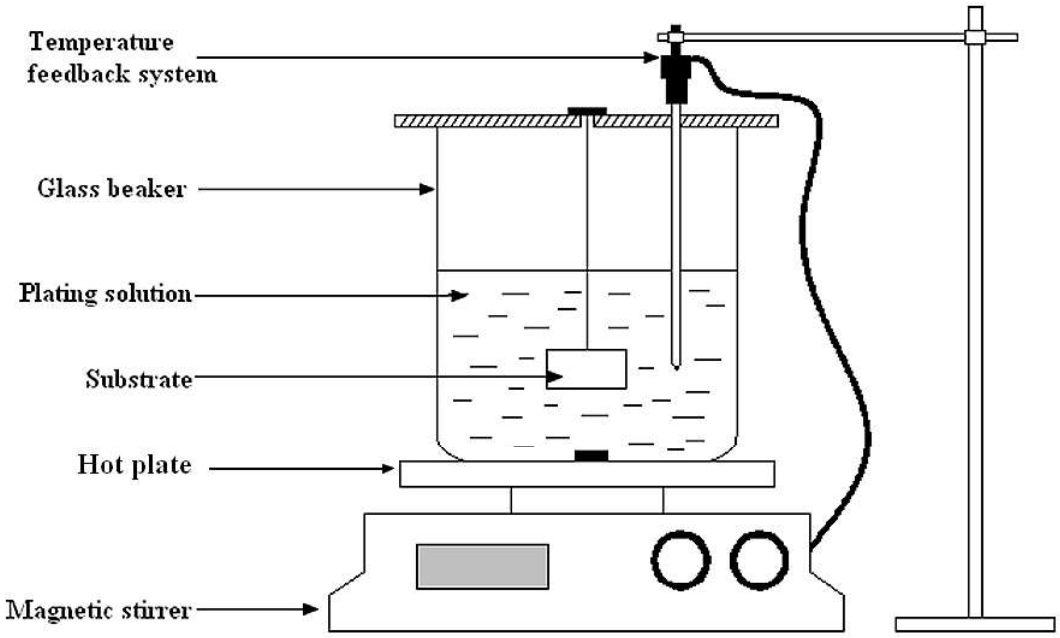

Fig. 1.2: A schematic diagram of a typical electroless plating setup

The substrate in an electroless plating setup can be coated from all sides as it remains immersed in the plating solution during coating. The coating process is elaborated below.

STEP 1: Cleaning and conditioning of the substrate surfaces are carried out in a 5% NaOH solution.

STEP 2: The substrate is etched to prepare the surface for better adhesion (5% H_2SO_4 and 5% H_2O_2 etchant are used)

STEP 3: To remove the etchant and prepare the substrate surface for catalysing the substrate is again dipped in 5% NaOH solution.

STEP 4: The substrate surface is then catalysed.

STEP 5: The substrate is then coated inside the plating solution bath, placed on the magnetic stirrer, at a defined temperature. In order to incorporate nano particles these particles are agitated in deionised water before introducing it into the solution.

STEP 6: This coated sample is rinsed well in deionised water to remove any residual solution from the coating surface.

1.3 Notable works in the field of electroless plating

After the initial framework laid down by Brenner and Riddell (Brenner and Riddell, 1946) for the deposition and application of electroless coatings, a number of other researchers came up with various new aspects of these coatings. Although before Brenner and Riddell's work of 1947 other researchers had contributed to the field of electroless coating. But their work suffered from the lack of a stable bath composition hence due to the spontaneous dissociation of the bath no effective coating thickness could be achieved during this period. Mclean and Karten (1954), used the reduction method to deposit nickel on small parts required for naval purposes. Gutzeit and Mapp (1954), advocated the 'Kanigen' process of Nickel-Phosphorus deposition as one of its kind in resisting corrosion due to its impervious nature. The Kanigen process was originally devised by the engineering department of General American Transportation Corporation in 1947 as a replacement for the more expensive and complicated electroplating process (Gutzeit and Mapp, 1954). Goldenstein et al. (1957), extensively researched the structure of the amorphous phase nickel deposits in 1957. They also established that at higher temperatures (300 ^{o}C) this metastable amorphous nickel decomposes into a mixture of Ni_3P and crystalline nickel. In the same year, Minjer and Brenner (1957), were able to measure the deposition rate and simultaneously they studied the effect of thiourea, a complexing agent, on bath chemistry. Gutzeit (1959), advocates in favour of a model of EN deposition proposed initially by Brenner and Riddell. This model explains the role of atomic hydrogen in the reduction of nickel during the deposition process. Although by the early 1960s researchers had established the deposition of copper, nickel, cobalt as well as certain alloys of nickel, chromium and iron etc. on various substrates like aluminium, iron and magnesium there remained the issue of bath stability, generation of the smooth substrate surface for coatings as well as the need for a catalytic surface to initiate the deposition. During the period 1960-1980, a number of patents were filed and research published addressing the issue of bath chemistry. Since the discovery of electroless Ni-B coatings in 1949 a lot of modifications and developments have made the Ni-B coating very versatile

in terms of their application as a tribo coating. Fig. 1.3 shows a brief timeline of the development of electroless Ni-B coatings since its discovery in 1949.

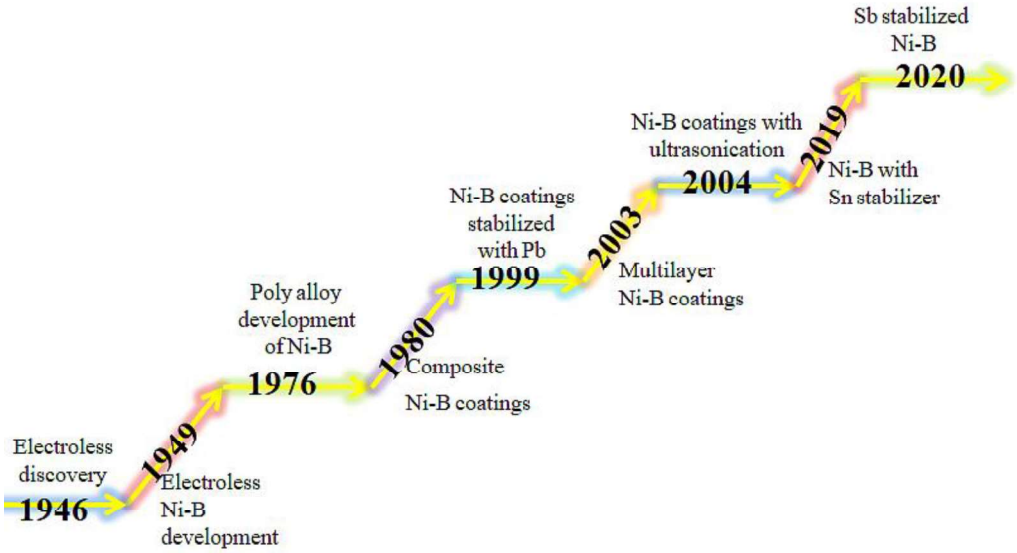

Fig. 1.3: Brief timeline of electroless Ni-B development in the last 5 decades (Vitry et al., 2022)

In recent times more and more research has come up for Ni-P and Ni-B coatings with the addition of alloys such as Mo, W, Cu etc and various nanoparticles. Hence, the study of the bath chemistry of Ni-B and Ni-B coatings has become important.

1.4 Bath chemistry of electroless Ni-P and Ni-B coatings

Tables 1.1 and 1.2 show typical Ni-P and Ni-B coating bath compositions. After pre-treatment, specimens are immersed in electroless Ni solution (bath). In this bath, nickel salts act as the primary source of nickel and a suitable reducing agent is used as the coating requirement (Ni-B or Ni-P). Besides these, the bath also consists of complexing agents and stabilizers. The primary function of the complexing agents is to act as a deterrent and prevent the pH of the solution to drop too fast. Simultaneously, these complexing agents also help to prevent the precipitation of nickel in the solution. Acetic acid, succinic acid and lactic acid (Mallory, 1991) are some of the popular monodentate anions used as complexing agents in EN platings. In order to prevent the spontaneous decomposition of

the plating bath, stabilizers are used. Such random decomposition may proceed with the evolution of an excess amount of hydrogen gas and the precipitation of Ni particles along with nickel phosphide. Heavy metal ions such as Sn^{2+}, Sb^{3+}, Hg^{+}, Pb^{2+} etc. are considered as good bath stabilizers (Mallory, 1991). Additionally, a strong acid or alkali is used to maintain the required bath pH. Table 1.3 lists some bath compositions of Ni-B coatings used by other researchers.

Table 1.1: A typical bath composition for electroless Ni-P plating (Park and Kim, 2018)

Bath composition	Amount	Operating conditions	Amount
Nickel sulphate	20-40 g/l	pH of the solution	5.2
Lactic acid	9-15 g/l	Deposition temperature (^{o}C)	90
Sodium hypophosphite	20-40 g/l	Deposition time (h)	2
Acetic acid	20-30 g/l	Bath volume (mL)	500
Lead nitrate	2 mg/l	Stirring rate (rpm)	200

Table 1.2: A typical bath composition for electroless Ni-B plating (Mukhopadhyay, Barman and Sahoo, 2018)

Bath composition	Amount	Operating conditions	Amount
Nickel chloride	20g/l	pH	12.5
Sodium borohydride	0.8 g/l	Coating duration	4 hours
Lead nitrate	0.0145 g/l	Deposition temperature	90±2^{o}C
Ethylenediamine	59 g/l	Bath volume	200mL
Sodium hydroxide	40 g/l		

The introduction of Phosphorus or Boron during the electroless nickel deposition, results in the deposition of either Ni-P or Ni-B on the substrate. This in turn imparts specific properties to these coatings. The borohydride-reduced (Ni-B) coatings exhibit better wear resistance and hardness. In contrast, the Ni-P coatings show better strength, ductility, fatigue strength (high phosphorus) and corrosion resistance (Townsend, 1994). The elementary reactions involved in electroless Ni plating processes are a combination of a reduction reaction and an oxidation reaction (equations (1.1), (1.2) and (1.3)) (Mallory, 1991).

Oxidation:

$$Reductant\ (Metal\ salts) \rightarrow Oxidationproduct + ne^{-} \quad (1.1)$$

Reduction:

$$mNi^{2+} + 2me^{-} \xrightarrow{Substrate\ surface} mNi \downarrow \quad (1.2)$$

Overall reaction:

$$mNi^{2+} + Reductant \xrightarrow{Substrate\ surface} mNi + Oxidation\ product \quad (1.3)$$

These reactions although describe the deposition of metal ions on the surface of the substrate material. They fail to account for all the phenomena observed during EN platings. The experimentally observed reactions are more complex than suggested above. Hence, to get a complete overview of the reaction mechanism one needs to study every reaction involving different reducing species, individually.

Over the last seven decades, a number of mechanisms have been proposed to explain the kinetics of the reaction of EN plating bath solution. The mechanism proposed by Brenner and Riddell, 1946, which later on came to be known as the "Atomic hydrogen mechanism", identified two core equations ((1.4) and (1.5)) to be the basis for this plating process.

$$Ni^{2+} + H_2PO_2^- + H_2O \rightarrow Ni + H_2PO_3^- + 2H^+ \quad (1.4)$$

$$NaH_2PO_2 + H_2PO_2 \rightarrow NaH_2PO_3 + H_2 \quad (1.5)$$

These reactions showed that the coating was made up of pure nickel (without any phosphorus), which was later on disproved experimentally. A solution to this ambiguity was proposed by Gutzeit (1959). He suggested that the presence of elemental phosphorus may be explained by the following reactions (equations (1.6) and (1.7)).

$$H_2PO_2^- + H \rightarrow H_2O + OH^- + P \quad (1.6)$$

$$H_2PO_2^- + H_2O \rightarrow H^+ + HPO_3^{2-} + 2H \quad (1.7)$$

Table 1.3: Bath composition of Ni-B as reported by different authors

	Ni^{2+} source (g/l)	Reducing agent (g/l)	Complexing agent (g/l)	Stabilizer (g/l)								pH regulator (g/l)	Temp
	Nickel chloride $NiCl_2$	Sodium Borohydride $NaBH_4$	Ethylene Diamine $C_2H_8N_2$	Thallium acetate $TlC_2H_3O_2$	Thallium nitrate $Tl(NO_3)_3$	Lead Nitrate Pb $(NO_3)_2$	Lead tungstate $PbWO_4$	Ethylene Thiourea $C_3H_6N_2S$	Thiourea CH_4N_2S	Sodium citrate $(Na_3C_6H_5O_7)$	Tin Chloride $SnCl_2$	Sodium hydroxide NaOH	
(Delaunois and Lienard, 2002)	20	1.05	90		0.11							90	95
(Delaunois and Lienard, 2002)	20	0.48	59			0.0145						39	95
(Narayanan and Seshadri, 2004)	30	0.8	90	0.016								90	95
(Krishnaveni, Sankara Narayanan and Seshadri, 2005)	30	0.8	90	0.016								90	95
(Vitry, Delaunois and Dumortier, 2008)	24	0.48	59				0.02					39	95
(Srinivasan, Meenakshi, Santhi, Thangavelu, & John, 2010)	6	12	59					0.0002				90	95
(Correa et al., 2012)	20	8	35						0.001			110	80
(Bonin et al., 2018)	24	0.602	59				0.021					39	95
(Bonin et al., 2019)	24	0.062	59								0.05 to 0.2	39	95
(Vijayanand et al., 2021)	30	0.8	90							30			85

From equation (1.6) it is observed that an excess of OH^- ion is produced this in turn increases the pH of the solution. Due to this increase in pH, the reaction in equation (1.7) speeds up thus resulting in more H^+ ions. This cyclic process generates a layered deposition of EN coatings on the substrates. However, this mechanism is unable to provide a proper explanation for the simultaneous reduction of both nickel and hydrogen during the EN plating process. Other mechanisms include the "Hydride transfer mechanism" (Gutzeit, 1955). Ni-B coatings which result from the reduction of nickel salts by borohydride (BH_4) ions typically involve the reactions shown below.

$$BH_4^- + 8OH^- \rightarrow B(OH)_4^- + 4H_2O + 8e^- \quad (1.8)$$

$$4Ni^{2+} + 8e^- \rightarrow 4Ni^0 \quad (1.9)$$

Although the above reactions demonstrate the reduction of Ni, they are unable to explain the presence of boron in the coatings. Gourbunova et al. (1973) have proposed a reduction by boron in the following mechanism.

$$2NaBH_4 + 2H_2O \rightarrow 2B + 5H_2 + 2NaOH \quad (1.10)$$

There are still other researchers who have presented findings that differ from the above-mentioned mechanism of reduction by borohydride.

1.5 Parameters affecting the deposition rate of EN plating

Wolfgang Riedel in his published work of 1991 (Riedel, 1991) has identified some parameters that have a considerable impact on the rate of deposition of the electroless coatings. One such observation for electroless Ni coating suggests the similar effect of bath temperature on both electroless Ni-B (reduced by borohydride) coatings and Ni-P (reduced by hypophosphite) coatings (Townsend, 1994). Glenn O Mallory (Mallory,1991) reported the effect of pH on a Ni-B (with dimethylamine borane as reductant) coating to be a function of certain variables as mentioned below:

$$Deposition\ rate = f(T, pH, Conc.Ni^{2+}, Red.agent, Conc.Red.agent, Bath\ loading).$$

Where,

T: Temperature

pH: pH of the solution bath

Conc. Ni^{2+}: Concentration of Ni ions

Red. agent: Type of reducing agent used

Conc. Red. agent: Concentration of the reducing agent

Temperature tends to have the most pronounced effect on the deposition rate of the coatings. Evidently, majority of the chemical reactions occurring in the bath during the plating process are endothermic. Hence, the addition of heat (increase in temperature) hastens the reaction and increases the rate of deposition. Caution must be taken not to overheat the bath as it may lead to spontaneous decomposition of the solution. The bath is typically maintained within 85-95 ºC.

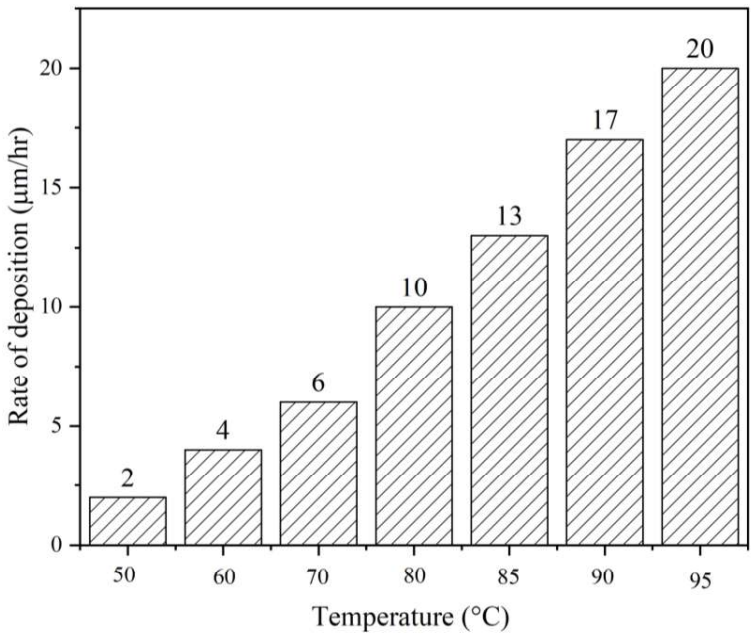

Fig. 1.4: Variation of the deposition rate with bath temperature (Townsend, 1994)

Fig. 1.4 reports the variation in the deposition rate against the bath temperature (Townsend, 1994). The solution bath temperature controls the properties of electroless Ni-B coatings

and this has been extensively reported in the literature. Delaunois et al. (2000) examined how the temperature of the bath affects the electroless Ni-B deposition on aluminum alloy using a borohydride as the reducing agent in the coating bath. They observed that with the increase in the bath temperature, the coating thickness also increased. Similarly, Gorbunova et al. (1973) reported that the deposition rate is directly proportional to the bath temperature. Oraon (2007) conducted a study that demonstrated a linear relationship between the coating deposition rate and bath temperature for shorter immersion periods. However, the deposition rate reaches a saturation point in case of longer immersion periods. Beyond that point, with the increase in bath temperature, the deposition rate eventually declines.

While exploring the impact of solution bath temperature using an acidic bath (DMAB), other researchers delved into the subject as well (Hamid et al., 2010). They attempted to deposit Ni-B coatings by immersing copper and steel substrates into the coating bath at temperatures of 60 °C and 80 °C for varying durations. Their findings unveiled that a lower coating deposition rate was attained when utilizing a lower coating bath temperature (60 °C) for both copper and steel. Furthermore, it was noted that the deposition rate on the copper substrate was lower than that of the steel substrate. It was also observed that the deposition rate did not exhibit a linear relationship with respect to plating time, and instead decreased as time progressed. This decline is attributed to the diminishing concentration of DMAB over time and the creation of oxidation products within the electroless plating baths, serving as plausible explanations for this phenomenon (Hamid et al., 2010).

The electroless nickel phosphorus (ENP) process involves various reactions that exhibit sensitivity to alterations in the pH of the solution. Specifically, when the pH is raised, the nickel-reduction reaction is accelerated, leading to more rapid deposition of nickel onto the substrate. Conversely, when the pH of the solution is increased, the reduction of phosphorus is impeded. This can be attributed to the generation of hydroxide ions as a byproduct of the phosphorus reduction reaction. Consequently, elevating the pH of the solution results in a reduction in the phosphorus content present in the coating. Additionally, it is important to note that the deposition rate of the EN process is

predominantly governed by the nickel reduction reaction. Thus, the deposition rate increased as the pH of the solution increased. This correlation indicates that manipulating the pH of the solution can effectively modulate the deposition rate during the EN process. Table 1.4, as reported by Baldwin and Such (2017), provides valuable insights into the influence of solution pH on both deposition rates. The data presented in the table underscores the relationship between pH and deposition rates, serving as a useful reference for understanding the impact of pH adjustments on the EN process.

Table 1.4: Variation of the deposition rate with solution pH (Baldwin and Such., 2017)

Sl. No.	pH	Plating thickness (mm)
1	4	3
2	4.5	7
3	5	10.5
4	5.5	13
5	6	14

The immersion time of the substrate in the solution bath determines the deposition thickness of the EN coatings. Oraon (2007) and Vitry et al. (2012), reported that with the increase in immersion time, the coating thickness also increased. The deposition rate initially, remains constant for nearly up to 2 hrs and thereafter it decreases steeply (without any bath replenishment). Oraon (2007), has concluded that although there is no dependency of coating thickness upon the concentrations of the reducing agent, there is a direct bearing of deposition time upon the coating thickness. Vitry et al. (2012), also report that for Ni-B electroless deposition there is an increase in the coating thickness initially (up to 4 min), with a growth rate exceeding 40μm/min. After this initial spike in the deposition rate, the coating gets densified and no further increase in coating thickness is observed for the next 4 to 7 minutes. After this, the coating tends to thicken almost linearly for 1 hr of immersion.

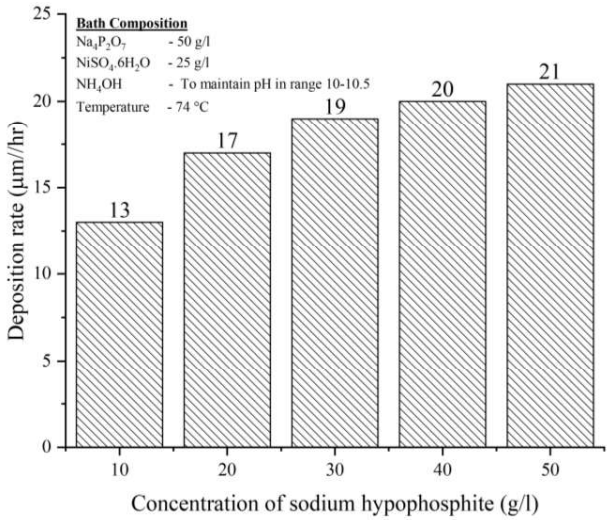

Fig. 1.5: Variation of the deposition rate with sodium phosphate concentration (Mallory, 1991)

Although the choice of reducing agent may have some effect on the deposition rate up to a certain concentration (depending on the type of reducing agent used) the deposition rate increases with an increase in the concentration of the reducing agent. Fig. 1.5 shows the variation of the coating deposition rate with a concentration of reducing agent. As can be observed, the deposition rate increases with the concentration of the reducing agent (sodium hypophosphite) up to a certain limit and then the rate becomes nearly constant.

1.6 Structure and properties of EN coatings

The surface morphology of the electroless coatings shows a typical cauliflower-like structure. In the case of Ni-P coatings, the phosphorus content tends to influence their structure and properties (Gould et al.,1981; Fan et al., 2012). The nodules of this cauliflower-like structure grow in size with the increase in the phosphorus content of these coatings (Fan et al., 2012). Goldenstein et al. (1957) have studied extensively the influence of phosphorus percentage in Ni-P coatings. They reported that in the as-deposited state, coatings with more than 7 wt % of phosphorus tend to be amorphous. On heat treatment, these amorphous structures crystallize into nickel and nickel phosphide (Goldenstein et al., 1957; Sribalaji et al., 2016). Additionally, researchers have also observed the presence of hollow grooves for multilayered Ni-P coatings.

In the as-plated condition, the Ni-B electroless coatings exhibit an amorphous nature, similar to the Ni-P coatings. Krishnaveni et al. (2012) have identified this amorphous nature by the presence of a single broad peak. The crystalline structures are generally indicated by sharp peaks, and in contrast, a broad peak implies a disorderly structure, inherent in the amorphous nature (Cullity, 1978). Ni-B deposits also show a cauliflower-like texture with a columnar morphology (Rao et al., 2005). Effectively the microstructure is a combination of amorphous and crystalline phases (Delaunois and Lienard, 2002; Dervos et al., 2004; Ziyua et al., 2006). Watanabe and Tanabe (1983) reported this amorphous structure based on the observations of the electron micrographs and electron diffraction patterns of the Ni-B films. Similar observations have been made by other researchers also (Srivastava et al., 1992; Evans and Schlesinger, 1994). The structure and properties of the Ni-B coatings are dependent on the boron content of these coatings (Gaevskaya et al., 1996; Anik et al., 2008; Vitry, Kanta and Delaunois, 2011; Vitry et al., 2012). Fig. 1.6 shows typical cauliflower-like features of electroless Ni-B deposition (obtained during the present study).

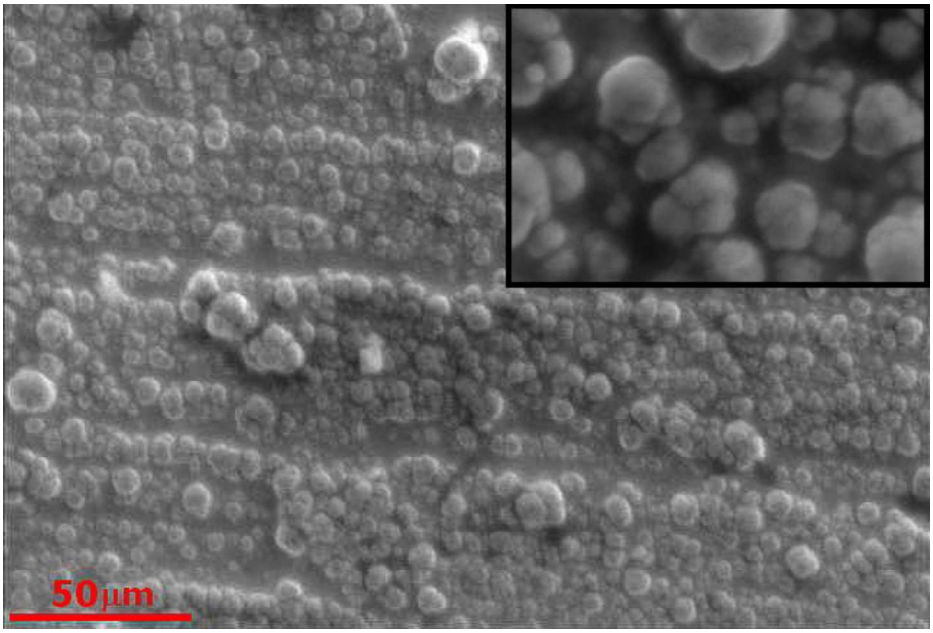

Fig. 1.6: Typical surface morphology of electroless Ni-B deposition

1.7 Physical and mechanical properties

1.7.1 Porosity, density and melting point

Porosity is one of the important properties of these coatings as they are expected to have good corrosion resistance; hence low pore density is a must. In general, EN plating shows a low porosity which further decreases with the increase in deposit thickness. Ernest et al. (1998) in their study of 1998 have corroborated the above statement. They have further added that beyond 50 μm deposit thickness, these coatings do not show any appreciable change in their pore density.

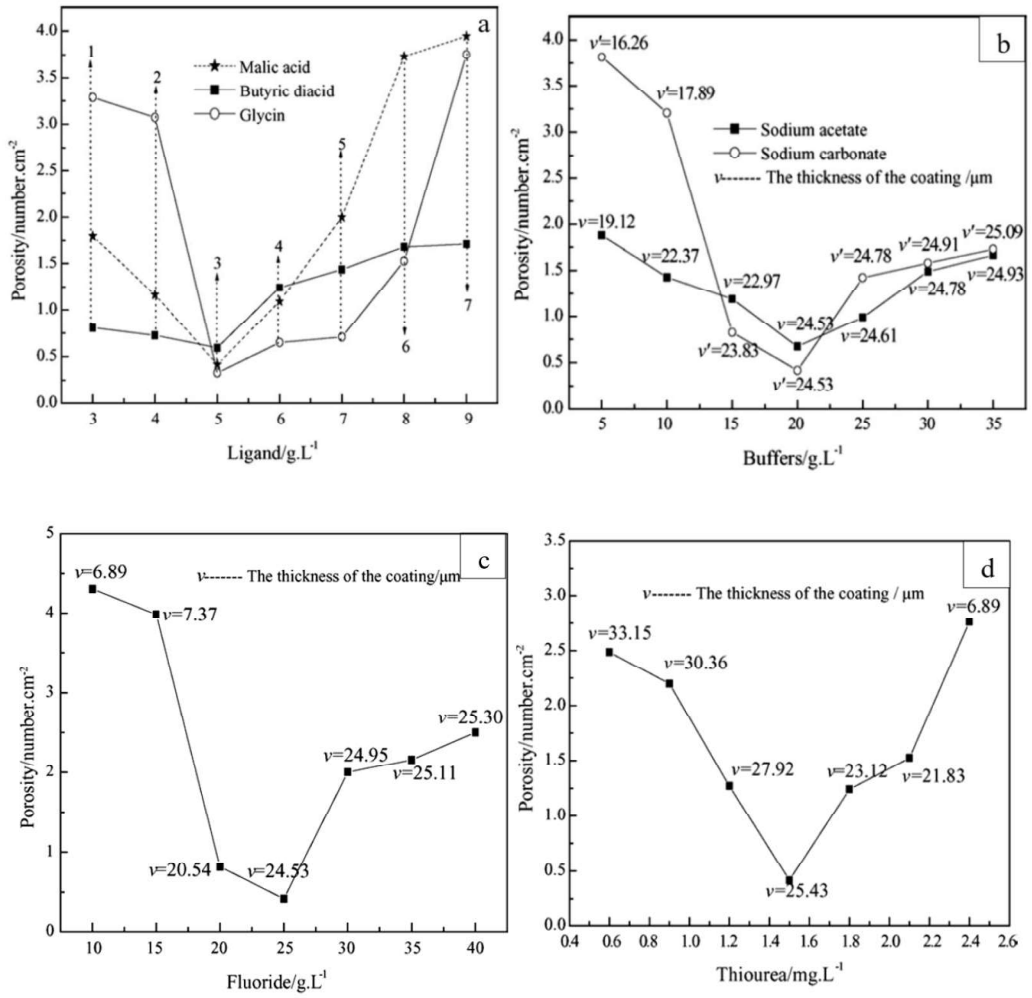

Fig. 1.7: Variation of the porosity/cm^2 with (a) Ligands, (b) Buffers (c) Flouride and (d) Thiourea concentration (Li et al., 2006)

Fig. 1.7 (a) to (d) shows the variation of the porosity with the addition of (a) Ligands, (b) Buffers (c) Flouride and (d) Thiourea concentration in Ni-P coatings (Li et al., 2006). They reported that a number of parameters such as ligand concentration, buffer agents, fluoride and thiourea affect the porosity of these coatings. They showed that certain ligands such as Mallic acid and Glycin have a more pronounced effect on the porosity as compared to Butyric diacid. They also concluded that the addition of buffers such as sodium acetate and sodium carbonate in low amounts (5 g/l) shows that the porosity is more in the case of sodium carbonate as compared to sodium acetate. Also, a lower value of porosity is observed in the case of thiourea as a stabilizer as compared to fluoride.

In the case of Ni-B coatings, with increasing boron content, electroless nickel-boron coatings show densities that are lower than those of pure bulk nickel (8.91 g/cm^3). 8.25 g/ cm^3 containing 5 wt% B is a generally accepted density of electroless Ni-B coatings (Sudagar et al., 2013). The melting point of nickel-boron coatings is between the melting point of pure nickel (1455 °C) and the Ni/Ni_3B eutectic temperature (1093 °C), making it impossible to determine with any accuracy the melting point of electroless Ni-B deposits.

1.7.2 Hardness

The hardness of as-deposited electroless Ni-P coatings ranges from 450-500 HV and on heat treatment the hardness increases substantially, to nearly 1000 HV (Sha et al., 2011). This improvement in the hardness of these coatings is attributed to the crystallization of the intermetallic Ni_3P phase; this has been substantiated through X-Ray Diffractometry, by a number of researchers (Rabizadeh et al., 2010; Islam and Shehbaz, 2011; Ma et al., 2014; Czagány et al., 2017). The amount of Ni_3P phase depends on the phosphorus content in the as-deposited coatings and the temperature of heat treatment (Rabizadeh et al., 2010; Czagány et al., 2017). In addition to this, heat treatment also improves abrasion resistance and substrate–coating adhesion (Mallory, 1991; Rabizadeh et al., 2010). In the case of electroless Ni-B coatings the precipitation of Ni_3B, inter-metallic phase, results in high hardness and wear resistance. Many researchers report the superior hardness and wear resistance of Ni-B coatings over its Ni-P counterpart (Riedel, 1991; Pal and Jayaram, 2018).

The addition of nanoparticles further improves the hardness of the Ni-B particles. The nickel-boron ions attach themselves to the surface of the particles that are added to the electroless Ni-B plating solution and then reduced onto the substrate surface. This leads to the entrapment of the particles by nickel-boron atoms, causing them to become embedded in the coating. The primary way in which inclusion particles improve the hardness may be explained by the following three phenomena:

- These particles provide resistance to the dislocation motion (Shakoor et al., 2014).
- The addition of these particles impedes the grain growth and in turn, increases the yield stress of the coating surface (Yazdani et al., 2018)
- Since these particles have high hardness and are spread across the surface, they tend to increase the average hardness of the coatings (Georgiza et al., 2017).

1.7.3 Residual stress

In case of the EN platings the total residual stress is a combination of intrinsic stress and thermal stress. Intrinsic stress results from the grain size and the crystal structure geometry evolves during the coating deposition and depends on the phosphorus content of the coatings (Parker, 2018). A 10 wt % Phosphorus in the coating generates neutral or compressive stresses. Phosphorus content below 10 wt % induces a tensile stress (Krishnan et al., 2006). Meanwhile, the thermal stresses are generated due to the difference in the thermal expansion coefficient of the coating and the substrate. Several authors have reported that the internal stress of the coatings depends not only on the phosphorus content of the coatings but also on the coating substrate as well (Parker and Shah, 1970; Mallory and Altura, 1983). As most of the EN coatings are deposited at 85 ºC to 95 ºC (bath temperature), hence on cooling to room temperature there occurs a contraction of nearly 0.1% for Ni-P platings (Parker, 2018). He observes that in case of aluminium and copper (high thermal coefficient of expansion) compressive stresses develop and for beryllium and titanium (low thermal coefficient of expansion) the stresses developed are tensile in nature. The tensile stress is responsible for the peeling, blistering and cracking of these coatings.

Compressive stress improves the adhesion of the coating and the substrate, hence moderate compressive stress is desirable in the case of coatings (Parker and Shah, 1970).

1.7.4 Ductility and tensile strength

Tensile strength and ductility are two factors which are predominantly dependent on the phosphorus content of the deposition. Duncan (1996) has theorised, based on the Ni-P equilibrium phase diagram, the correlation between the various phases present and the mechanical properties. At ambient temperature, it is observed that in addition to the α-Ni phase, there also exists β and γ phases. The β phase is a solid of phosphorus (4.5 %) in nickel. This is a crystalline phase. On the contrary, the γ phase is amorphous in nature and contains around 11 % to 15% of phosphorus. These phases are metastable and tend to decompose into Ni_3P and α- nickel on heat treatment (Duncan, 1996). Similar observations have also been made by other investigators (Kreye et al., 1986). Fig. 1.8 represents the effect of phosphorus content on the ductility of the coatings as demonstrated by Duncan.

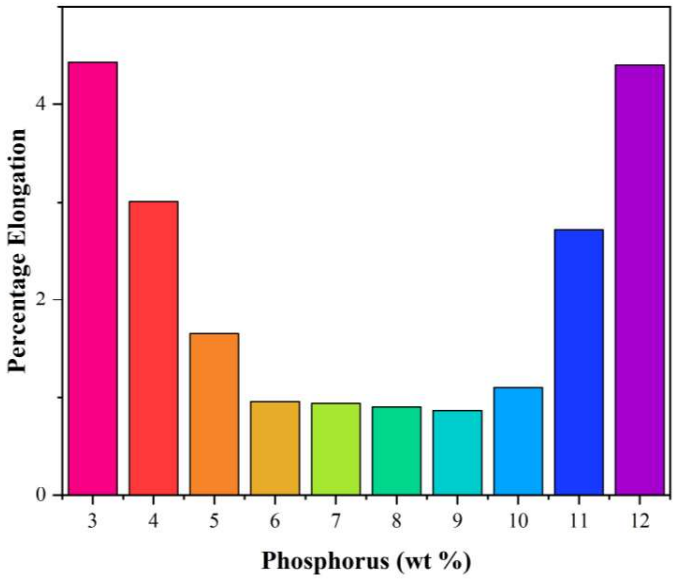

Fig. 1.8: Variation of ductility on the phosphorus coatings of electroless Ni-P deposition (Duncan, 1996)

It can be observed from Fig. 1.8 that low as well as high phosphorus coatings are more ductile as compared to medium phosphorus coatings. Medium phosphorus coatings tend to have a mixture of the α and β phases and also are highly stressed (Duncan, 1996), hence low ductility is achieved. Fig. 1.9 shows the variation in tensile strength with the phosphorus concentration. Duncan (1996) has reported a higher tensile strength for the medium and high phosphorus depositions. The low phosphorus depositions have predominantly β-phase solid solutions but with an increase in phosphorus the amorphous nature increases, as γ phase is formed. This transformation results in a stressed microstructure, hence initially the tensile strength also increases but when the structure becomes completely amorphous tensile strength decreases.

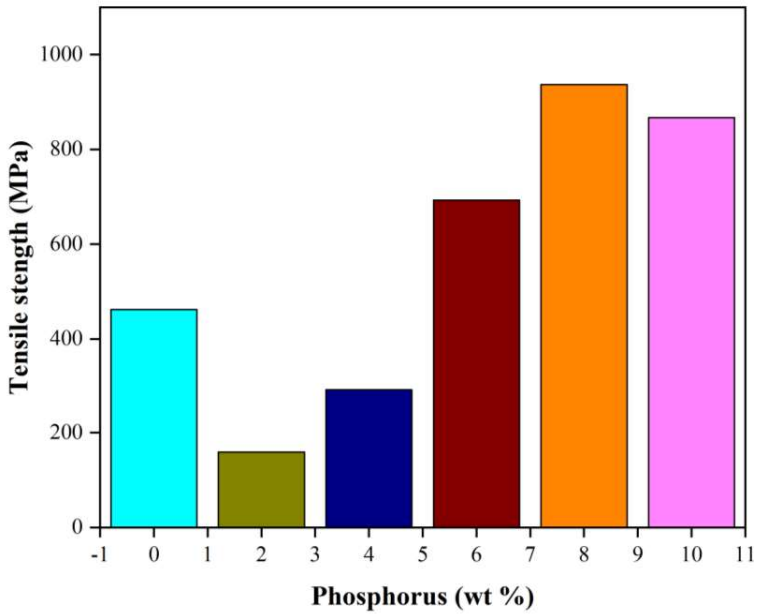

Fig. 1.9: Effect of phosphorus content of electroless Ni-P deposition on its tensile strength (Duncan, 1996)

1.7.5 Surface roughness

One of the important factors in the evaluation of friction behaviour and wear characteristic of coatings is surface roughness. More often than not, surface roughness decides whether the friction coefficient would be high or low for two contacting surfaces (Goettems et al., 2017). They also reported that between the substrate and Ni-P coatings,

the latter showed a reduced friction coefficient. Vitry et al. (2008), also observed similar smoothening behaviour for Ni-B coated aluminium alloy. They also reported a decrease in the average surface roughness values for the heat-treated Ni-B coatings owing to the structural modification that occurs due to heat treatment. Electroless nickel-boron deposit's roughness is affected by the substrate's roughness. The coating grows in columns that are locally perpendicular to the surface. In the case of a smooth substrate, the alignment of the columns in the coating will be even smoother than the substrate itself because the columns will be parallel to each other. If the substrate is rough, however, the columns will form a "fan-like" arrangement, making the coating rougher than the substrate.

1.8 Tribo-behaviour of EN coatings

Wear is defined as the removal of material from solid surfaces as a result of one surface moving over another. Wear can occur from one of the several wear mechanisms which are also called modes of wear. The precise combination of wear mechanisms depends on contact conditions. Typical wear mechanisms include: adhesive, abrasive, fatigue, corrosive, fretting, erosion and chemical wear. It is common that in real contact, more than one wear mechanism is acting at the same time. Owing to their high hardness, EN coatings also sport high wear resistance and abrasion resistance. The superior wear resistance capabilities of EN coatings have been established by many researchers (Gawne and Ma, 1988; Barker, 1993; Baudrand and Bengston, 1995; Berkh et al., 1996). Also, the co-deposition of tungsten in binary EN coatings has resulted in an improvement in the wear resistance of these coatings. Due to this high wear resistance, these coatings are considered a replacement for hard chromium and high alloy materials.

Taber wear index (TWI) is a method to calculate the wear resistance of materials. The TWI is a measure of weight loss of a material obtained under a load of 10 N rotated for 1000 cycles using the abrasive wheels (CS-10). As compared to hard chromium which has a TWI of 0.5 to 0.7, the as-deposited Ni-P shows a value of 9.6. the as-deposited Ni-B

however shows a value of 1.4 to 2 TWI which is comparable to that of hard chromium. Hence such coatings may replace hard chromium (Krishnan et al., 2006).

In theory, a surface's hardness can be used as an indicator of how well it resists wear. There are many other factors, such as the surface texture and the applied stress, that influence a surface's wear properties. Electroless nickel deposit's wear resistance is affected by phosphorus content and the kind of heat treatment the as-deposited sample goes through. Heat treatment is likely to improve the coating's hardness and in turn its wear resistance. However, at high heat treatment temperatures, grain coarsening occurs and it may reduce the coating's wear resistance. Literature shows that the amount of wear on coatings that had been subjected to laser irradiation was significantly less than that of coatings that had been either as-deposited or furnace-annealed from an amorphous alloy (Tsujikawa et al., 2005). The higher hardness obtained by suitable heat treatment methods makes them preferable for wear-resistant applications. Although it should be noted that after being heated to 400° Celsius in an environment of 5% H_2 and 95% Ar, the Taber wear index of a Ni-B coating dropped very steeply to 13 (Kanta et al., 2010). When it comes to Taber abrasion resistance, the coating itself is more important than the adhesion between the coating and substrate. If the application only requires high wear resistance as in the case of sliding surfaces or flow through pipes, electroless Ni-B coated on an aluminium substrate may be more effective as compared to plated steel (Kanta et al., 2009).

A study by some researchers conducted a scratch test and demonstrated strong adhesion of the electroless Ni-B deposition onto a substrate Al alloy (Vitry et al., 2008). According to some researchers (Srinivasan et al., 2010b), the primary reason for the high wear resistance of electroless Ni-B is the columnar structure of these coatings. This structure helps in retaining the lubricant even during conditions of adhesive wear. EN coating displays a wear mechanism which is typically either abrasive or adhesive or a mixture of both of these phenomena. Since nickel and iron are highly soluble in one another, an adhesive wear mechanism controls the deterioration of as-coated Ni-B coatings (from counter-face material). Particle incorporations are common in electroless nickel, and it is discovered that some of the engineered coatings have superior wear behaviour to the parent material. Adding tungsten to Ni-P coatings increases their wear resistance

(Palaniappa and Seshadri, 2008). This may be because tungsten is strengthening the nickel matrix in a solid solution. When the electroless Ni-P deposit wears away, it's because nickel atoms in the coating are attracted to iron atoms in the counter disc. In some instances, oxide particles adhere to the coated pin/counter disc interface leading to a negative wear depth curve (Palaniappa and Seshadri, 2008). This accumulation of oxides also serves as a lubricant at the interface, reducing the coefficient of friction for the heat-treated coatings.

Also, the deposition of both ZrO_2 and tungsten is observed to improve the wear behaviour of the Ni-P (Gay et al., 2007). It is found that better abrasion resistance of steel could be achieved by the addition of tungsten carbide (WC) as reinforcement with a Ni-P matrix increasing it by a factor of thirteen. While improving electroless deposited binary Ni-P on the same substrate resulted in an increase in abrasion resistance by a factor of three. The higher abrasion resistance of Ni-P-Tungsten carbide composite coating may be due to the Ni matrix which acts as a supporting member and holds the particles within the matrix, which allows the electroless coating to resist excessive damage due to the shearing action of the sliding counterpart. Several other soft and hard particulates, such as alumina (Alirezaei et al., 2005), boron carbide (Araghi and Paydar, 2010) and silicon carbide (Sarret et al., 2006) have found their acceptance as particle inclusion in these type coatings.

Annealing electroless nickel coatings at temperatures higher than 400 degrees Celsius, as most researchers have found, has a negative impact on the coating's ability to withstand wear. This occurs as a result of the formation of intermetallic phases, which result in a decreased adhesion of the coating to the substrate. The wear tracks were analysed by Novák et al. (2010), and they found abrasion to be the dominant wear mechanism. They also concluded that at an annealing temperature higher than 450 °C excessive intermetallics were formed causing delamination of the coating. They suggested using Al_2O_3 fibre reinforcement in the coating, which was shown to reduce flaking and increased the resistance to wear in comparison to a binary Ni–P coating. According to the findings of (Ebrahimian-Hosseinabadi et al., 2006), there is a reciprocal relationship between the volume percentage of B_4C particles and the amount of wear resistance exhibited by Ni-P-B_4C. The coating's resistance to wear improved with increasing volume percentage up to 25%, after which it began to degrade at a faster rate. They determined that the decrease in

wear resistance of the Ni-P-B_4C coating was due to the Ni matrix losing its ability to effectively support and retain the particles within the matrix. The incorporation of SiO_2 nanoparticles helps to slow the dislocation movement of the composite coatings, which allows for the subsequent crystallisation of an amorphous Nickel-Phosphorus matrix at the appropriate elevated temperatures. Table 1.5 lists the specific wear rate improvements for Ni-P-TiO_2 with the addition of 4g/l nano-TiO_2 (Makkar et al., 2014). It can be seen from the table that there is an improvement in the wear resistance Ni-P-TiO_2 against the binary Ni-P coating.

Table 1.5: Comparison of wear rates between Ni-P and Ni-P-TiO_2 (nano) with load and sliding velocity (Makkar et al., 2014).

Coatings	Load (N)	Specific wear rate (* 10^{-6} mm^3/Nm)	Sliding Velocity (m/s)	Specific wear rate (* 10^{-6} mm^3/Nm)
Ni-P	1.00	7.85	0.10	8.00
	1.50	25.00	0.20	15.00
	2.00	61.78		
Ni-P-TiO_2	1.00	1.43	0.10	1.50
	1.50	3.93	0.20	4.48
	2.00	18.9		

1.9 Corrosion

The electroless nickel acts as a barrier coating. The substrate material is protected from the detrimental action of the environment. This is necessary due to the homogeneity and nearly impervious nature of these coatings. These coatings in their deposited form are amorphous and highly resistant to corrosion. The amorphous nature and lack of grain or phase boundaries impart excellent anti-corrosive properties to these coatings. It has been observed that the corrosion resistance of these coatings decreases with heat treatment. This is owing to the fact that heat treatment tends to bring about a microstructural change in these coatings from amorphous to relatively crystalline. Tomlinson and Carroll (1990) studied the correlation between surface roughness, coating thickness and corrosion potential. They found that for a given substrate roughness the corrosion potential increased with coating thickness.

1.10 Nanoparticle reinforced coatings

More than 20 types of composite particles have been used in reinforcing EN coatings. Namely, SiC, WC, diamond, TiC, Cr_3C_2, Al_2O_3, SiO_2, Cr_2O_3, TiO_2, ZrO_2, CeO_2, YSZ,Fe_3O_4, $K_2Ti_6O_{13}$, Si_3N_4, MoS_2, PTFE, BN, Talc, B_4C, CaF_2, polymer, and graphite (Liu et al., 2007; Matsubara et al., 2007; Yu et al., 2011; Afroukhteh et al., 2012a, 2012b; Ashassi-sorkhabi and Es, 2013; Sharma and Singh, 2013; Ma et al., 2014; Hsu et al., 2015; Islam et al., 2015; Luo et al., 2015; Murty et al., 2015; Soleimani et al., 2015; Wang et al., 2015; Wu et al., 2015; Wang et al., 2015; Wang et al., 2015; Ardakani et al., 2016; Dadkhah and Ansari, 2016; Sharma and Sharma, 2016; Shi et al., 2016; Farrokhzad, 2017; Li et al., 2017; Sadreddini et al., 2017; Xie, 2017). Recently, CNT has also been included in this group of reinforcements. As has been categorically reported in the literature these nano reinforcements have improved the hardness and wear resistance of the coatings (Xu et al., 2005; Bigdeli and Allahkaram, 2009; Ranganatha et al., 2012; Karthikeyan and Ramamoorthy, 2014; Sadreddini and Afshar, 2014). A study from 2014, reports an improvement in the wear resistance of the electroless Ni-P coatings reinforced with TiO_2 (Makkar et al.,2014). Table 1.5 shows the comparison in the wear rate of the as-deposited Ni-P coatings and as-deposited Ni-P-TiO_2 coatings. The wear rate of the reinforced coatings in all the cases is less than 30% of the coatings prepared without any TiO_2 inclusion.

One of the primary requirements of particle reinforcement in the electroless EN coating is the need for good dispersion of these ceramic particles. Nanoparticles are difficult to keep suspended in a solution because they have a large surface energy, which causes them to clump together. This can be prevented by air injection, vigorous agitation, or ultrasonic vibration. Surfactants can also be used to help prevent agglomeration (Riedel, 1991). Sometimes with the combined use of these methods, one can achieve a good suspension of nanoparticles. Before selecting a nanoparticle for reinforcement, it is necessary to consider the factors like type, size, concentration and properties of the embedded particles, as they play the primary role in determining the characteristics of the

composite coatings (Chen et al., 2010; Rabizadeh and Allahkaram, 2011; Yang et al., 2011).

1.11 Summary of literature review

The available literature shows extensive work done in the field of nanocomposite reinforced electroless Ni-P coatings, in contrast, the reports for electroless Ni-B coatings are much less elaborate. The reports on the reinforced Ni-B coatings include reinforcement with SiC, SiO_2, diamond, graphite, Al_2O_3, Si_3N_4, CuO (Kaya et al., 2008; Krishnaveni et al., 2012; Ekmekci and Bulbul, 2015; Georgiza et al., 2017). Most of the early works concentrate on the preparation and characterization of the coatings and not on their tribo-nature. More recently, Yazdani et al., 2018, have presented their findings regarding the wear-resistant properties of Ni-B-CNT coatings. They have proposed that with the increase in the CNT content of the coatings, there is an increase in the crystallinity. Also, they reported an improvement in the friction coefficient and the wear rate of the as-plated coatings. This is attributed to the self-lubricating effect brought about by the incorporation of CNT. As it has been suggested by the available literature the addition of the nanoparticles changes the following properties: hardness, wear resistance, crystallinity, crystal structure also texture and morphology of the EN coatings. The tribo-study of the Ni-B-nano particles is still a field of interest for modern-day researchers. Although a few researchers have studied the Ni-B coatings as Ni-B-Diamond (Kaya et al., 2008), Ni-B-Si_3N_4 (Krishnaveni et al., 2012) and Ni-B-CNT (Yazdani et al., 2018), there still exists a whole range of nanoparticles whose influence on the tribo-character of the Ni-B plating has not been studied at length. The purpose of this research is t conduct a detailed study of the tribo-mechanical properties of such reinforced coatings.

1.12 Research plan

Based on the literature survey, research objectives and outline of the work are defined.

1.12.1 Objectives

Based on the literature survey following objectives have been derived.

- To prepare sound Ni-B and Ni-B-reinforced nano composite coatings by electroless process.
- To characterise the coatings by microstructural evaluation and SEM, EDS and XRD.
- To study the mechanical properties and wear characteristics of the as deposited coatings.
- To study the corrosion resistance of the reinforced coatings as compared to the as-deposited Ni-B coatings.
- To compare the best Ni-B-reinforced coatings with the corresponding Ni-P-reinforced coatings.

1.12.2 Outline of the work

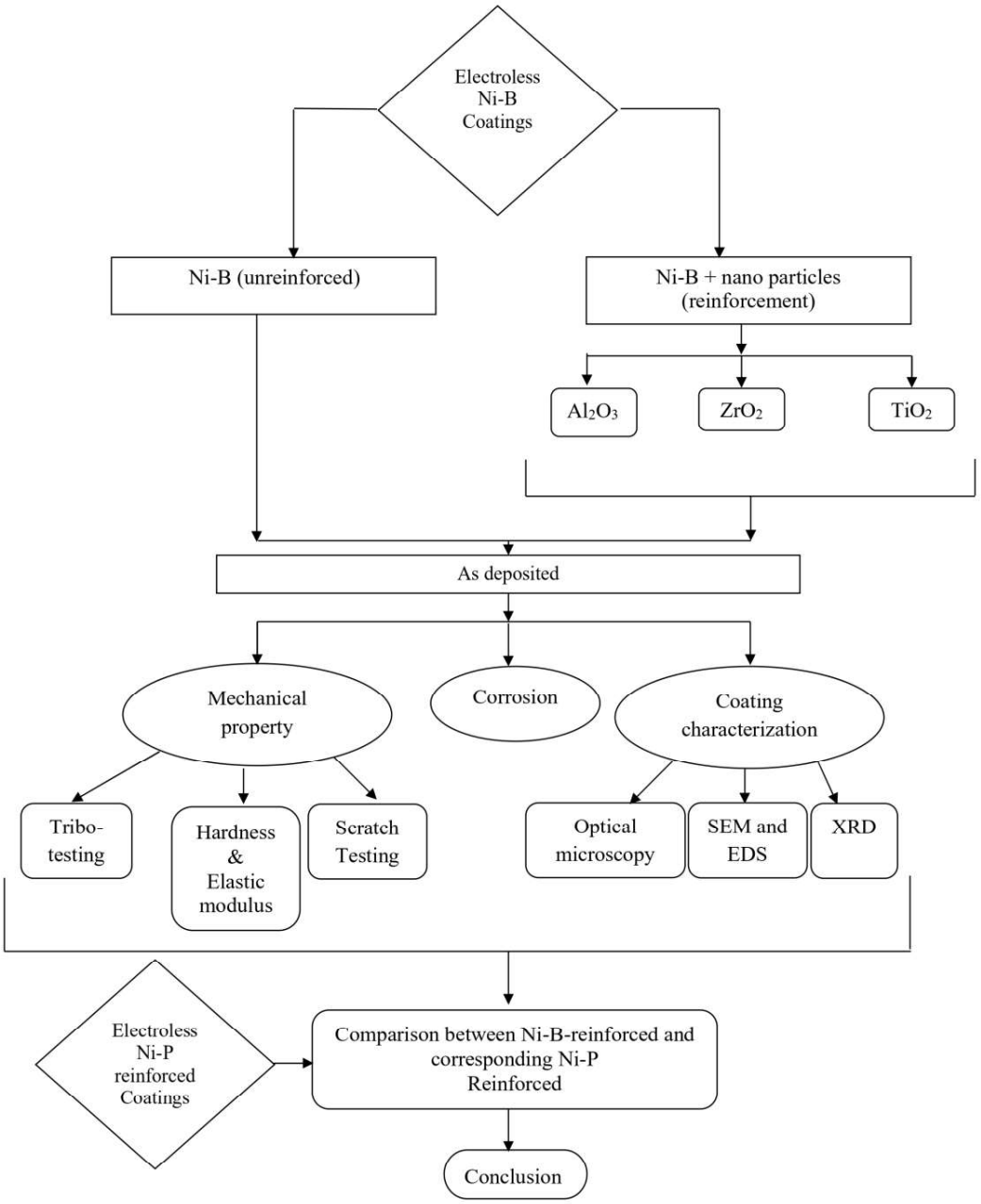

Fig. 1.10: Outline of the work

1.13 Closure

In this chapter, the literature survey provides an overview of the current state of research on electroless Nickel depositions incorporated with nanoparticles. The findings of this survey suggest that there is a growing body of evidence to support the importance of Nickel depositions in industrial applications. However, there are still many unanswered questions relating to the tribological aspect of electroless Ni-B reinforced with nanoparticles. This literature survey has also raised a number of questions that warrant further research. For example, what are the effects of nanoparticle reinforcement on the mechanical aspect of these coatings? How the presence of nanoparticles influences the electrochemical corrosion response of these as-deposited coatings? The ensuing chapters have tried to answer these questions in detail.

This page is intentionally left blank

Chapter 2: Materials and methods

Outline: *2.1 Bath composition and coating deposition, 2.2 Surface morphology study, 2.2.1 Optical microscopy, 2.2.2 Scanning Electron Microscope, 2.2.3 X-Ray Diffraction, 2.3 Micro Vicker's Hardness test, 2.4 Nanoindentation test, 2.5 Scratch test, 2.6 Corrosion test, 2.6.1 Potentiodynamic polarization test, 2.6.2 Electrochemical impedance spectroscopy, 2.7 Wear and Friction test, 2.8 Closure*

2.1 Bath composition and coating deposition

An electroless bath, also known as an autocatalytic bath, is a chemical solution used in plating applications to deposit metal coatings onto a substrate. Unlike electroplating, which relies on electrical current to drive the deposition of metal ions onto a substrate, an electroless bath uses a chemical reduction reaction to achieve the same goal. In an electroless bath, a reducing agent in the solution reacts with metal ions to form metal atoms, which then deposit onto the substrate. The substrate must be chemically treated to make it receptive to the metal coating, and a catalyst is often added to the bath to facilitate the reaction.

In the case of the present study, primarily 3 kinds of nanoparticle-reinforced coatings were deposited namely Nickel-Boron-Alumina (Ni-B-Al_2O_3), Nickel-Boron-Zirconia (Ni-B-ZrO_2) and Nickel-Boron-Titania (Ni-B-TiO_2). Steel substrates of dimension 15 mm X 15 mm X 5 mm and cylindrical substrates of dimension 30 mm length and 6 mm diameter were deposited upon. Fig. 2.1 shows two typical coated substrates used in the present research. Prior to the deposition, these substrates were polished using corundum embed emery papers of grades 800, 1200, 1600 and 2000 to obtain a good surface finish. The primary bath composition used for depositing both coatings is given in Table 2.1. The Ni ion source is $NiCl_2$ and ethylene diamine acts as a complexing agent. Heavy metallic lead ions are used to stabilize the bath so that the bath does not decompose untimely. The pH of the bath was maintained at 12.5 by using sodium hydroxide pellets. As the coating progressed the pH of the bath was replenished by adding sodium hydroxide

solution to the bath externally. The Ni-B coating was reduced by sodium borohydride solution added just before the introduction of the substrate in the bath. Additionally, to deposit the ternary Nickel-Boron-nano particle composite coatings, nano powders of varying composition (avg. particle size-30 nm, SRL, India) was used as reinforcement. The Ni-B coating was reduced by sodium borohydride solution added just before the introduction of the substrate in the bath. Before adding the nano powders were sonicated in an ultrasonicator in presence of surfactant. Sonication was done at a frequency of 60 kHz for 15 min, to make sure that no lumps of agglomerated nano powder remain when they are introduced into the coating bath. A colloidal solution was achieved by this ultrasonication process.

Table 2.1 shows the bath composition used for the deposition. The deposition was carried out for a period of 1 hr. The bath temperature was maintained at 85 ± 3° C. These polished specimens underwent all the necessary cleaning process such as ultrasonic cleaning in deionised water, acid pickling as well as cleaning with ethanol to ensure a completely dry and contaminant free surface. To ensure that the deposition was carried out in a contaminant-free environment the glassware used were also properly cleaned and finally rinsed using deionised water before the commencement of the coating. Fig. 2.2 shows the schematic diagram of electroless coating setup used in the present research.

Table 2.1: Bath composition

Chemicals	Use	Amount
Nickel chloride hexahydrate	Nickel source	20g/l
Ethylene diamine	Complexing agent	80-100ml/l
Sodium hydroxide	Buffer to maintain pH	35-40g/l
Lead nitrate	Stabilizer	0.06g/l
Sodium borohydride	Reducing agent	0.2-0.3 g/l
Nanoparticles	Reinforcements	Varying amount

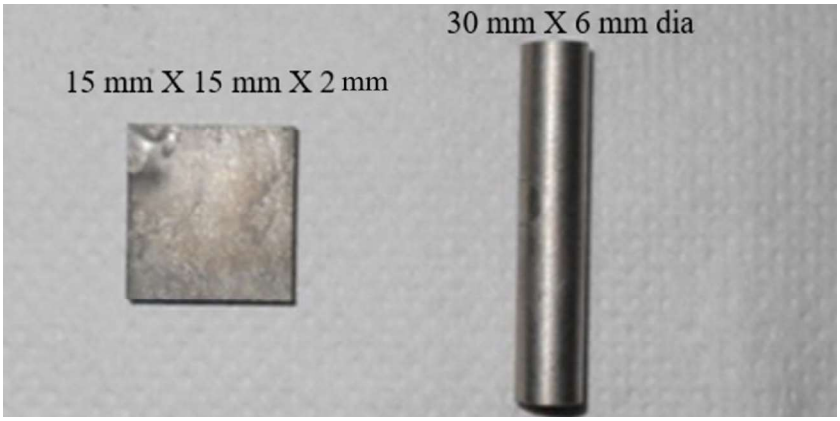

Fig. 2.1: Coated substrates used in the study

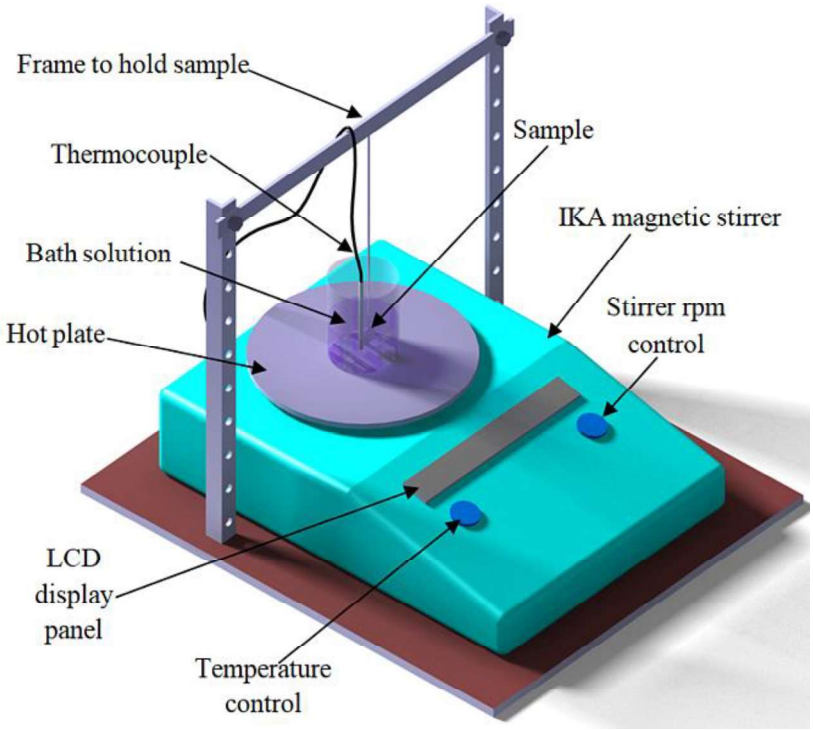

Fig. 2.2: Pictorial representation of electroless coating setup

2.2 Surface morphology study

After depositing a sound coating, the next important step is the coating characterization and the morphology study. The coatings were studied initially under an optical microscope to verify whether the whole substrate surface was coated with the Ni-

B bath. To further identify the nanoparticles (Alumina, Zirconia and Titania) the as-deposited samples were analyzed under an FESEM (Field Emission Scanning Electron Microscope). The SEM analysis was adjunct by EDS scanning. The phase identification was done by analyzing XRD (X-Ray Diffraction) patterns of the coating. Also, RAMAN spectroscopy was used to identify phases that were not visible in the XRD patterns. The current microstructural investigation aims to study the distribution of reinforcing particles, nodule structure and phase element identification in the deposited samples. The coating thickness is calculated using equation (2.1).

$$T = \frac{W*10^4}{A*\rho} \tag{2.1}$$

Where T is the coating thickness in 'μm', W difference in the weight of the sample in 'gm' before and after coating, ρ coating density in 'gm/cm^3', and A is the coating surface area in 'cm^2'.

2.2.1 Optical microscopy

Optical microscopy refers to a type of microscopy that uses visible light and lenses to magnify and observe objects that are too small to be seen with the naked eye. It is an important tool for analyzing the microscopic structure of materials. In optical microscopy, a sample is placed on a stage and illuminated with light that passes through a series of lenses to form an enlarged image. The magnification of the image depends on the type of lens used and the numerical aperture of the system. The resolution of the image is determined by the wavelength of the light used and the quality of the lens system.

The primary purpose of the microscopic analysis is to verify the integrity of the deposition before analyzing the samples under an SEM. Due to magnification limitations; optical microscopes are not suited for detecting particles in the nano range. The optical microscope Leica DM2700 M is used in this work. Fig. 2.3 shows the microscope used in this study.

Fig. 2.3: Optical microscope used in the study

2.2.2 Scanning Electron Microscope

Fig. 2.4 shows the FESEM (Field Emission Scanning Electron Microscope) used in the present research. Scanning electron microscopy (SEM) is a tool for observing microstructure in great detail with a resolution of around 1 nm at high magnification. In SEM, a beam of electrons is directed at the sample surface, producing signals in the form of secondary/backscattered electrons or characteristic X-rays. These signals representing surface structures are captured by detectors and used to produce images on a computer screen. Light elements (atomic number < 9) are difficult to detect in most common SEM machines, but FESEMs, or field emission scanning electron microscopes, having field emission guns (FEGs) attachment are better suited for this purpose. FESEMs are capable of detecting light elements and provide excellent-resolution imaging. Additionally, FESEM is superior for compositional analysis using energy dispersive spectroscopy (EDS)

attachment. EDS measures the energy of X-rays produced by heating the electron beam on the material surface, allowing for the identification of elements. The EDX spectrum is displayed as a plot between X-ray counts and energy, and elemental mapping is also possible in EDS to show the distribution of X-rays and different elements in the sample.

Fig. 2.4: Field Emission Scanning Electron Microscope

2.2.3 X-Ray Diffraction

The basic idea behind X-ray diffraction is that monochromatic X-rays interfere constructively with crystalline material. These X-rays are made by a cathode ray tube. They are then filtered to make them monochromatic, collimated to focus them, and sent toward

the sample. If the conditions of Bragg's Law ($n = 2d\ sin\theta$) are met, when the incident rays hit the sample, they create constructive interference and a diffracted ray.

Fig. 2.5: X-Ray diffraction instrument

According to this rule, the lattice spacing and diffraction angle in a crystalline sample are proportional to the wavelength of the electromagnetic radiation being used for the diffraction. It is necessary to detect and analyse the X-rays that have been diffracted. Due to the amorphous material's random orientation, scanning it across a range of 2θ angles should expose the material to all possible diffraction directions of the lattice. Diffraction peaks can be converted to d-spacings, which then allow for their identification.

XRD is a non-destructive approach. Fig. 2.5 shows the XRD instrument used in the present research. The coating phase structure is investigated using a (Bruker D8 advance, USA) Diffractometer equipped with a $Cu\ K\alpha$ ($\lambda = 1.54059$) as the radiation source and an Inel CPS 120 hemispherical detector. During the XRD test, the scanning speed (1.0°/min) and width (0.02°) are held constant. Based on other related research, the diffraction angle (2θ) is chosen to be between 20° and 120°. The nature of XRD plots can

quickly identify if a certain phase is crystalline or not. The phase is termed crystalline if the diffraction peak is crisp, whereas diffused peaks are features of the amorphous phase.

2.3 Micro Vicker's hardness test

One common technique for determining a material's hardness is the Vicker's hardness test. It involves using a square-based pyramidal diamond indenter and applying a load to make an indentation on the test surface. The applied force in this test can range from 1 gf to 120 kgf, and the indentation time is limited to 10 to 15 seconds. The Vickers hardness test is favored due to its ease of performance, independence of indenter size and applied load, and the ability to use the same indenter for different materials.

In general, the coatings under study vary in thickness from 15 μm to 60 μm, hence Vicker's microhardness test becomes a very handy tool to evaluate the material thickness of the coating. The hardness of materials is typically differentiated into three groups based on the penetration depth (d) of the indenter: nano-hardness (d < 1 μm), micro-hardness (d = 1-50 μm) and macro-hardness (d > 50 μm). This classification helps distinguish between the hardness of materials at different length scales and can provide useful information about their properties and behavior. The hardness value is determined by measuring the lengths of the two diagonals of the projected area of the indentation after the removal of the indenter. The image of a typical pyramid indenter with a square base is shown in Fig. 2.6 (b).

Vickers Microhardness (HV) is assessed in this study utilizing the LECO Microhardness Tester LM248AT (Fig.2.6 a) in accordance with the ASTM E384-17 standard. At five random locations on the coatings, a 100gf load is applied with a dwell duration of 15 seconds. The diagonals (shown in Fig. 2.6 (b) termed as d_1 and d_2) of the impressions are individually recorded using a micrometer attached to the hardness tester. The dedicated software installed on the computer linked to the microhardness tester allows for the instantaneous display of the microhardness results. This software serves as an interface between the microhardness tester and the computer, facilitating data transfer and analysis.

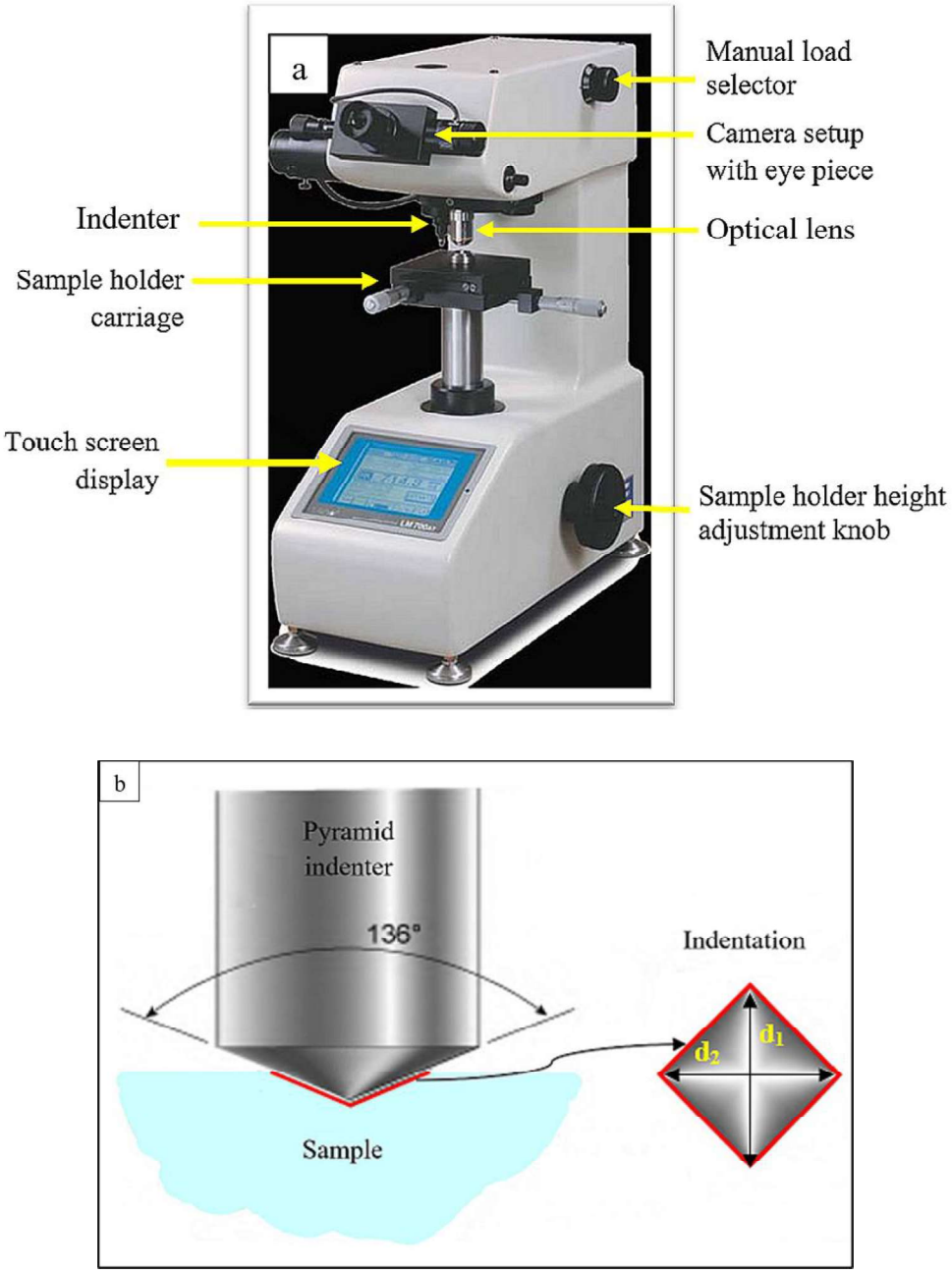

Fig. 2.6: (a) Vickers Micro hardness tester and (b) Schematic diagram of a typical pyramid-type indenter

Vickers Micro hardness is computed using the equation (2.2).

$$HV = 1854.4 * [F / (dv) 2] \quad (2.2)$$

Where F the applied indentation load in gf is, dv is the mean of the two diagonals d_1 and d_2 length of indentation impression (μm). Average of 10 readings is reported as the average micro Vicker's hardness.

2.4 Nanoindentation test

Nanoindentation is a popular method for measuring nano/micro-scale properties like creep resistance, hardness, fracture toughness, elastic modulus for thin films and coatings. This method calculates contact area indirectly from penetration depth without imaging the indent. The nano-indentation tester used in the study is an Anton Parr NHT3 model. Fig. 2.7 shows the nano-indentation tester. This nano-indentation tester can measure depths from 20 nm to 200 μm and loads from 0.1 to 500 mN. Various protocols such as advanced matrices, user-defined sequences, CMC (continuous multi cycles), sinus mode, and multiple samples protocols, are all supported by the instrument. Standard Berkovich diamond indenters having a tip diameter 100 nm was used to indent the samples. The peak load, dwell time and loading-unloading rate were 10 mN, 10s and 0.33 mN/s, respectively.

Fig. 2.7: Anton Parr NHT3 nano-indentation instrument

The underlying principle for calculating the elastic modulus follows the Oliver and Pharr method to generate the load-displacement curve which in turn gives the elastic modulus of the specimen. Oliver and Pharr's 1992 nanoindentation data analysis method uses the specimen's elastic unloading response to calculate the tip–sample contact size at unloading. The stiffness of elastic contact is based on Hertz' theory.

This gives the stiffness of contact as shown in equation (2.3)

$$S = \frac{dP}{dh} \tag{2.3}$$

The effective elastic constant is given by equation (2.4):

$$E_e = \left(\frac{\sqrt{\pi}}{2}\right)\left(\frac{S}{\sqrt{A_c}}\right) \tag{2.4}$$

Where, $E_e = 1/[(1 - v_{sample}^2)/E_{sample} + (1 - v_{indenter}^2)/E_{indenter}]$, from this equation the term $(1 - v_{sample}^2)/E_{sample}$ may be obtained as the indenter properties are known and the E_e is calculated from the equation 2.4. Fig. 2.8 shows a typical loading-unloading curve as obtained from the nano-indentation test.

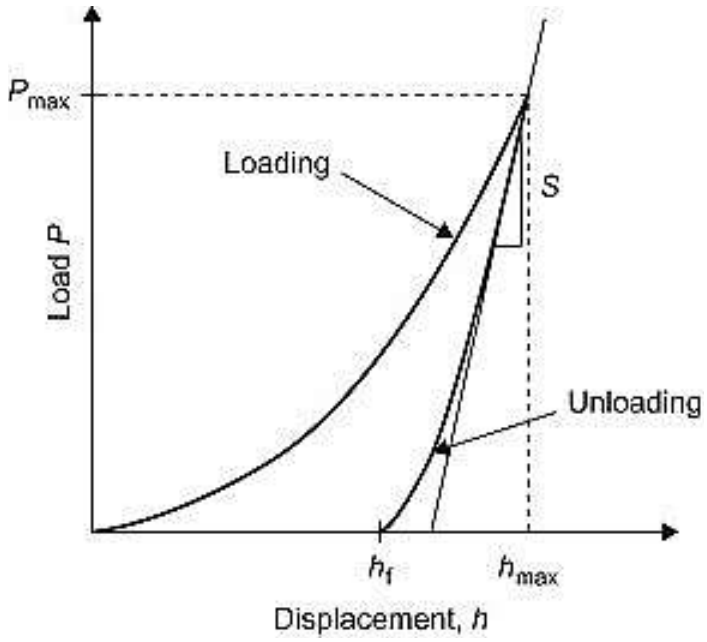

Fig. 2.8: A Typical loading-unloading curve

2.5 Scratch test

The coatings resistance to permanent deformation against a linearly moving diamond indenter was evaluated using a scratch test. The instrument used was Ducom Scratch tester TR-101-IAS. Fig. 2.9 shows the scratch tester and its various components. In order to conduct the scratch indentation test, a diamond indenter (conical shape) with Rockwell C hardness having a hemispherical end is used. The nose radius of the indenter is 200 µm and the flank angle was 120°. Scratches were captured for analysis with the help of the scratch tester's built-in image acquisition system, which featured a camera with a resolution of 5 megapixels. The scratch tester is connected to a computer by means of the 'Winducom 2010' software in order to allow for the input and visualisation of test parameters.

Fig. 2.9: DUCOM Scratch tester

In order to determine the scar widths, the 'Scar View 2016' software was utilised. In accordance with the standard set by ASTM G171-03, the scratch hardness (GPa) was calculated by using the applied load in addition to the average width of the scratch. Scratch hardness, better known as scratch hardness number, is calculated by equation (2.5).

$$H_s = \frac{8}{\pi}\frac{F_N}{w^2} \quad (2.5)$$

' F_N ' is the normal load applied during scratch, given in N and ' w ' is the measured scratch width in mm. The average traction load and the normal load that was applied are used in the calculation to determine the coefficient of friction.

The testing was done at a constant loading condition of 20 N, 30 N, and 40 N. The specimen was scratched for a stroke length of 5 mm and an indentation speed of 0.1mm/s. Scarview imaging software was used for obtaining optical images. An average hardness of 3 scratches for each load is reported in this study.

2.6 Corrosion test

Fig. 2.10 shows the potentiostat setup used for the study. Corrosion measurements are vital for figuring out how various materials react to corrosive environments.

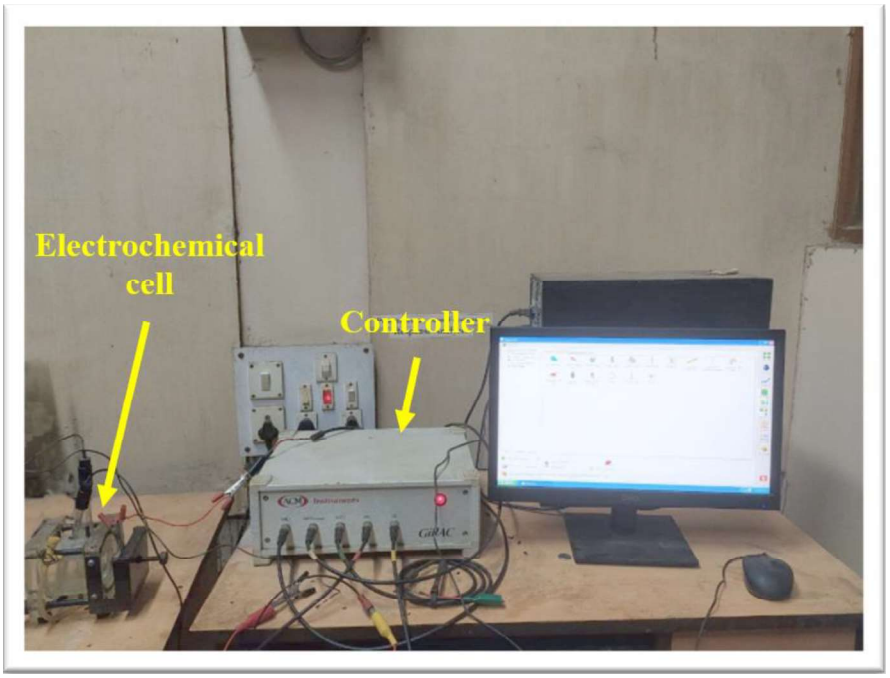

Fig. 2.10: Electrochemical corrosion setup (Potentiostat)

Planning and enacting preventative measures to restore the component's functional properties is aided by knowing the materials response to corrosion. Electrochemical methods are superior to other methods for revealing important details about the corrosion process. Furthermore, it allows for the possibility of reducing corrosion by regulating the electrode potential. In the present study potentio-dynamic polarization technique and EIS (Electrochemical Impedance Spectroscopy) method are used as yard stick to determine the corrosion resistance of the specimen under study.

2.6.1 Potentiodynamic polarization

In simple terms, Polarization Technique is a method in electrochemistry that studies the behavior of metal electrodes in a corrosive environment by shifting the potential of the working electrode from its open circuit potential and measuring the current as a function of time or potential. The Open Circuit Potential (OCP) of a metal refers to the potential of the metal when it is not connected to any external circuit. This potential reflects the equilibrium state of the metal and can be used to determine its corrosion potential, dissolution potential, or equilibrium potential. The potential-time relation in a corrosive environment shows how the protective films on the metal surface form and break down, as indicated by changes in the corrosion potential. An increase in the corrosion potential indicates the formation of protective films, while a decrease in the corrosion potential indicates the breakdown of these films. Anodic polarization occurs when the potential of the working electrode is shifted in a positive direction, causing it to become the anode and electrons to be removed from it. This leads to the oxidation of metal ions from the electrode surface, causing the electrode to corrode. The current flowing through the electrode during anodic polarization is proportional to the rate of metal ion oxidation. In contrast, cathodic polarization occurs when the potential of the working electrode is shifted in a negative direction, causing it to become the cathode and electrons to be supplied to it. This leads to the reduction of metal ions from the electrode surface, which may form a protective film that slows down the corrosion rate. The current flowing through the electrode during cathodic polarization is proportional to the rate of metal ion reduction.

In the Polarization Technique, an electrochemical cell with three electrodes is used. The working electrode, which is the test sample, is placed in a container filled with a corrosive solution. The reference electrode and the counter electrode are also placed in the container, and all three electrodes are connected to a potentiostat. The potentiostat is used to control the potential of the working electrode and to measure the current flowing through the electrode. The reference electrode provides a stable reference potential for the measurement, while the counter electrode supplies or removes electrons from the solution to complete the circuit. The arrangement of the three electrodes and the use of the potentiostat allows for the controlled manipulation of the potential of the working electrode and the measurement of the corresponding current.

The experimental data obtained during the Polarization Technique, including the potential and current values, are stored in a connected computer using dedicated software. This recorded data is then used to plot different graphs, such as a Tafel plot. A Tafel plot is a semi-logarithmic plot of the applied voltage versus the current density. This plot provides valuable information about the corrosion behavior of the metal, including the corrosion rate, the corrosion current density (I_{corr}) and the corrosion potential (E_{corr}). The nonlinearity of the Tafel plot near zero overvoltage indicates the presence of half-cell reactions, which contribute to the total current flowing through the electrode. The Tafel extrapolation technique can be used to determine these corrosion parameters once the interpolated data has been plotted. Fig. 2.11 shows a typical Tafel plot with the specific anodic and cathodic parts. The Tafel region is the linear portion of a Tafel plot, which is a graphical representation of the relationship between electrode potential and the logarithm of the corresponding current density in electrochemical reactions. The Tafel region occurs at high overvoltage and indicates the rate-determining step in the electrochemical reaction.

The Tafel extrapolation method is considered a rapid and accurate method for measuring the corrosion rate of metals and alloys. This is based on the Tafel equation, which relates the reaction rate and the overvoltage in an electrochemical reaction. The Tafel extrapolation method can provide continuous monitoring of the extremely low corrosion rate, making it useful in a variety of applications, including the prediction and control of corrosion in industrial and natural environments. However, the accuracy of the

Tafel extrapolation method can be influenced by several factors, such as temperature, electrode geometry, and solution composition, and it may not always be equivalent to the accuracy of other methods, such as weight loss or electrochemical impedance spectroscopy.

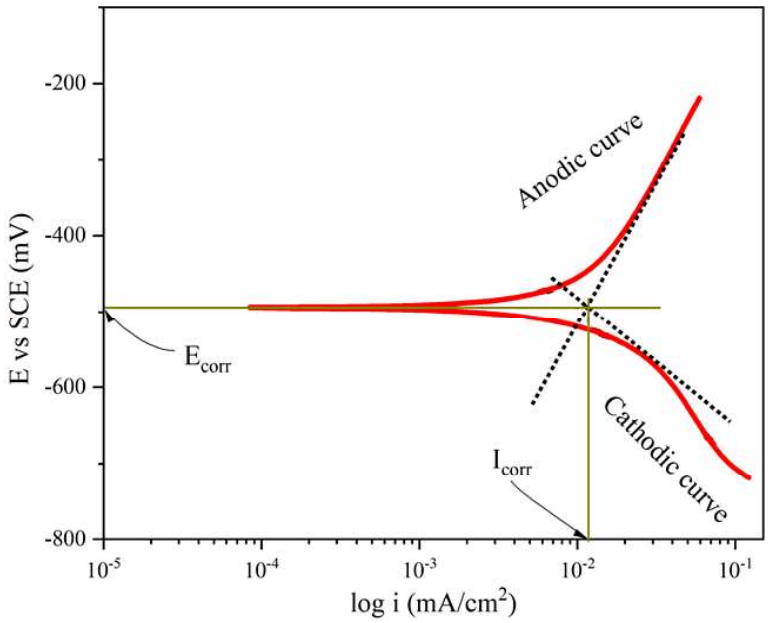

Fig. 2.11: Typical Tafel curve

2.6.2 Electrochemical impedance spectroscopy

Electrochemical impedance spectroscopy (EIS) is a technique used to study the behavior of electrochemical systems, such as corrosion and battery performance. It is based on the measurement of the electrical impedance of the system over a range of frequencies. EIS provides information about the resistance, capacitance, and inductance of the system, and the interactions between these components can be used to determine important parameters, such as the corrosion rate and the degree of corrosion inhibition. The technique is widely used in materials science, corrosion engineering, and electrochemistry, and it provides valuable information for the optimization and control of electrochemical processes.

In Impedance Spectroscopy or Electrochemical Impedance Spectroscopy (EIS), the electrode impedance is plotted against frequency to study the behavior of electrical circuits and to determine the impedance properties of materials such as resistance, capacitance, and inductance, as a function of frequency. During Impedance Spectroscopy test, a small voltage signal is applied to the corroding surface and the resulting current is measured. The equivalent electrical circuit of the material is then used to analyze the electrochemical system. This method is non-destructive. The information obtained from EIS provides valuable insights into the corrosion process and helps in developing strategies to mitigate it. The Randle's circuit is a widely used equivalent circuit model in Impedance Spectroscopy and is often used to analyze electrochemical systems. A typical circuit is shown in Fig. 2.12 (a).

In this circuit, R_{sol} represents the solution resistance between the working electrode and reference electrode, R_{ct} represents the charge transfer resistance or polarization resistance at the interface between the solution and electrode, and C_{dl} represents the double layer capacitance.

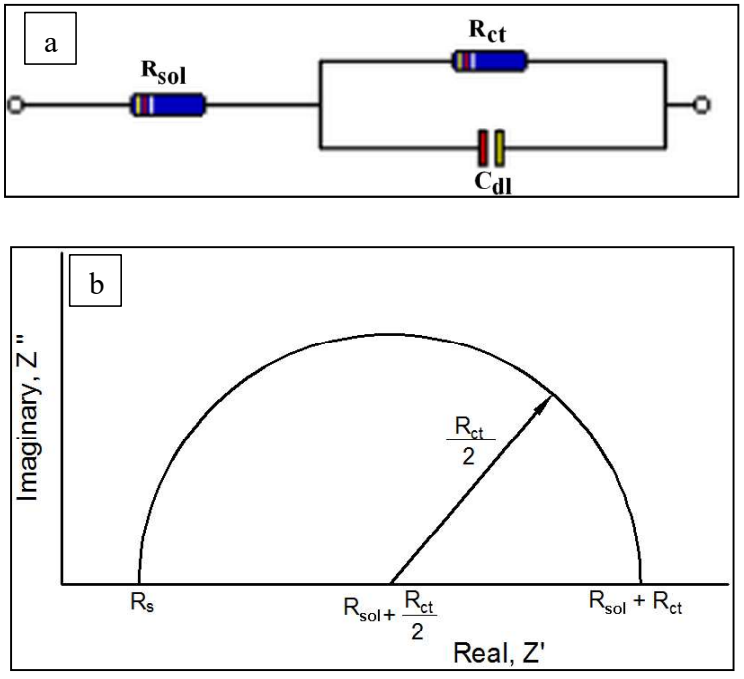

Fig. 2.12 (a): Randle's circuit obtained from Gill AC instrument
(b) Typical Nyquist curve

Fig. 2.12 (b) shows the typical Nyquist curve. The frequency response analyzer included with the potentiostat generates a sinusoidal potential across the sample and measures the phase angle and magnitude of the induced current. The impedance is then calculated from these measurements, across a wide frequency range (from 10^{-3} Hz to 10^{5} Hz). The data collected by the potentiostat and frequency response analyzer is transmitted back to the computer attached to the instrument and can be stored for further analysis. The stored data is represented as a Nyquist plot, which is a graphical representation of the real and imaginary parts of the impedance as a function of frequency. An area of $1cm^2$ of the samples was subjected to the corrosive action of 3.5 wt. % NaCl solution. 1mV/s scanning speed was maintained throughout the test.

2.7 Wear and Friction test

In the present study, the TR-208-M2 pin on disc tribotester is employed for conducting sliding wear tests under room temperature and dry conditions. The testing unit is shown in Fig. 2.13. The procedure follows the guidelines set by the ASTM G99-05 standard. The cylindrical work sample is held vertically against a rotary counter disc made of EN31 material (with a hardness of 63 HRC), which has a hardness significantly greater than the material being tested. Dead weights are added to the pan attached to the loading lever, which is operated manually, to apply loads. The control unit connected to the computer sets the speed and duration of the test through specialized software. The frictional force is measured using a beam-type load cell with a range of 0-100 N and accuracy of 0.1 ± 2% N. The software displays the real-time variation trend of the test material's friction coefficient. The data collected during the test is used by the installed software to plot a graph. After each test, the specimen's mass loss is measured with a sensitive digital balance, and the wear rate is determined by dividing the mass loss by the sliding distance.

Fig. 2.13: Pin-on-disk tribotester

2.8 Closure

This chapter provides a comprehensive overview of the experimental procedures employed in the study. The chapter begins by detailing the process of electroless deposition, including the materials and techniques used to produce these coatings. Next, the chapter goes on to explain the basic material characterization methods, which include the measurement of XRD, SEM and EDAX. This is followed by the description of various tests conducted on the samples such as hardness, nano indentation, scratch, wear test and corrosion tests. These tests are critical to understanding the properties of the materials being tested and provide a baseline for comparison to other materials. Each of these tests provides unique insights into the behavior of the materials being tested and allows for a detailed understanding of their properties and performance characteristics.

This page is intentionally left blank

Chapter 3: Nano-Alumina reinforced electroless Ni-B coatings

Outline: *3.1. Introduction, 3.2 Experimental details, 3.3 Results and discussion, 3.3.1 Zeta potential of colloidal alumina solution, 3.3.2 Coating morphology, 3.3.3 Raman spectroscopy, 3.3.4 X-Ray Diffraction, 3.3.5 Micro Vicker's hardness and elastic modulus, 3.3.6 Scratch resistance, 3.3.7 Wear and friction behaviour, 3.3.8 Corrosion, 3.4 Closure*

3.1 Introduction

Ni-B coatings are chemically more stable than pure EN coatings (Gültekin et al., 2021). The addition of nanoparticles like alumina, silica, silicon carbide, etc. may further enhance the properties of Ni-B coatings (Ekmekci and Bulbul, 2015; Georgiza et al., 2017). ENB coatings show a density that is consistently less than pure nickel's, which measures 8.9 g/cm^3, and this density reduces as the boron concentration increases. Coatings that contain 5 wt% B are commonly acknowledged to possess a density of approximately 8.25 g/cm^3. It is difficult to determine the melting point of nickel-boron accurately. Although it is observed that the Nickel-Boron melts in the range between 1093 °C and 1455 °C. 1093 °C is the eutectic temperature of the Ni/Ni_3B and 1455 °C is the pure nickel's melting temperature.

The addition of nanoparticles improves the mechanical properties such as hardness due to the morphological changes brought about in the electroless binary Ni-B matrix (Georgiza et al., 2017). Further, the addition of reinforcement particles, which offer both dispersion and particle hardening, can lead to a reduction in grain sizes and an increase in hardness. It is essential to establish the ideal quantity of these particles, as an excessive amount can cause a decline in wear resistance and mechanical strength due to the formation of agglomerated ceramic nanoparticles that cannot be integrated into the surface matrix (Doğan et al., 2020).

Secondary particle reinforcement comes in two distinct varieties. The first category contains particles that are utilized for the purpose of enhancing the base material's

properties, such as its resistance to wear, abrasion, and corrosion. These are primarily hard metal oxides, carbides, and nitrides (Grosjean et al., 2001; Alirezaei et al., 2004; Aal, Hassan and Rahim, 2008; Bhattacharyya et al., 2023). Particles that are naturally lubricious and soft fall into the second category (Leo, Staia and Hintermann, 2005; Hu et al., 2009; Sharma and Singh, 2011). Examples of this type of particle include polytetrafluoroethylene (PTFE), boron nitride, and molybdenum sulphide, among others.

Alumina is one of the most prolific second-phase materials used in the case of surface modification of coatings as well as composite materials (Purohit and Vagge, 2016; Sarbishei et al., 2016; Mahdavi et al., 2020). Owing to the high hardness of alumina particles, the incorporation of these particles results in improved mechanical properties like hardness and elastic modulus in composite materials. Besides this, these particles also increase the wear resistance.

The literature although provides ample observation on electroless Ni-P-Alumina coatings, a lacuna persists in regards to the Ni-B-nano Alumina coatings. Li et al., 2018, have investigated the effect of alumina reinforcement on the hardness and corrosion resistance of electrodeposited Ni-B coatings. Ekmekci and Bulbul (2015) have studied the nano alumina reinforced electroless Ni-B, but their investigation is limited to the characterization of these coatings. The literature lacks a detailed investigation into the wear behavior and elastic modulus of the Ni-B-nano Alumina coatings. Furthermore, a study into the correlation of these mechanical properties to the colloidal stability of the alumina nanoparticles in the solution has not been explored yet. Besides, the present research also attempts to find the effect of varying concentrations of nano alumina on the mechanical behavior of electroless Ni-B coatings.

The present chapter involves the study incorporating varying amounts of nano alumina particles into the Ni-B coatings and obtaining sound coatings (reinforced with alumina). The resulting coatings were subjected to various characterization techniques such as X-Ray diffraction pattern analysis, Raman spectroscopy and analysis of scanning electron micrographs combined with the EDX study. Additionally, the coatings shall undergo hardness testing, elastic modulus evaluation via nanoindentation method, wear

study (behavior and mechanism) and electrochemical corrosion testing. It is expected that the reinforced coatings would perform better as compared to the unreinforced counterpart.

3.2 Experimental details

The as-received alumina nanopowders (20-30 nm) were first sonicated in the presence of Sodium Dodecyl Sulphate (SDS) in deionised water to form a colloidal suspension of alumina particles. SDS is a suitable surfactant for the dispersion of alumina particles (Xu et al., 2017). The ultrasonication was done using a probe-type sonicator at a frequency of 60 kHz and 120 W. Sonication was carried out for one hour until a proper colloidal state was reached and the particles do not settle to the bottom. Before the coating process, the alumina colloidal solution was subjected to a zeta potential test using a Zetasizer Nano ZS (Malvern, United Kingdom) to determine the saturation concentration of alumina in the coating bath. Ni-B-Nano alumina with varying alumina concentration namely: 2.5 g/l, 5 g/l, 7.5 g/l, 10 g/l and 12.5 g/l were deposited using a basic bath solution. The constituent bath elements are presented in Table 3.1. The coatings were deposited at a temperature of 85 °C ± 3 while keeping the bath continuously agitated at 300 rpm. All the coatings were deposited for a duration of 1 hr.

Post-coating, the coated specimens were subjected to Raman spectroscopy using a Raman spectrometer (Renishaw Invia, UK) which employs an Argon laser that has an excitation wavelength of 514 nm. These parameters are appropriate for recording the Raman spectra of thin films and embedded nanoparticles (Mandal et al., 2016). Various other tests were conducted to observe the surface morphology, hardness, elastic modulus, tribo behaviour and potentiodynamic polarization test (Manning, 1980). The details of these tests are presented in Chapter 2.

3.3 Results and discussion

3.3.1 Zeta potential of colloidal alumina solution

Alumina nanoparticles of 20-30 nm average diameters were commercially obtained. Fig.3.1 (a) shows the alumina suspension in the absence and presence of surfactant (SDS). The addition of SDS helps to keep the nanoparticles suspended in the

solution for days, while the solution without surfactant can be observed with sedimentation at the bottom of the beaker. This ability to keep the particle suspended allows the nanoparticles to be embedded in the coating during the deposition. Fig. 3.1 (b) shows the SEM of dry un-sonicated agglomerates of alumina powder

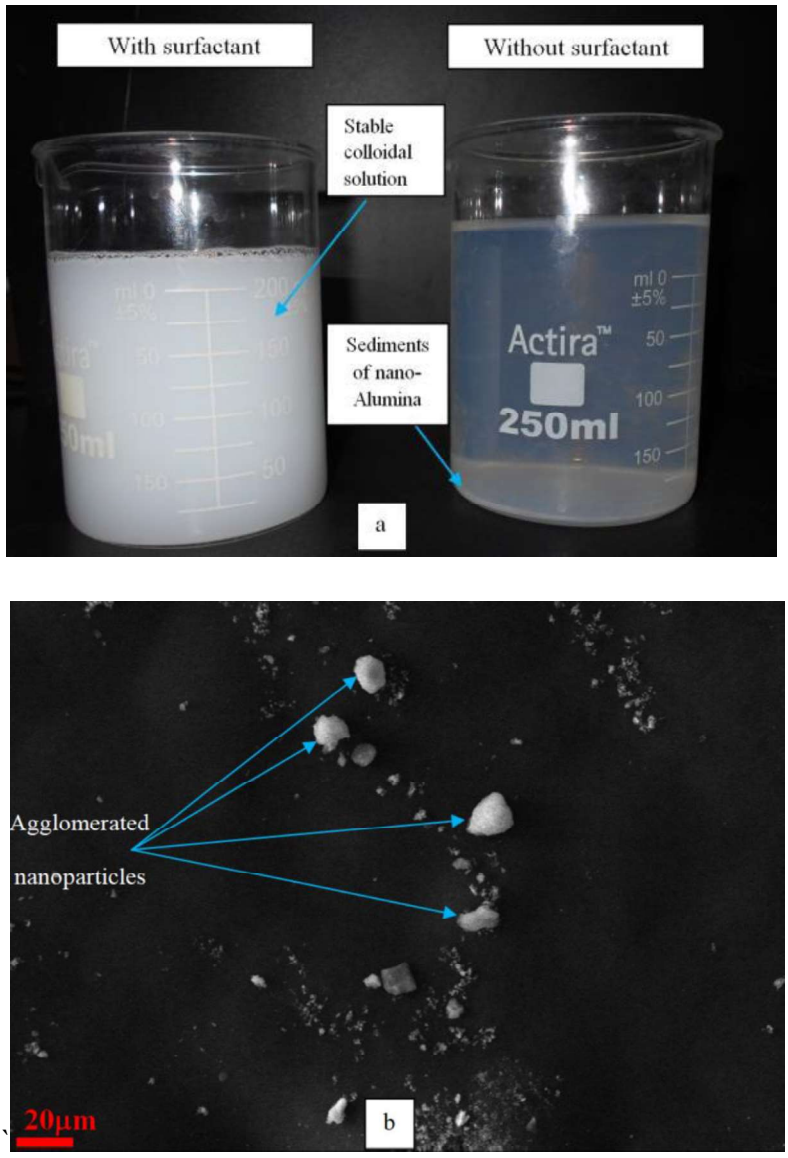

Fig. 3.1: (a) Image of a colloidal suspension of alumina particles after allowing it to settle for 4 hrs, in presence and absence of sodium dodecyl sulphate (SDS); (b) SEM image of nano Al_2O_3 agglomerates.

Zeta potential is the surface potential of the nanoparticles relative to the boundary of the diffused layer when the particle is in suspension. Any nanoparticle in suspension

with a surface charge tends to form a double layer by attracting oppositely charged ions towards its surface. Fig.3.2 shows the schematic diagram of a typical nanoparticle with a negative surface charge. It attracts positive ions which get attached, in a dense packing, adjacent to the surface. This layer is known as the stern layer. The stern layer is followed by the diffused layer, with loosely held ions. The zeta potential is the electrokinetic potential difference between the slipping plane and the particle surface. The slipping plane is the boundary between the outer diffused layer and the particle surface. The outer diffused layer is a region of ions that are attracted to the particle surface. The zeta potential is important because it determines the stability of a colloidal dispersion (International Standardization Organization (2012)). Several researchers have determined the stability of colloidal solutions using the Zeta potential as a standard (Jiang et al., 2009; Lu and Gao, 2010). In general, a zeta potential value of ± 40 to ± 60 of a suspension is considered as having good stability. A value of ± 30 to ± 40 is considered to represent a colloidal suspension of moderate stability (Freitas and Müller, 1998; Hunter, 2013; Shah et al., 2014; Kumar and Dixit, 2017). A zeta potential value in the range of ± 10 to ± 30 is considered as representing a suspension with insipient stability and any value below this range i.e.: 0 to ± 10 causes flocculation in the suspension and results in the sedimentation of the submerged particles.

A surfactant comes in handy in situations where the suspended particles need to remain suspended for a long duration, which is a requirement of electroless coating. The presence of surfactant also improves the wettability of the particles (Maestro et al., 2015). The surfactants are adsorbed onto the solid particulate surface and provide an overall charge to the engulfed particles. As a result, all particles of similar nature tend to possess like charges of finite magnitude on their periphery. This causes repulsion of like particles and prevents flocculation. Thus, the suspended particles do not coagulate and remain suspended for a longer duration of time. Fig. 3.3 shows a schematic diagram of a lone alumina particle surrounded by surfactants that impart a net charge on to the surface. Fig. 3.4 shows the measure of zeta potential of nano alumina of varying concentrations at a pH of 12, which is the solution bath pH of the coatings under study. The zeta potential was measured in the presence and absence of surfactants. The surfactant used is Sodium Dodecyl Sulphate (SDS), anionic surfactant. It was observed that the zeta potential value

changed from a moderate stability solution potential to a good stability solution potential. This is attributed to the ability of the surfactant to wet solid surfaces as well as its ability to impart a net charge (in the present case, a negative charge) to the particles.

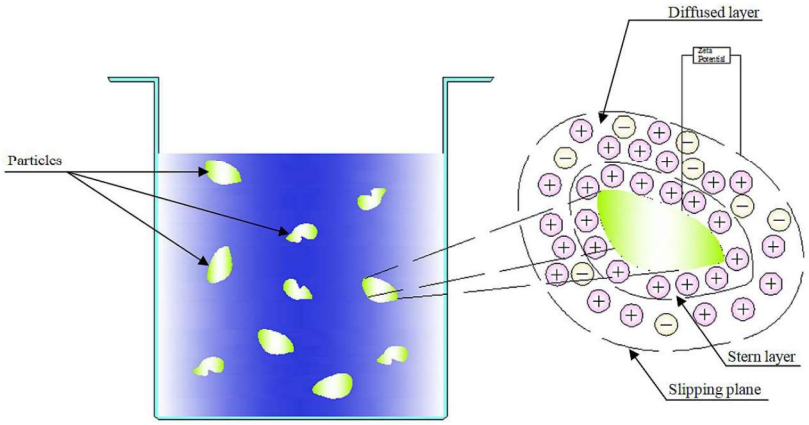

Fig.3.2: Schematic drawing showing a typical suspended particle surrounded by ions forming the basis for zeta potential measurement

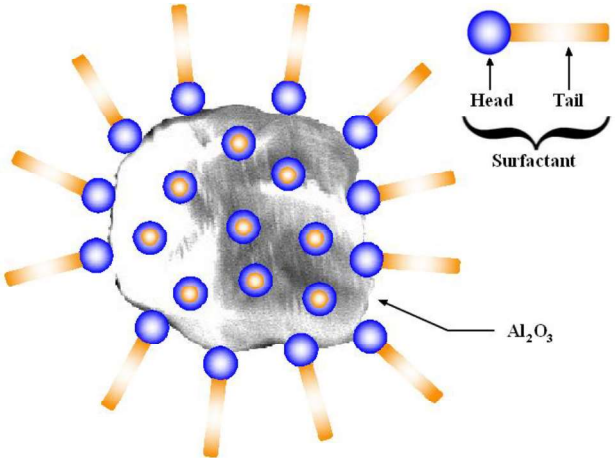

Fig. 3.3: Schematic diagram of lone alumina particle surrounded by surfactant

The zeta potential value drops beyond alumina wt % of 10. With the increase of the wt % of alumina to 15 % the zeta potential value significantly decreased from a good stability zone (-52 mV) to a moderately stable zone (-39 mV), for the solution with surfactant. The solution without surfactant also shows a similar trend. This could be due to the agglomeration of nanoparticles. These nanoparticles owing to their high surface charge tend to agglomerate if there is a high concentration of such particles in the solution. In the

present case, beyond 10 wt % of alumina, nanoparticles are unable to stay suspended in the solution, at a pH of 12.

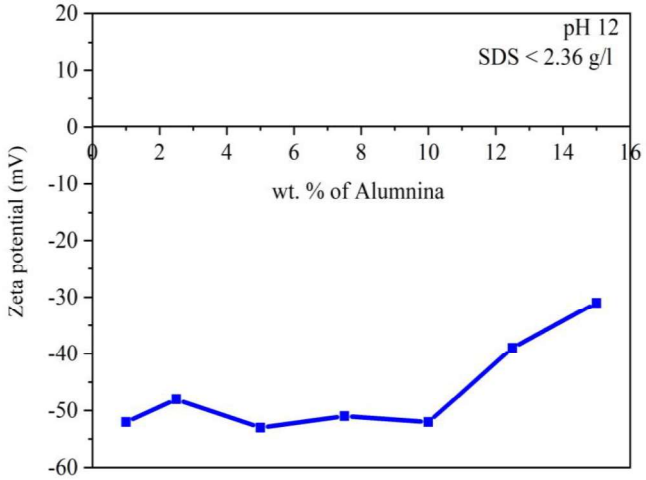

Fig. 3.4: Variation of zeta potential with alumina wt % in a solution of pH 12

3.3.2 Coating morphology

The coating morphology is identical to cauliflower-like nodules spread throughout the surface. Various literature hints at the fact that the size of these nodules may have a bearing on the hardness and wear resistance. Fig. 3.5 (a) to Fig. 3.5 (f) show typical nodular microstructure which is a characteristic feature of electroless coatings. Fig. 3.5 (a) for Ni-B binary coating shows larger nodules as compared to reinforced coatings shown in Fig. 3.5 (b) to Fig. 3.5 (f).

Table 3.1: Coating bath composition

Sl.No.	Chemical	Manufacturer	Function	Amount in bath
1.	Nickel chloride	Merck (US)	Nickel source	18-20g/l
2.	Ethylene diamine	Merck (US)	Complexing agent	45-50 ml/l
3.	Lead nitrate	Merck (US)	Stabilizer	0.05-0.06 g/l
4.	Sodium hydroxide	Merck (US)	Maintains pH	35-40 g/l
5.	Sodium borohydride	Merck (US)	Reducing agent	0.5 g/l
6.	Nano alumina	SRL Chem (India)	Reinforcement	Varying amount
7.	SDS	SRL Chem (India)	Surfactant	2.36 gm

* The bath temperature was maintained at 85°C ± 3.

Table 3.2: Coating nomenclature

Sl. No.	Description of the coating	Nomenclature
1.	Ni-B binary coating	Ni-B
2.	Ni-B + 2.5 wt % nano alumina	Ni-B-2.5
3.	Ni-B + 5 wt % nano alumina	Ni-B-5
4.	Ni-B + 7.5 wt % nano alumina	Ni-B-7.5
5.	Ni-B + 10 wt % nano alumina	Ni-B-10
6.	Ni-B + 12.5 wt % nano alumina	Ni-B-12.5

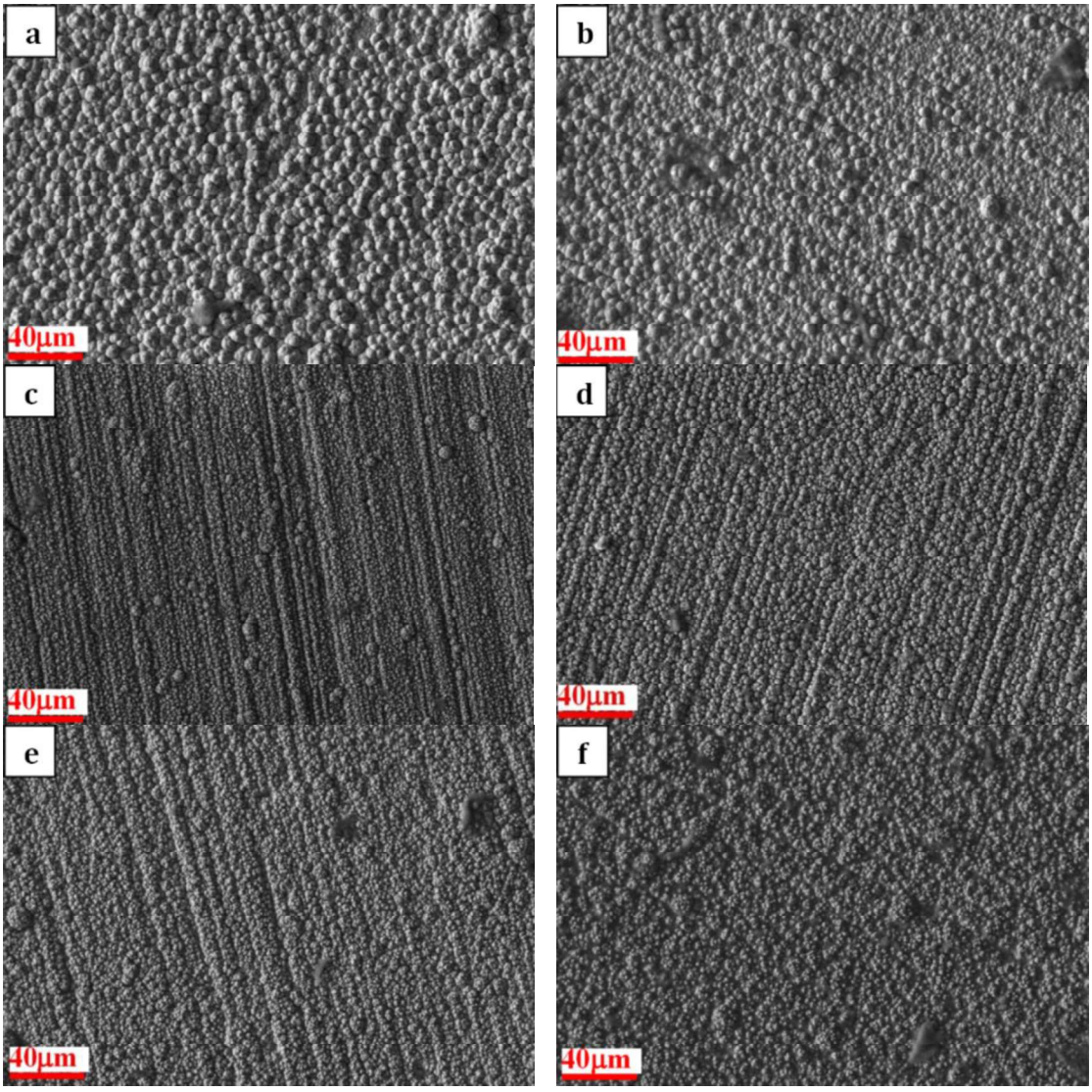

Fig. 3.5: Nodular microstructure of (a) Ni-B, (b) Ni-B-2.5, (c) Ni-B-5, (d) Ni-B-7.5, (e) Ni-B-10 and (f) Ni-B-12.5

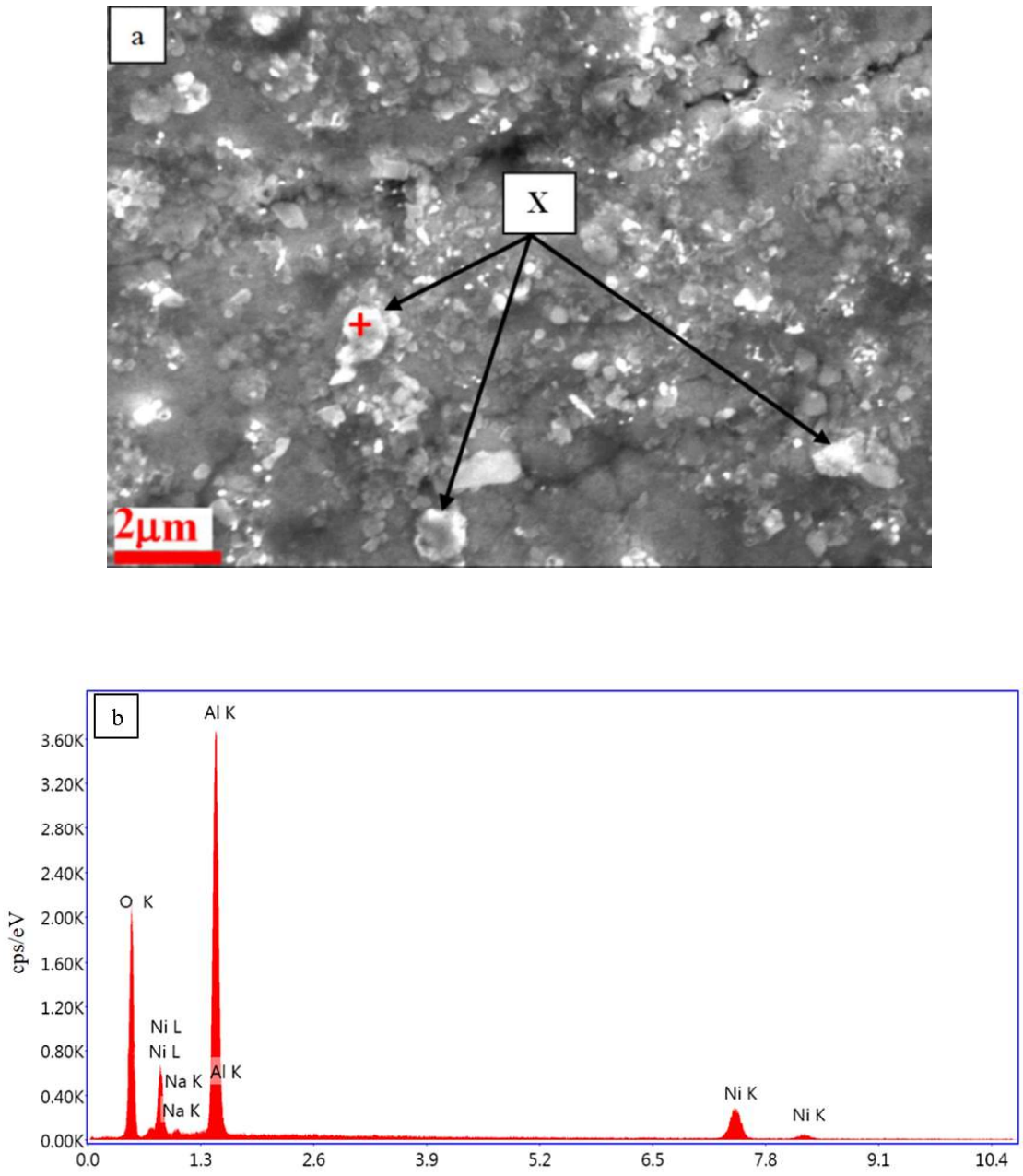

Fig. 3.6: (a) SEM image of the subsurface region of the Ni-B-10 coating, (b) point EDX of the coating surface (marked by '+')

The decrease in size of the nodular structure may be due to the structural refinement brought about by the inclusion of alumina nanoparticles. Although no clear trend in the nodular size could be established among the reinforced coatings, it may be concluded that as compared to the binary Ni-B coating the reinforced coatings show a more refined nodule.

Fig. 3.6 (a) shows agglomerated alumina nanoparticles perched on the coating surface partially or completely covering the nodular gaps. Several patches of agglomerated alumina nanoparticles (denoted by X in Fig. 3.6 (a)) can be seen blanketing the nodular gaps partially or fully. This forms an impermeable layer of Ni-B matrix and nano-alumina reinforcement protecting the substrate. (Ernst et al., 1997) reported that electroless coatings are dense as the coating grows by nodule overlap. As can be observed from Fig. 3.6 (a) the nanoparticles seem to have embedded themselves in the nodular gaps and micro porosities of the Nickel-Boron matrix. Fig. 3.6 (b) depicts the EDX map of the Ni-B-10 coating subsurface. Prominent Aluminium K-α peaks can be observed in the EDX pattern. The presence of sodium is due to the addition of sodium hydroxide and Sodium borohydride in the bath during the coating process.

3.3.3 Raman spectroscopy

Fig. 3.7 depicts the Raman spectroscopy of the coated samples. The peaks signify the presence of a stable α-Al_2O_3 and not the γ-Al_2O_3. According to Laha et al. (2005), the γ-Al_2O_3 does not show any visible peak in the Raman spectrum. The band at 539 cm^{-1} shows the characteristic peaks of α-Al_2O_3, while the bands at 321 cm^{-1} and 306 cm^{-1} show the spectrum corresponding to $Al(OH)_3$ (Ruan et al., 2001). This is quite possible as the electroless deposition is performed in a solution with deionised water as the solvent. The coating bath temperature is maintained at around 85 °C. This facilitates the chemical bonding of alumina with water and results in the formation of the hydroxide. The band at 539 $cm^{-1}$and 446 cm^{-1} correspond to Al-O-Al distortion and the ones at 321 cm^{-1} and 306 cm^{-1} are caused by stretched vibrations due to the formation of Al-O bonding (Ruan et al., 2001). Raman data is significant to the study because due to the low percentage of adsorption of alumina into the coating, it often becomes difficult to identify the alumina peaks by the X-Ray diffraction method.

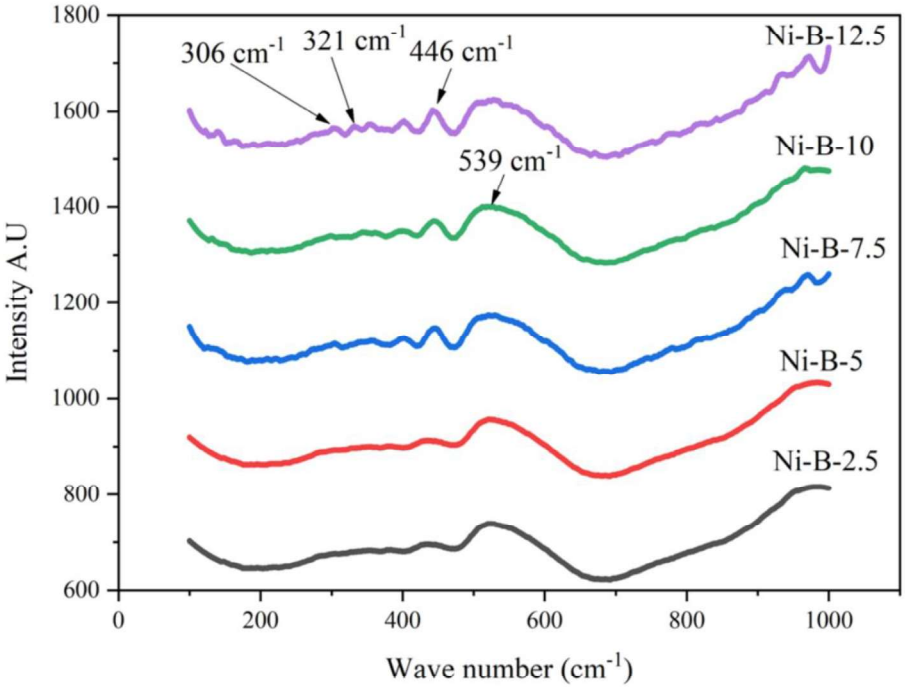

Fig. 3.7: Raman spectrum of the coated specimens

3.3.4 X-Ray Diffraction

The diffraction pattern analysis of the coatings reinforced with alumina is shown in Fig. 3.8. XRD helps to identify the nature of as-deposited coatings. The characteristic Ni peak is identified at 2θ value of around 45° for all the coatings (Vitry et al., 2012). The broad peak identified indicates an amorphous nature of the coating. Although as reported by Delaunois and Lienard (2002), the structure is often found to be a mixture of crystalline and amorphous structures. Dervos et al. (2004) and Ziyuan et al. (2006), also supported the presence of the mixed structure in electroless coatings. The identification of boron tends to be difficult via XRD because of the low solubility of boron in solid nickel (0.03 wt %) (Ziyuan et al., 2006). The boron is often identified in the form of some Ni-B inter-metallic as Ni_3B and Ni_2B when the coatings are subjected to heat treatment (Hamid et al., 2010). It can be deduced from the XRD pattern that the addition of alumina does not affect the structure of the coating although it may change the morphology of the coatings (from coarser to finer nodules) (Hu et al., 2018).

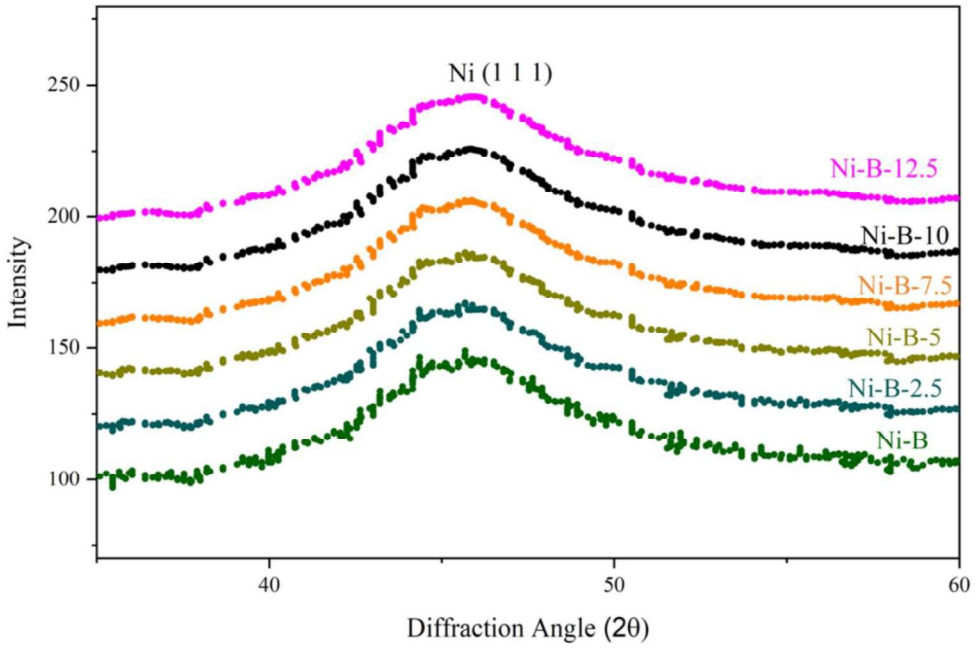

Fig. 3.8: X-Ray diffraction of the specimens under study

3.3.5 Micro Vicker's hardness and elastic modulus

Fig. 3.9 shows the hardness values obtained for the coatings. With the addition of nano Al_2O_3, the hardness increases as expected. This is attributed to the desired hard nanoparticle inclusion, which when embedded in the softer Ni-B matrix, transfers the applied load from the matrix to the reinforcements (nano Al_2O_3). This sharing of load causes a hardness value. Further, these nanoparticles obstruct the flow of material. When a load is being applied during hardness test this also helps to restrict the size of indentation as a result a higher value of hardness is obtained. Although the hardness improves with the addition of nanoparticles it should be noted that the standard deviation of the hardness values for the coating Ni-B-12.5 is much higher than the other coatings as indicated by the error bars. This fluctuation in hardness values is a result of the inhomogeneous distribution of nano-Al_2O_3 powders in the case of the Ni-B-12.5 coating caused by the higher degree of agglomeration of alumina beyond a concentration of 10 g/l. Fig 3.10 represents the elastic modulus in graphical format. The elastic modulus increases with the addition of nano-particles. It can be seen that unlike the hardness a clear trend is not observed for the elastic modulus values. The elastic modulus (E) increases from 75.9 GPa for binary Ni-B

to 122.9 GPa for the reinforced Ni-B-10 coating. This may be due to the dispersion strengthening resulting from the addition of nanoparticles (Sarbishei et al., 2016; Mahdavi et al., 2020).

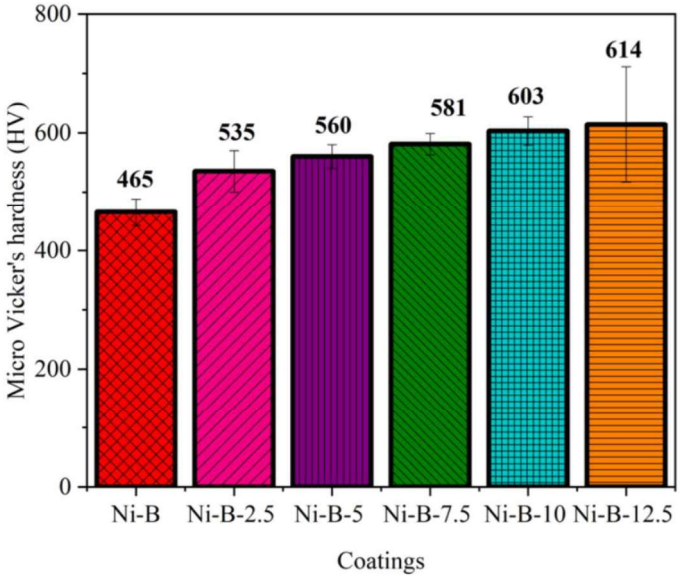

Fig.3.9: Micro Vicker's hardness of coatings taken at 100 gf load

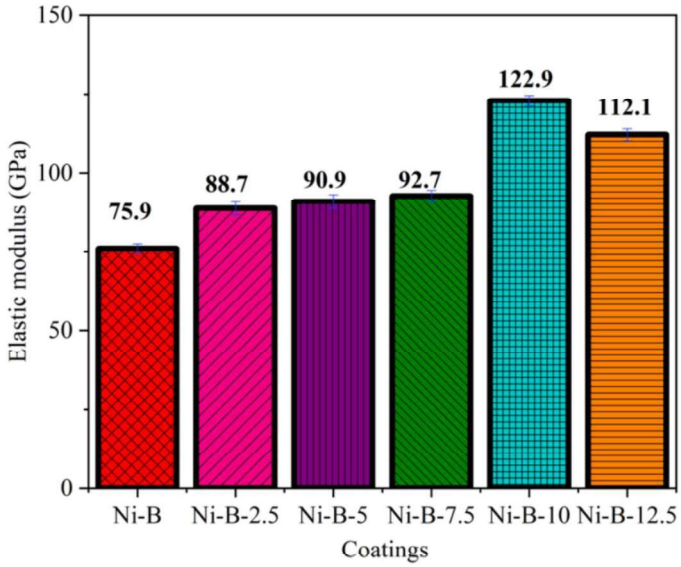

Fig. 3.10: Elastic modulus of the coatings obtained at a loading-unloading rate of 20mN/min

Fig. 3.11 shows the loading/unloading curve for the variation of normal force against the applied depth of penetration of the indenter. The curve is obtained by employing

the depth method. In this method, the load is allowed to vary up to a maximum depth of 500 nm and once the maximum depth is reached the load is released. The loading and unloading rates were maintained at 20 mN/min. The pattern of the curves obtained is quite similar to one another. The area under each curve represents the energy absorbed by the respective coating to reach the desired penetration depth of 500 nm. The loading-unloading curve for Ni-B-10 coating encompasses the largest area among the coatings. This is also corroborated by its elastic modulus value of 122.9 GPa which is the largest for the coatings reinforced with nano alumina.

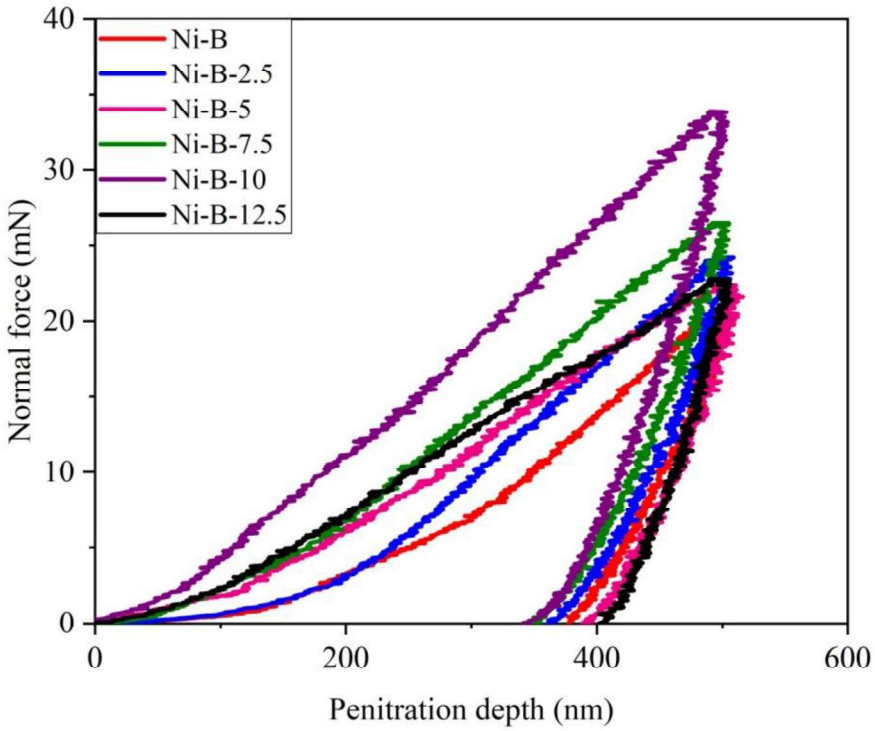

Fig. 3.11: Loading and unloading curve showing the variation of normal force with the penetration depth

It must be noted that although the percentage addition of alumina in the coating bath of Ni-B-12.5 is more (12.5 g/l) as compared to Ni-B-10 coating, still the resulting elastic modulus is less as compared to Ni-B-10. In the present case, due to the excessive agglomeration of alumina (beyond 10g/l concentration), proper inclusion and uniform distribution of alumina may not be achieved in the Ni-B-12.5 coatings, as a result, lower dispersion

strength and a lower elastic modulus are obtained. It should be mentioned here that more alumina in the coating bath does not necessarily mean more absorption of alumina in the coating. The adsorption of alumina depends on the degree of agglomeration and sedimentation of the colloidal solution.

3.3.6 Scratch resistance

Fig. 3.12 (a) and (b) display the optical images of surface scratches on two types of coatings: as-deposited binary Ni-B and as-deposited Ni-B-10 g, respectively.

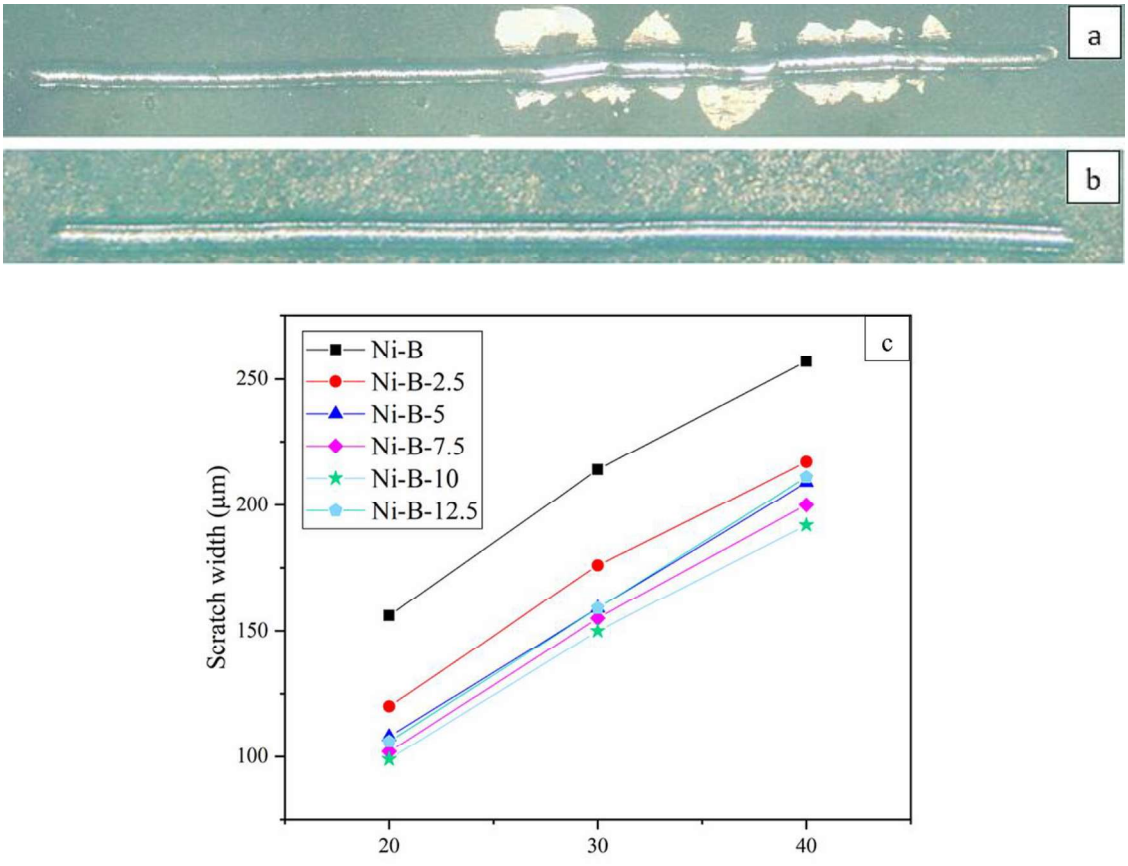

Fig. 3.12: Scratch on binary (a) Ni-B, (b) scratch on Ni-B-10 and (c) scratch width of Ni-B and alumina reinforced coatings

The hardness of the scratch is inversely proportional to the square of its width, as indicated by equation (2.5). Therefore, a narrower scratch width corresponds to a higher scratch hardness. In Fig. 3.12 (a), the as-deposited Nickel-Boron coating exhibits a peel-off

phenomenon, identifiable by a bright white patch. However, this peel-off is not observed in the Ni-B-10 coating shown in Figure 3.12 (b). Nano inclusions present within the subsurface of the coatings play a significant role in acting as load-bearing elements in composite electroless Ni-B coatings. They contribute to the distribution of the applied load, enabling effective dissipation of energy resulting from the penetration and movement of the diamond indenter during the scratching process. Conversely, the absence of nanoparticles in the as-deposited Ni-B coatings hinder the facilitation of load transfer. Consequently, the energy generated by the applied load remains concentrated in the surrounding area. This concentrated energy causes the coating to peel off, releasing the excess localized energy. In Figure 3.12 (c), the measurement of scratch width in the reinforced Ni-B-10 coatings demonstrates a notable improvement compared to the as-deposited binary Ni-B coating. This indicates that the incorporation of TiO_2 nanoparticles enhances scratch hardness up to an alumina concentration of 10 g/l and mitigates the occurrence of peel-off.

3.3.7 Wear and friction behaviour

The coatings under study were subjected to a dry sliding wear test at loads of 1 Kgf and 2 Kgf and a sliding speed of 100 rpm. The specific wear rates at these loads are shown in Fig. 3.13 (a) and 3.13 (b). These figures show that with the increase in the amount of reinforcement (nano alumina) from 0 g/l to 10 g/l in the coating bath, the wear resistance of the coatings also increases. This is due to the increase in the percentage inclusion of hard nanoparticles in the coating. The hard alumina nanoparticles when embedded in the softer Ni-B matrix obstruct the sliding motion and do not allow the interacting coating surface to be removed easily. The corresponding data for the variation in frictional force is shown in Fig. 3.14. Here the increase in frictional force along with the addition of nanoparticles is evident. However, there seems to be a break in trend at 12.5 g/l of alumina in addition to the coating. At points, ‘a’ and ‘b’ in Fig. 3.14 sudden drop in frictional force is visible for coating reinforced with 12.5 g/l alumina. This may be due to the pluck-out of patches of nanoparticles from the coating surface.

This makes the coatings weak and subsequent removal of the coating layer occurs at certain instances. The alumina patches are formed as a result of excessive agglomeration. As discussed earlier, beyond 10 g/l concentration the agglomeration of alumina becomes severe which is detrimental to the stability of the colloidal solution and the suspension stability of nano alumina in the coating bath. Also, there are instantaneous spikes in frictional force at certain points as seen in Fig. 3.14. This is more evident in the case of the coatings with a higher concentration of nanoparticles (10 g/l and 12.5 g/l). This may be attributed to the three-body abrasion caused due to the reattachment of the plucked-out nanoparticles back into the softer matrix of the specimen surface. Fig. 3.15 shows the coefficient of friction of the binary Ni-B and the various alumina reinforced Ni-B coatings. The coefficient of friction increases with the addition of nanoparticles as these are hard and irregular shaped particles and thus increase the friction coefficient of the interacting pair (coating surface and the counter disk). But for the coating Ni-B-12.5 the coefficient of friction decreases due to the high concentration of alumina in the solution bath that renders the colloidal solution is unstable. This unstable solution results in agglomeration of the alumina particles and sedimentation. Hence the effective concentration of nanoparticles decreases in the coating and in turn the coefficient of friction also decreases.

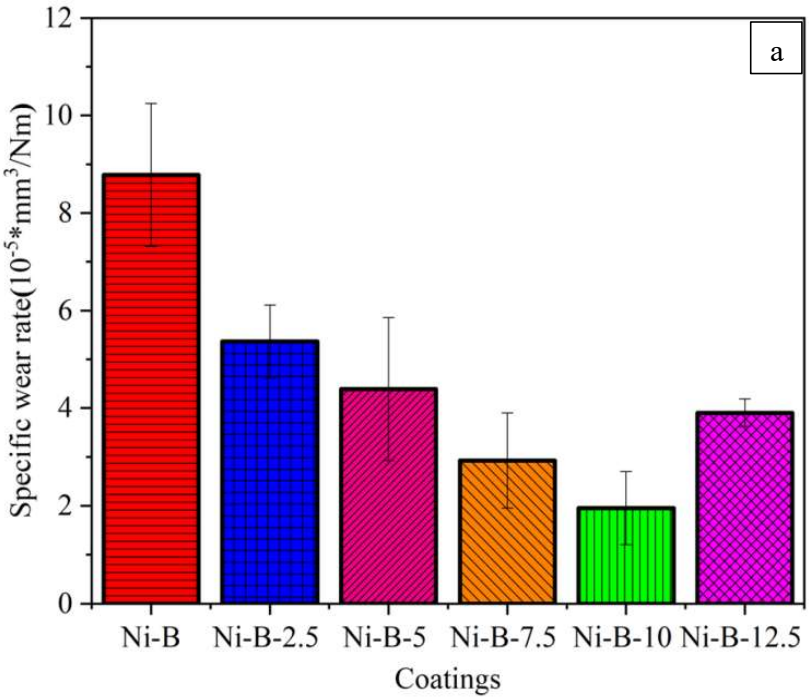

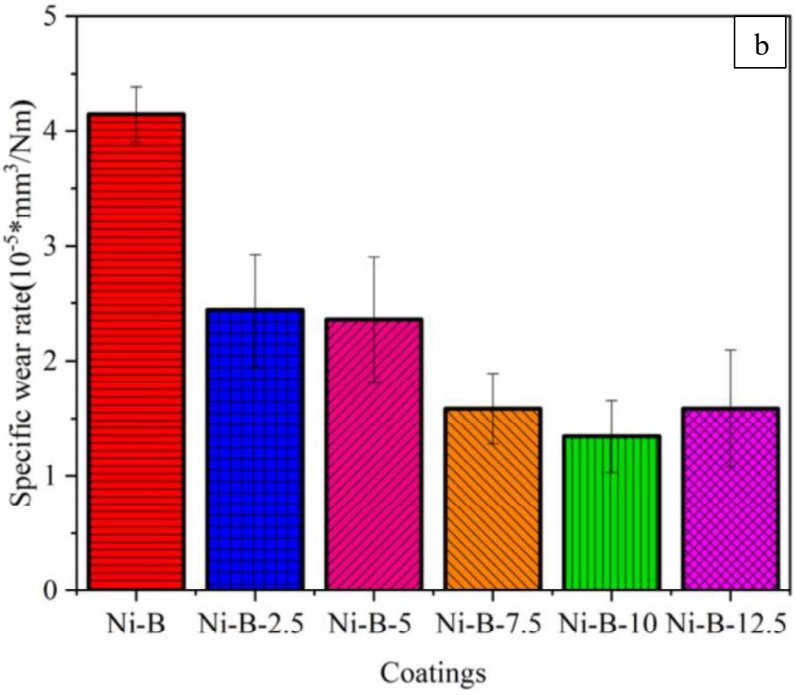

Fig. 3.13: Specific wear rate of the specimen under a load of (a) 1 kgf and (b) 2 kgf

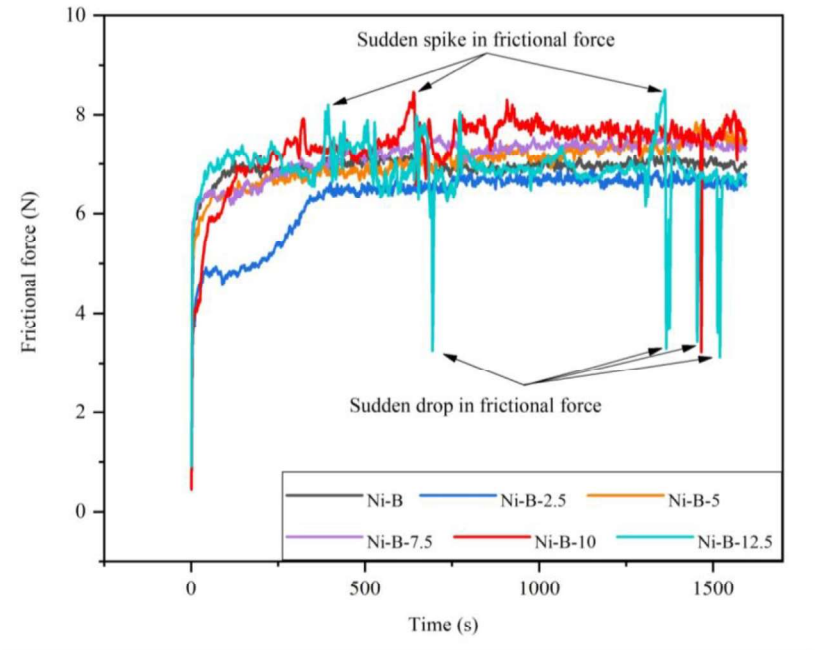

Fig. 3.14: Variation of frictional force with time for the coatings under study

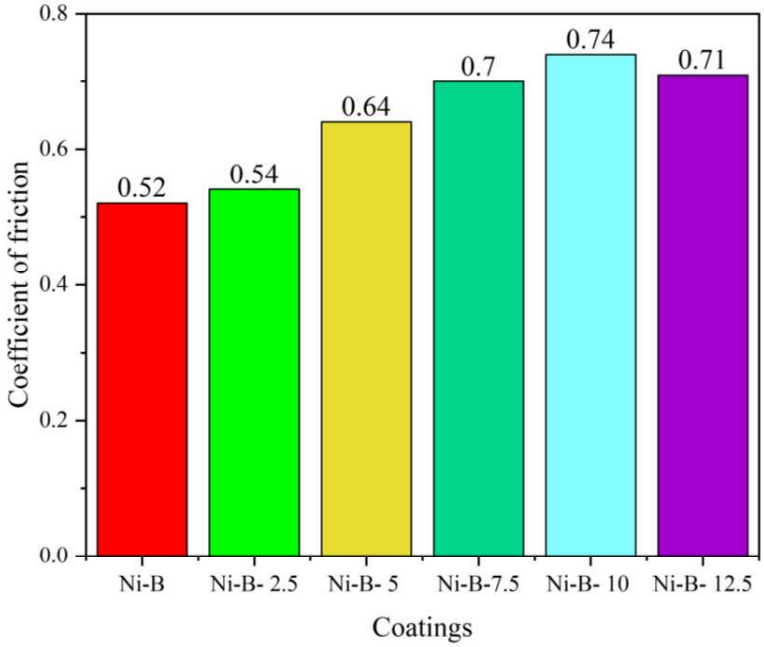

Fig. 3.15: Coefficient of friction for the coatings under study

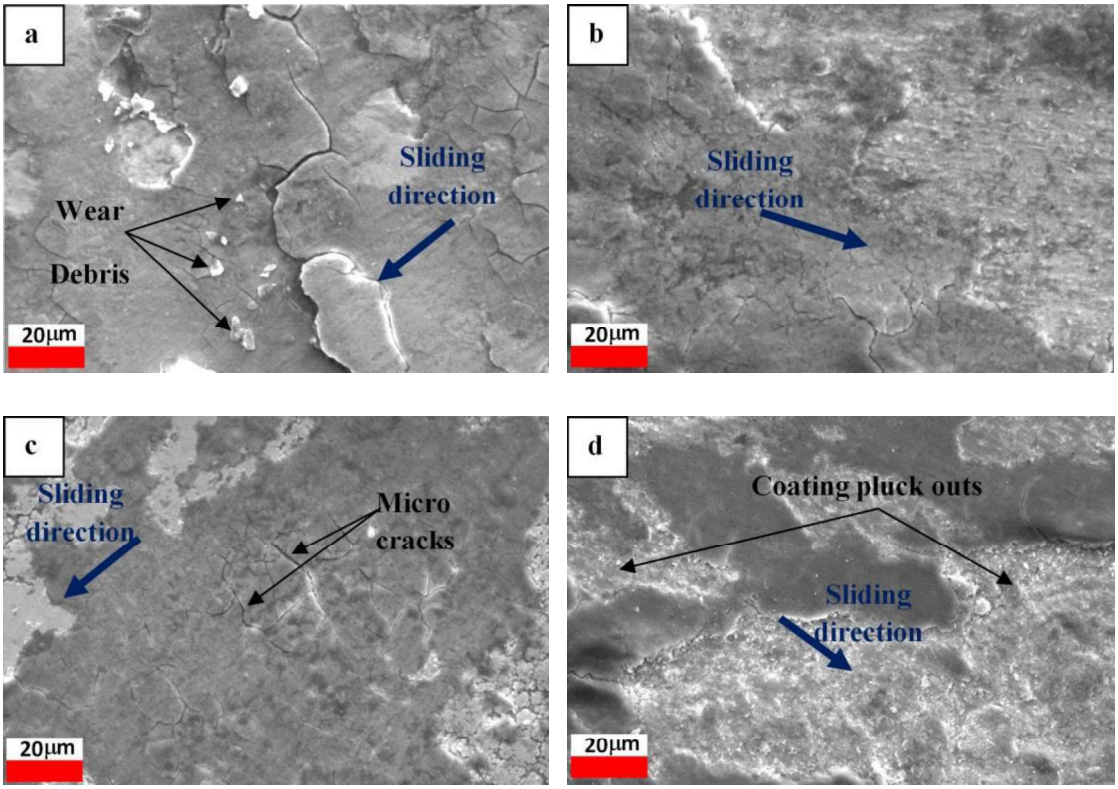

Fig. 3.16: Wear morphology of (a) Ni-B, (b) Ni-B-5, (c) Ni-B-10 and (d) Ni-B-12.5

Fig. 3.16 shows the worn surface of the coatings. A similar mechanism can be observed in all the coatings. A combination of abrasive and adhesive wear seems to be the dominating wear phenomenon (Gawne and Ma, 1987; Correa et al., 2013). Fig. 3.16 also shows micro-cracks and pluck out of worn patches due to the sliding motion and interaction of the coatings with the hard EN 31 counterpart.

3.3.8 Corrosion

Fig. 3.17 shows the Tafel curves for the coatings under study. Electroless coatings are highly corrosion resistant. These coatings do not act as sacrificial layers instead they form a noble and almost impervious layer upon the substrate. Thus obstruct the substrate from coming directly in contact with the corrosive environment. To achieve this, the coatings need to be non-porous.

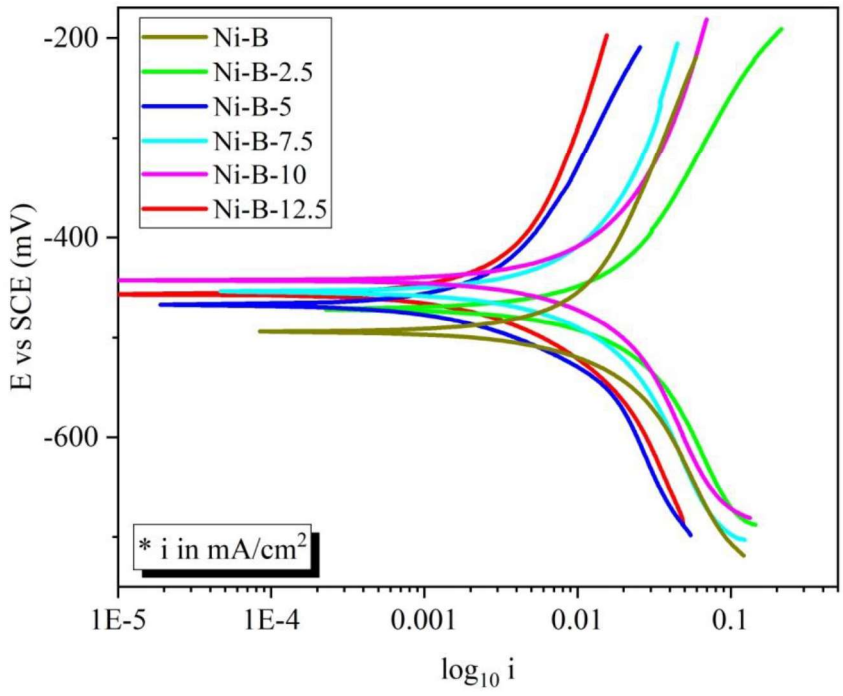

Fig. 3.17: Tafel curves (Anodic and cathodic) for the coatings under investigation

An added advantage of these coatings is the absence of any grain boundaries that act as inherent sites for excessive corrosion (Sha et al., 2011). Hamid et al., (2010)

discussed the detrimental effect that heat treatment has on the electrochemical corrosion resistance of the EN coatings. They found that although heat treated coatings show improved surface micro-hardness and increased sliding wear resistance but due to warping of the coatings, heat treatment tends to decrease the corrosion resistance. The improved micro-hardness and wear resistance is attributed to the formation of hard inter-metallic phases like Ni_3B and Ni_2B and also the transformation of coatings to a more or less crystalline structure from an amorphous structure of the as-deposited coatings. A high temperature of 800 °C and above tends to cause severe flaking due to the decrease in adhesion of these coatings with the underlying substrate layer (Biswas et al., 2017). Hence, for optimal design, parity has to be maintained between the mechanical properties and corrosion behavior of these coatings.

Table 3.3 shows the corrosion potential and current for the coatings. The corrosion current increases along with the incorporation of alumina nanoparticles until the Ni-B-10 but start to decline as the amount of alumina is further increased in the bath. This may be attributed to the agglomeration of nanoparticles which reduces the effective surface covered by the nanoparticles as compared to the case when they are more or less dispersed (as is for the coatings with a lower amount of alumina addition).

The best performing coating among the alumina reinforced coatings as per corrosion protection is Ni-B-10 because, with the further addition of alumina (12.5 g/l) to the coating bath, the colloidal solution tends to display insipient stability as shown by the zeta potential value in Fig. 3.4. The E_{corr} value increases from -494.54 mV (binary Ni-B coating) to a nobler (more positive value) value of -421.02 mV for the Ni-B-10 coating. This shift of corrosion potential is also an indicator of the improved corrosion resistance of the Ni-B-10 coating. Although researchers argue that I_{corr} value provides a better representation of the electrochemical corrosion behavior of surfaces, in the present research in addition to the corrosion current the corrosion potential also follows a similar trend. This is strong evidence in favor of the improved corrosion potential of the reinforced specimens. As observed from Table 3.3, E_{corr} value suggests a decreased performance of Ni-B-12.5 coating against the 3.5 % NaCl solution used as the corrosive environment.

Table 3.3: Corrosion potential and current for the coatings under study

Sl.No.	Specimen	E_{corr} (mV)	I_{corr} (mA/cm^2)
1	Ni-B	- 494.54	0.01126
2	Ni-B-2.5	- 471	0.01103
3	Ni-B-5	- 467.64	0.009
4	Ni-B-7.5	- 458.08	0.004
5	Ni-B-10	- 421.02	0.0026
6	Ni-B-12.5	- 456.83	0.0092

3.4 Closure

In the present chapter, the study conducted determined the influence of the addition of alumina nanoparticles on the microhardness, elastic modulus, wear resistance and the electrochemical response of the coatings. The improvement in the properties was brought about by the dual effect of improved hardness and refinement of the nodular morphology of the coatings. In this chapter as observed, Ni-B-10 coating shows the most balanced response to the mechanical, tribological and corrosion-resistant properties. With the increase in the concentration of alumina nanoparticles to 12.5 g/l, the wear resistance, elastic modulus and corrosion resistance decrease. Hence, amongst the alumina reinforced coatings under study the Ni-B-10 coating seems to be the most appropriate to use where coatings with low wear and high corrosion resistance are required.

Chapter 4: Nano-Titania reinforced electroless Ni-B coatings

Outline: *4.1. Introduction, 4.2 Experimental details, 4.3 Results and discussion, 4.3.1 Coating morphology, 4.3.2 X-Ray Diffraction, 4.3.3 Micro Vicker's hardness and elastic modulus, 4.3.4 Scratch resistance, 4.3.5 Wear and friction behaviour 4.3.6 Corrosion, 4.4 Closure*

4.1 Introduction

Titania nanoparticles or titanium dioxide (TiO_2) are widely used inclusions in bulk composite materials and composite coatings. These have applications in various industries such as cosmetics, paper, paint, and electronics, among others. TiO_2 is highly valued for its excellent properties such as high refractive index, chemical stability, low toxicity, and photocatalytic activity, making it useful for various applications. As nanoparticles, TiO_2 has even more attractive properties, such as unique optical and electronic properties, higher reactivity and increased surface area. One of the most important applications of TiO_2 nanoparticles is in the field of photocatalysis, where they are used to degrade pollutants and organic matter in air and water. They are also used as UV filters in sunscreens and other personal care products, and as whitening agents in food, cosmetics, and other applications.

In the present study the characterization and tribomechanical behavior of TiO_2 incorporated Ni-B coatings are investigated. The hardness and mechanical properties are expected to improve as per the evidence collected from the literature. In order to, analyze the coating they are subjected to couple of characterization techninques and mechanical testing methods. These include EDAX SEM, XRD, tribo test, nanoindentation test, hardness test and corrosion response of the coatings.

4.2 Experimental details

The following sections show the various characterization studies and mechanical property evaluation of the Ni-B-TiO_2 (nano) samples. The coating nomenclature is given

below.

Table 4.1: Coating Nomenclature

Sl. No.	Coating description	Nomenclature
1.	Nickel-Boron binary coating	Ni-B
2.	5 g/l TiO_2 (nano) reinforced electroless Nickel-Boron	Ni-B-5g/l TiO_2
3.	10 g/l TiO_2 (nano) reinforced electroless Nickel-Boron	Ni-B-10g/l TiO_2
4.	15 g/l TiO_2 (nano) reinforced electroless Nickel-Boron	Ni-B-15g/l TiO_2

In the present investigation, four different coatings were prepared which include the as-deposited Ni-B and the composite ternary coatings prepared with varying quantities of TiO_2 as shown in Table 4.1. Mild steel substrates having a length and breadth of 15 mm * 15 mm and thickness of 2mm were coated and used for the characterization and hardness tests. Cylindrical specimens of diameter 6 mm and length 30 mm are deposited to study the wear behaviour of the coatings. In order to get a fine surface finish, these specimen surfaces were polished using abrasive papers of varying grades. Table 4.2 provides the main bath constituents utilized for depositing the coatings. The details of the equipment used and their specifications are provided in the Chapter 2.

Table 4.2: Coating bath composition for Ni-B-TiO_2

Sl. No.	Chemicals	Role	Amount
1	Nickel chloride hexahydrate	Nickel source	20g/l
2	Lead nitrate	Stabilizer	0.06g/l
3	Sodium hydroxide	Maintain pH	35-40g/l
4	Ethylene diamine	Complexing agent	80-100ml/l
5	Sodium borohydride	Reducing agent	0.2-0.3 g/l
6	Titania	Reinforcements	Varying amount

4.3 Results and discussion

4.3.1 Coating morphology

Fig. 4.1(a) shows the spot EDAX of the point marked as ‘X’. Fig. 4.1 (b) shows the SEM image of the as-deposited coating Ni-B- 10 g/l TiO_2 and the SEM image of Ni-B- 15 g/l TiO_2 coatings is shown in Fig. 4.1 (c). In course of the deposition, the nano Titania particles get lodged into the porosities and voids of the electroless Ni-B matrix, as observed in Fig. 4.1 (b). The rate of deposition of the coatings is given by dividing the coating

thickness with the time of deposition. An hour of deposition resulted in an average coating thickness of around 17-20 µm. The thickness of the coatings is calculated by the equation (2.1). A number of researchers have reported a similar coating thickness for electroless Ni-B coatings (Kaya et al., 2008; Krishnaveni et al., 2012). Using equation 2.1. the coating thickness is calculated.

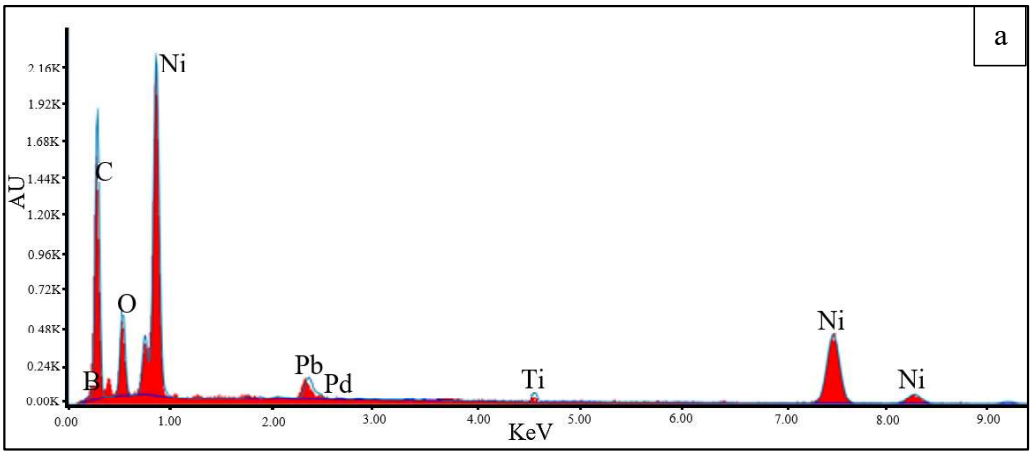

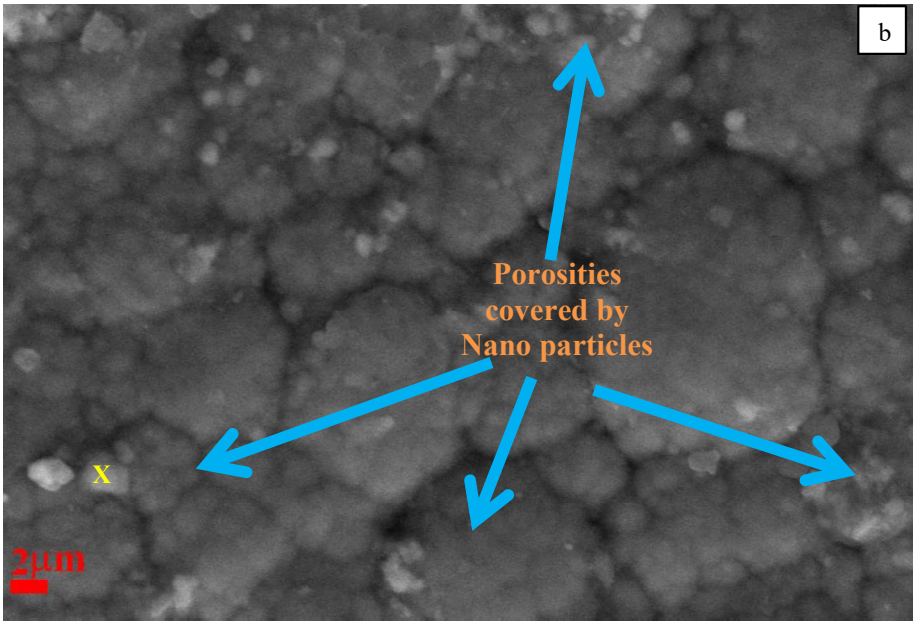

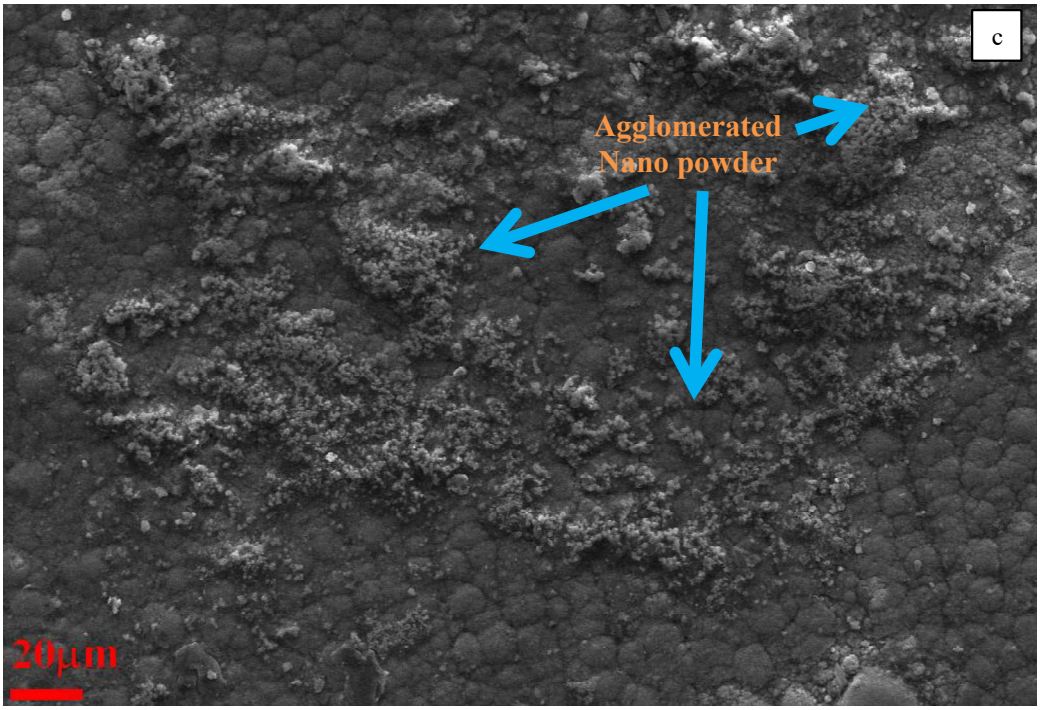

Fig. 4.1: (a) Spot EDAX of Ni-B- 10 g/l TiO_2, SEM image of (b) Ni-B- 10 g/l TiO_2 as deposited (c) Ni-B-15 g/l TiO_2

There was no visible difference in the thickness of the coatings even after the addition of the nanoparticles. This is probably because during Ni-B coating there is a high amount of evolution of hydrogen gas that pushes out the excessive nanoparticles from the matrix. Due to this the actual amount of nanoparticle incorporation is limited. This has been reported by several researchers working with alumina nanopowder (Narayanan and Seshadri, 2001; Krishnaveni et al., 2008; Krishnaveni et al., 2012). In Fig. 4.1 (b), the structure resembling the florets of cauliflower can be observed. This is a characteristic feature of such coatings (Rao et al., 2005). The boron content is often considered to be the factor on which several mechanical properties and the coating microstructure are dependent (Gaevskaya et al., 1996; Anik et al., 2008; Vitry et al., 2011; Vitry et al., 2012).

4.3.2 X-Ray Diffraction

Fig. 4.2 shows the X-Ray diffraction patterns of as-deposited coatings. The as-deposited binary Ni-B coating shows only one broad peak of Nickel at an angle (2θ) of

around 45°. This indicates a purely amorphous nature of the as-deposited Ni-B coatings. With the addition of Titania nanoparticles some crystallinity is observed indicated by sharp peaks in Fig. 2. This mixed nature of the Ni-B XRD patterns is reported in the literature. A number of Ni peaks with varying orientations are seen in the XRD patterns. This crystallinity also affects the mechanical behaviour of the coatings. Boron has low solubility in nickel hence during coating deposition when the boron diffuses distortion occurs in the Ni lattice as a result broad peaks are seen. This distortion decreases because of the addition of nanoparticles; hence a mixture of crystalline and amorphous peaks is observed for TiO_2-reinforced coatings. At angle (2θ) of around 36° Fe-C and at 65° Fe peak is observed. This is due to the substrate material.

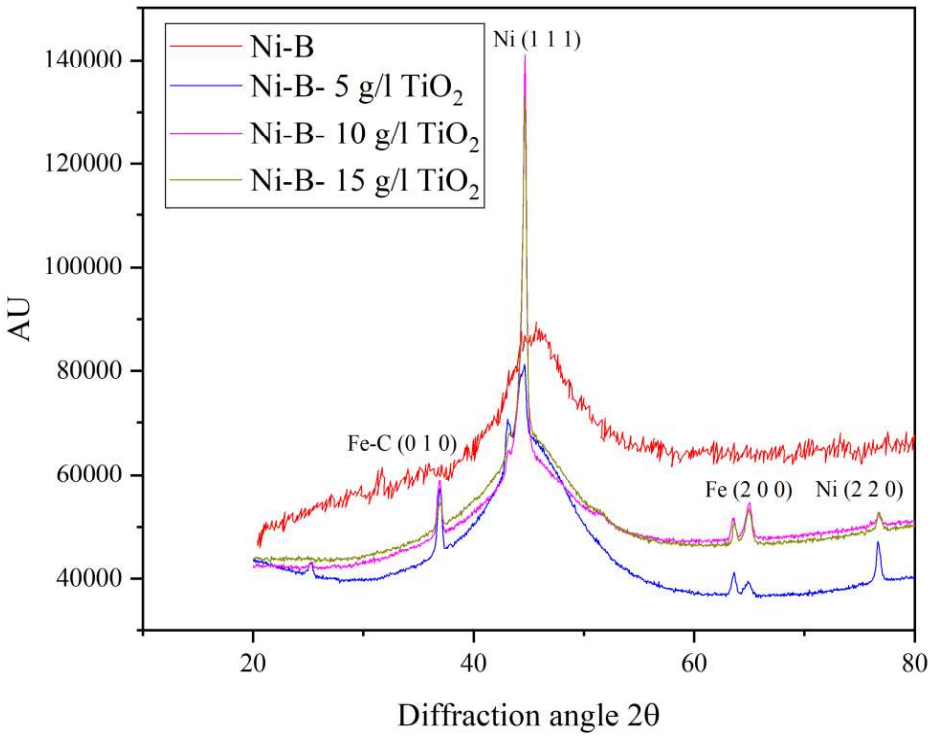

Fig. 4.2: XRD pattern of coatings

4.3.3 Micro Vicker's Hardness and elastic modulus

Fig. 4.3 shows the microhardness of the coatings under study. The microhardness values increase with the addition of nanoparticles. This is attributed to the incorporation of

hard titania nanoparticles in the coatings. The bulk hardness of TiO_2 is around 10 GPa. These hard particles are responsible for the increased average hardness of these reinforced coatings. The nanoparticles have a high surface-to-volume ratio hence the nanoparticles surface interaction with the matrix is high. Due to this interaction, the nanoparticles act as a load-bearing member in the composite coatings. Thus, the mechanical properties of the coatings are significantly improved. The hardness increases from 465 HV of binary Ni-B to a maximum value of 580 HV for Ni-B- 10 g/l TiO_2. An increase of around 25 % is observed for the coatings.

This trend of increasing hardness is seen up to Ni-B- 10 g/l TiO_2 coating. A further increase of nano TiO_2 concentration in the coating results in decreased hardness due to the agglomeration of these nanoparticles at higher concentrations, hence the nanoparticles are perched on the surface instead of getting embedded in the Nickel-Boron matrix. The evidence of excessive agglomeration is seen in Fig. 4.1 (c). Also, from the same figure the distribution of nanoparticles is found to be uneven and this results in the erratic nature of various mechanical properties.

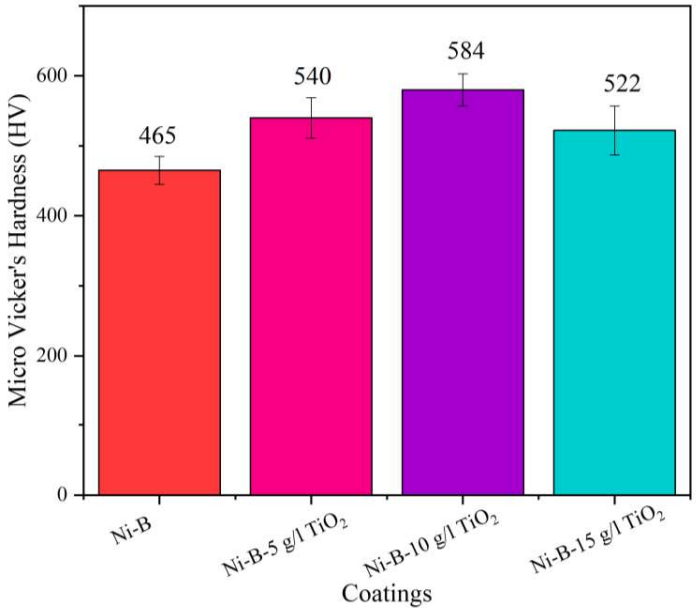

Fig. 4.3: Micro Vicker's hardness of coatings

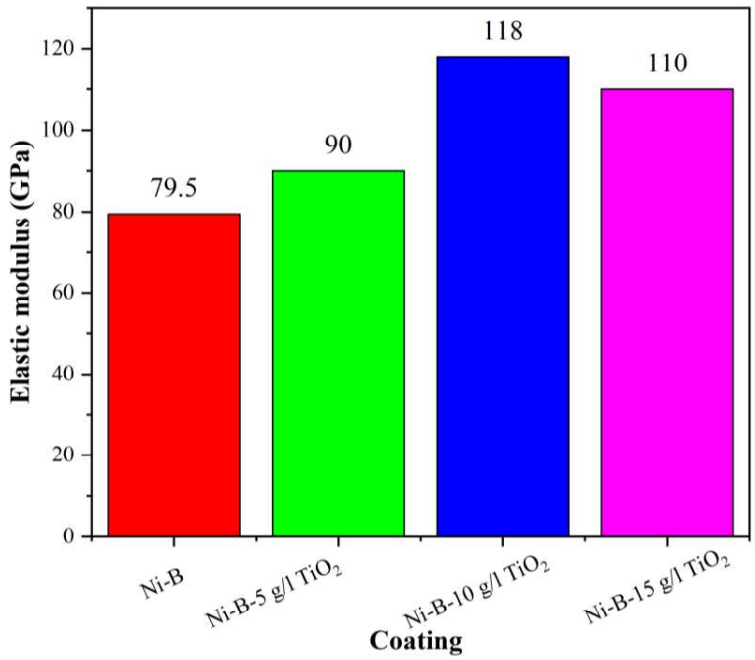

Fig. 4.4: Elastic modulus of coatings

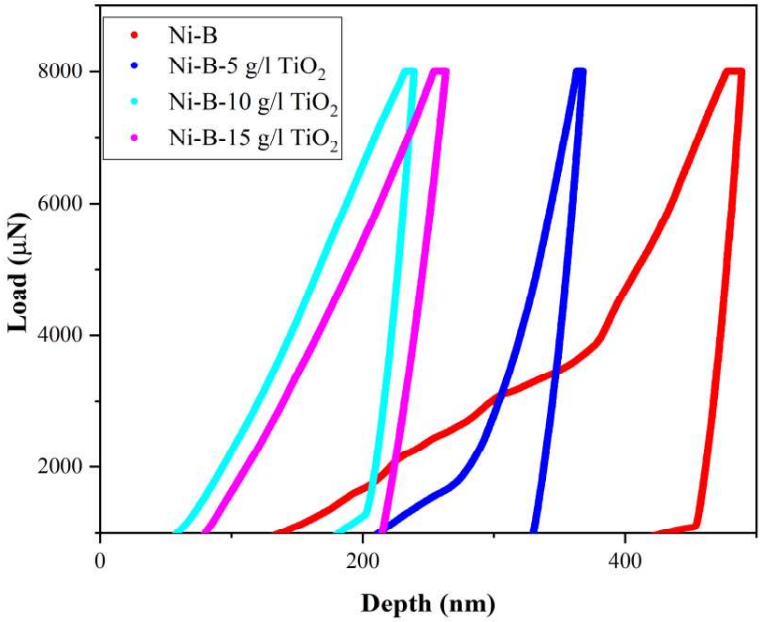

Fig. 4.5: Loading- Unloading curves of coatings

Fig. 4.4 shows the elastic modulus of the coatings under study. The elastic modulus values are 79.5 GPa, 90 GPa, 118 GPa and 110 GPa respectively for Ni-B, Ni-B-5 g/l TiO_2,

Ni-B-10g/l TiO_2 and Ni-B-15 g/l TiO_2. Fig. 4.5 shows the loading-unloading curves for the nanoindentation test. The loading and unloading curves show plastic deformation and low recovery after unloading. The depth of penetration is the lowest for Ni-B-10 g/l TiO_2 showing that the material is comparatively harder than the other coatings. The elastic modulus obtained is the highest for the Ni-B-10 g/l TiO_2 at 118 GPa as seen in Fig. 4.4. The unloading curves in Fig. 4.3.5 show a higher slope than the loading curves indicating a steeper recovery rate once the load was unmounted. The binary Ni-B coating showed wide penetration for the same loading conditions as compared to the nano-reinforced coatings. The nanoparticle reinforcement in the coatings seems to inhibit the dislocation motion hence causing a lower range of penetration depth. Also, from the shape of the loading-unloading curves, it may be concluded that for Ni-B the degree of deformation is more as compared to nanoparticle-reinforced coatings. Beyond the concentration of 10 g/l, which is likely the saturation level for nanoparticle adsorption, with further increase in the concentration of nanoparticles the coating properties deteriorate. This deterioration of the coating is seen in the case of Ni-B-15 g/l TiO_2, where the elastic modulus decreases by around 8 % as compared to the Ni-B-10 g/l TiO_2.

4.3.4 Scratch resistance

Fig. 4.6 (a) and (b) show the optical image of the scratch on the surface of as-deposited binary Ni-B and as-deposited Ni-B-10 g/l TiO_2, respectively. Scratch hardness is inversely dependent on the square of the scratch width thus a low scratch width results in a higher scratch hardness as given by equation 2. In Fig. 4.6 (a) a coating peel-off is observed for the as-deposited Nickel-Boron, marked by a bright white patch, but the same is not visible for the Ni-B-10 g/l TiO_2 coating (Fig. 4.6(b)). The nano inclusions within the subsurface of the coatings often act as load-bearing members in the composite electroless Ni-B coatings and help to distribute the applied load. This allows for the dissipation of the energy caused due to the penetration and travel of the diamond indenter during the scratching. In the case of the as-deposited Ni-B coatings, due to the absence of nanoparticles, this phenomenon of load transfer is not facilitated as a result; the energy developed due to the applied load remains concentrated in the vicinity. This in turn causes the coating to peel off to release this excess localized energy. In Fig. 4.6 (c), the scratch

width of reinforced Ni-B-10g/l TiO_2 coatings indicates a marked improvement over the as-deposited binary Ni-B. From Fig. 4.6 (c) it is observed that for the applied loads of 20N, 30N, and 40N the Ni-B-10g/l TiO_2 coatings show a scratch hardness of 4.8 GPa, 3.2 GPa, and 2.6 GPa, respectively (using equation 2). For the same loading conditions, the as-deposited Ni-B coatings show a lower scratch hardness of 2.1 GPa, 1.7 GPa, and 1.5 GPa, respectively for applied loads of 20N, 30N, and 40N.

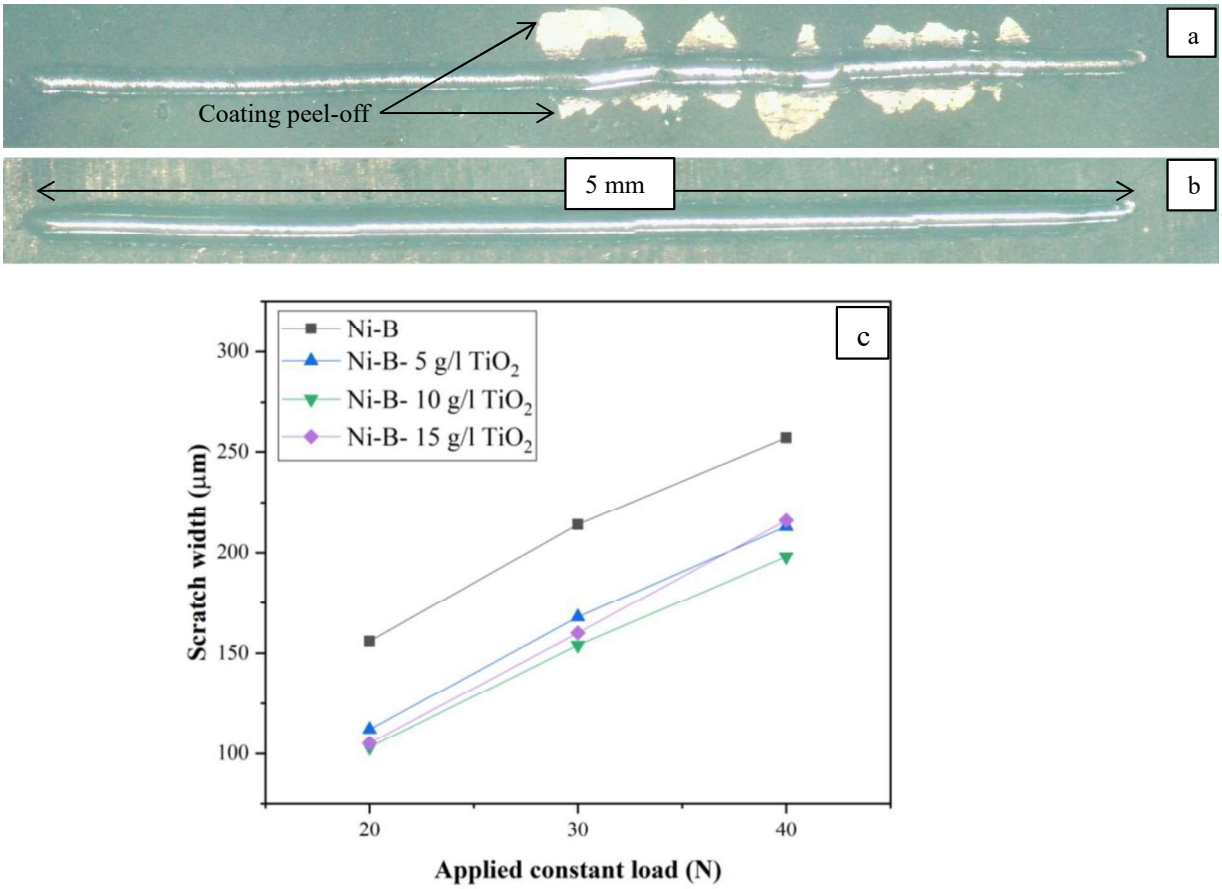

Fig. 4.6: (a) Optical image of scratch taken on Ni-B, (b) Ni-B- TiO_2 taken at load 20 N and (c) Scratch width of as-deposited coatings at applied loads 20 N, 30 N and 40 N taken at an indentation speed of 0.1 mm/s.

The coating Ni-B- 10 g/l TiO_2 scratched under an applied load of 20 N shows an increase in the scratch hardness of nearly 2 times as compared to Ni-B. This decreases 1.5 times for the 40 N applied load. This is because the scratch hardness depends inversely on

the square of scratch width and hence a slight change in the scratch width will result in a high change in the hardness of the samples. The corresponding scratch width of Ni-B- 10 g/l TiO_2 coating is 103 µm, 154 µm, and 198 µm for 20N, 30N, and 40N, respectively. The scratch width of Ni-B coating is higher with values of 156 µm, 214 µm, and 257 µm for the same set of loads. Beyond the applied load of 40 N excessive coating peel-off was seen even for the reinforced coatings.

4.3.5 Wear and friction behaviour

The results of the tribo analysis (specific wear rate) of the specimens are shown in Fig. 4.7. The addition of TiO_2 led to an initial increase in the specific wear rate. This increase was observed until the concentration of TiO_2 nanoparticles reached 10 g/l thereafter, the wear resistance started to decrease with further addition of TiO_2 nanoparticles, and the wear rate increased. The specific wear rates for Ni-B, Ni-B with 5 g/l TiO_2, Ni-B with 10 g/l TiO_2, and Ni-B with 15 g/l TiO_2 were found to be $8.8 * 10^{-5}$ mm^3/Nm, $5.2 * 10^{-5}$ mm^3/Nm, $3.2 * 10^{-5}$ mm^3/Nm, and $4.6 * 10^{-5}$ mm^3/Nm, respectively.

This increase in wear resistance is attributed to the multiple functions that the nanoparticles perform in the coating. Firstly, the nanoparticles embedded throughout the coating hinder the dislocation motion, making it harder for the dislocation to move freely through the coating (Gül et al., 2009). As a result, the process of deformation and material failure is slowed down. Secondly, the increased frictional force caused by the nanoparticles requires more force to remove the coating. Therefore, the nanoparticles act as load-bearing members (Yang et al., 2017) and distribute the force applied throughout the coating to prevent stress from congregating in a single location and causing failure.

However, it is necessary to note that the concentration of TiO_2 nanoparticles has to be carefully controlled. Higher concentrations of nanoparticles have a high surface energy, leading to a higher agglomeration rate. During the coating process, this results in the nanoparticles accumulating in large quantities and sinking to the base of the beaker. This, in turn, results in a decrease in the effectiveness of the addition of nanoparticles due to decreased adsorption of nanoparticles into the coating.

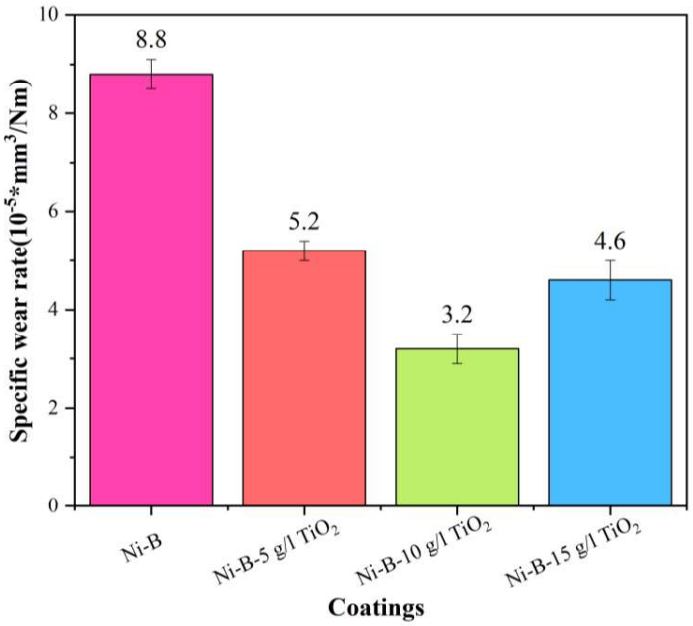

Fig. 4.7: Specific wear obtained at a load of 10 N

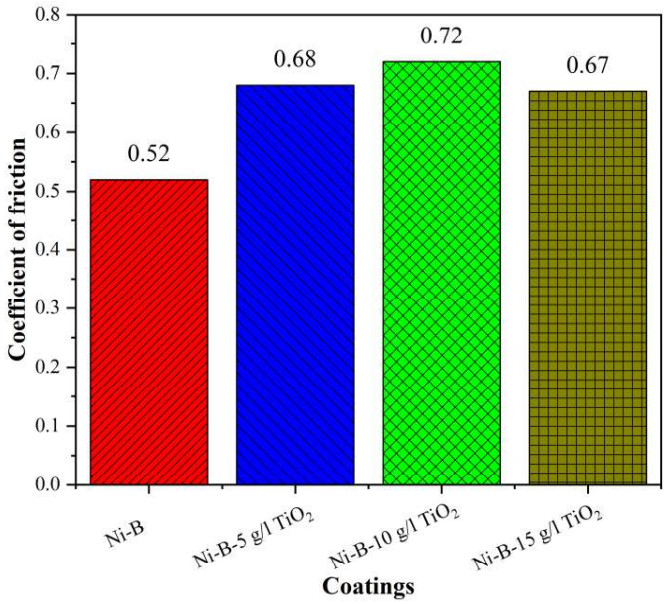

Fig. 4.8: Coefficient of friction values obtained during the Tribo test

Fig. 4.8 demonstrates that the coefficient of friction (COF) also increases with the addition of nanoparticles. The COF is a necessary parameter to analyze the sliding wear of a material with respect to its counterpart (EN31). The COF seems to increase with the

addition of nanoparticles, which in turn increases the resistance of the coating against the sliding motion. This may be because, during the sliding motion of the coating against the harder counterpart on the Pin on Disk tester, the nanoparticles attached to the surface of the coatings dislodge and form a layer between the coating and the counterpart, similar to a three-body abrasion. These nanoparticles being harder than the coating matrix of Ni-B, provide more resistance to the sliding motion. Similar observations are made in the case of Alumina reinforced Ni-B, where the sliding force is shown to increase with the increase in the concentration of nanoparticles. The COF of Ni-B-10 g/l TiO_2 increases to 0.72 from 0.52 for the binary Ni-B coating. This substantial increase in COF results in better wear resistance properties as shown in Fig. 4.7. However, in the case of Ni-B- 15 g/l TiO_2 due to agglomeration the adsorption of nanoparticles into the coating decreases hence the COF also decreased from 0.72 for Ni-B- 10 g/l TiO_2 to 0.67 for Ni-B- 15 g/l TiO_2. In summary, the incorporation of nanoparticles into the coatings increases wear resistance and friction coefficient up to a certain concentration (10 g/l). Beyond that, the wear resistance decreases, and the specific wear rate again increases.

4.3.6 Corrosion

Fig. 4.9 shows the Tafel curves from the potentiodynamic test conducted to study the corrosion resistance of the coatings under study. Table 3 shows the data obtained by plotting the Tafel slopes on the cathodic and anodic curves. The E_{corr} value increased with the addition of TiO_2 nanoparticles up to a concentration of 10 g/l but with a further increase to 15 g/l a decline in the value is seen. The increase of E_{corr} towards a nobler (more positive) value indicates better corrosion resistance. On the contrary, the corrosion density of the coating should be as low as possible for better corrosion resistance. As seen from Table 3, the I_{corr} decreases from 0.0113 for binary Ni-B to a lower value of 0.003 for the Ni-B-10 g/l TiO_2. Except for the Ni-B coating which shows dominant anodic corrosion, the rest of the coatings show more balanced corrosion as the difference between the anodic and cathodic slopes is very minimal. The coating however did not follow the trend of improved corrosion resistance with increased nanoparticle concentration. This may be due to the agglomeration and sedimentation of the nanoparticles due to their high concentration in the

solution. As shown in Fig. 1 (c) the coating Ni-B-15 g/l TiO_2 shows patches of agglomerated nanoparticles on the surface this results in a non-uniform distribution of the nanoparticles in the coating hence the coating's resistance to the corrosive environment of 3.5 % NaCl decreases. This in turn results in a decrease in E_{corr} of Ni-B-15 g/l TiO_2 coating by around 28 mV as compared to the Ni-B-10 g/l TiO_2. The corrosion current density on the other hand increases drastically to more than twice that of the Ni-B-10 g/l TiO_2 coating.

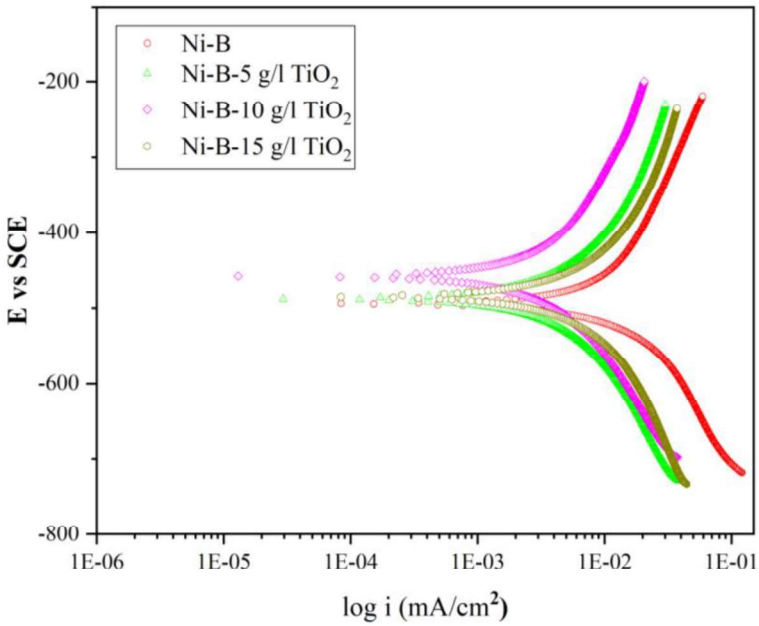

Fig. 4.9: Tafel curves for the as-deposited coatings Ni-B, Ni-B- 5 g/l TiO_2, Ni-B- 10 g/l TiO_2, Ni-B- 15 g/l TiO_2

Table 4.3.: Data obtained from the tafel curves

Sl.No.	Specimen	E_{corr} (mV)	I_{corr} (mA/cm^2)	βa (mV/dec)	βc (mV/dec)
1	Ni-B	- 494.54	0.0113	365.8	196.5
2	Ni-B-5 g/l TiO_2	- 488	0.0047	254	260
3	Ni-B-10 g/l TiO_2	- 457.26	0.003	235	216
4	Ni-B-15 g/l TiO_2	- 485.02	0.007	276	278

4.4 Closure

This study envisages the effect of the addition of nano titania on the

tribomechanical behaviour of the Ni-B coatings. Samples were coated with titania concentrations of 0 g/l, 5 g/l, 10 g/l and 15 g/l. These were then characterized and tested. Ni-B-10 g/l TiO_2 shows the most favourable results as concluded from the tests conducted and with further increase in nanoparticle concentration the wear resistance, mechanical properties and electrochemical corrosion resistance deteriorates.

Chapter 5: Nano-Zirconia reinforced electroless Ni-B coatings

Outline: *5.1 Introduction, 5.2 Experimental details, 5.3 Results and discussion, 5.3.1 Coating morphology, 5.3.2 Micro Vicker's hardness and elastic modulus, 5.3.3 Wear and friction behaviour, 5.3.4 Scratch resistance, 5.3.5 Corrosion, 5.4 Closure*

5.1 Introduction

Zirconium dioxide (ZrO_2) is a versatile material widely used in various technological applications due to its appealing properties. It finds application as a gate dielectric in fuel cell electrolytes and has been extensively employed in catalysis, including supporting catalysts like Au, Ag, and Cu in the water gas-shift reaction. However, the characteristics of zirconia are influenced by its different structural polymorphs. Zirconia exhibits three distinct stable phases: monoclinic phase is stable up to 1175ºC, followed by transformation into the tetragonal phase, which remains stable up to 2370ºC, and eventually transitioning into the cubic phase. With their notable hardness, they are highly suitable for reinforcing particles in their nano form.

In the present chapter, Zirconia reinforced electroless Ni-B coatings have been evaluated on their mechcanical, tribological and electrochemical corrosion behaviour. Due to the fact that zirconia has a bulk average hardness of approximately 10 GPa, the resulting composite coatings may have a higher bulk average hardness as a result. Additionally, due to the size of these zirconia nanoparticles, it is anticipated that they will be able to cover the nodular gaps and pores of the softer Nickel-Boron matrix, which will result in the coatings being of a higher quality. The present research uses ultrasonication to form a colloidal solution of nanoparticles and water which when poured into the coating bath (which is continuously being stirred over a magnetic stirrer) helps to deposit a coating with uniform distribution of nanoparticles. The coatings have been examined using scanning electron microscopy, energy dispersive x-ray spectroscopy, and X-ray powder diffraction in order to validate the aforementioned qualities.

5.2 Experimental details

The mild steel samples undergo various cleaning methods before being deposited. This includes polishing the samples with emery papers using grades 800, 1200, 1600, and 2000 to render all the samples smooth and samples have the same surface roughness. This is followed by ultrasonic cleaning, acid pickling, and drying of the samples. The samples are then deposited in a chemical bath after being exposed to a heated $PdCl_2$ solution, to make the surface more reactive, for ease of deposition.

Table 5.1. Coating Nomenclature

Sl. No.	Coating description	Nomenclature
1.	Ni-B binary coating	Ni-B
2.	1 g/l ZrO_2 (nano) reinforced electroless Ni-B	Ni-B- 1g/l ZrO_2
3.	5 g/l ZrO_2 (nano) reinforced electroless Ni-B	Ni-B- 5g/l ZrO_2
4.	10 g/l ZrO_2 (nano) reinforced electroless Ni-B	Ni-B- 10g/l ZrO_2
5.	15 g/l ZrO_2 (nano) reinforced electroless Ni-B	Ni-B- 15g/l ZrO_2

Electroless Ni-B coatings are deposited over mild steel substrates. Also, coatings are deposited incorporating zirconia in the coatings. The coating nomenclature is given in Table 5.1. The bath composition is shown in Table 5.2. The bath solution is prepared in a volume of 250 ml in a clean beaker. The deposition is done using a magnetic stirrer (IKA, India) with a temperature control module. Nickel chloride hexahydrate acted as the source of Ni^{++} ions in the solution. Ethylenediamine is used as a complexing agent. The primary function of the complexing agents is to act as a deterrent and prevent the basic pH (12-14) of the solution to drop steeply. Simultaneously, these complexing agents also help to prevent metallic nickel precipitation in the solution. Sodium borohydride provides the free electrons to reduce the Ni^{++} ions. A temperature of 85° ± 3° Celsius was maintained throughout the deposition time of 1 hour. Before being introduced into the coating bath the nano ZrO_2 was sonicated at 60 Hz in an ultrasonicator in deionised water.

Various tests were conducted to observe the Surface morphology, elemental composition, hardness, elastic modulus, scratch resistance, tribo behaviour and corrosion response. These tests helped to evaluate the property of these zirconia incorporated

coatings. The following section presents the results of the tests conducted on the coatings. The details of these tests are presented in chapter 2.

Table 5.2. Bath composition

Sl.No.	Chemical	Function	Amount in bath
1.	Nickel chloride	Nickel source	18-20g/l
2.	Ethylene diamine	Complexing agent	45-50 ml/l
3.	Lead nitrate	Stabilizer	0.05-0.06 g/l
4.	Sodium hydroxide	pH buffer	35-40 g/l
5.	Sodium borohydride	Reducing agent	0.5 g/l
6.	Nano Zirconia	Reinforcement	1 g/l, 5g/l, 10 g/l, 15 g/l
7.	SDS	Surfactant	2.36 gm

5.3 Results and discussion

5.3.1 Coating morphology

Fig. 5.1 (a) to (d) shows the SEM microstructure of the coated specimen. The typical cauliflower-like microstructure is observed for the entire set of the specimen. During electroless deposition, the nucleation and growth of individual grains are responsible for this cauliflower-like morphology. The activated surface of the substrate provides excellent spots for the beginning of nucleation. The metallic ions of Ni-B then tend to overlap with each other and grow in a vertical direction facilitating a columnar microstructure. Simultaneously, the Ni-B covers the nanoparticles and entraps the nanoparticles inside the porosities of these columnar growths.

Figure 5.1 (b) to (d) shows the zirconia nanoparticles embedded in many such pores created due to the basic columnar microstructure of the electroless Ni-B matrix. Fig. 5.1 (a) shows binary Ni-B coatings with porosities. Fig. 5.1 (d) shows a lower presence of zirconia nanoparticles on the surface as compared to Fig. 5.1 (c), although the amount of nanoparticles added during the deposition process is more for the coating. This may be attributed to the fact that at a concentration of more than 10 g/l of zirconia nanoparticles, the agglomeration was higher and as a result the adsorption of the nanoparticles was low. Also, as evident during the coating process, the majority of the nanoparticles got settled at the bottom of the beaker and did not participate actively in the coating process.

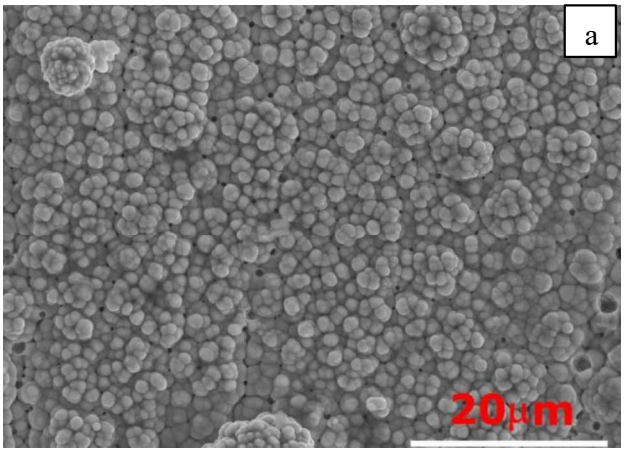
a
20µm

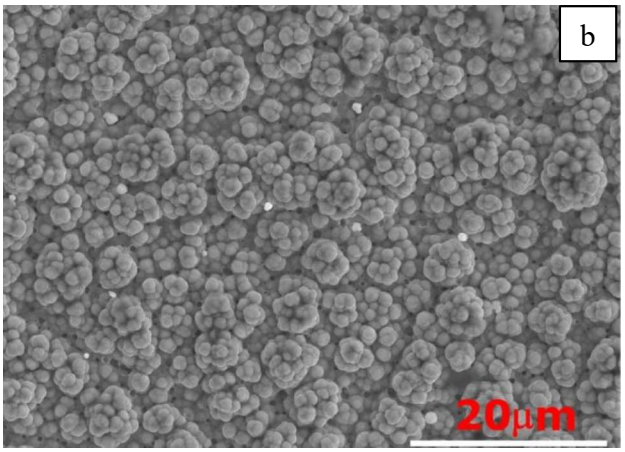
b
20µm

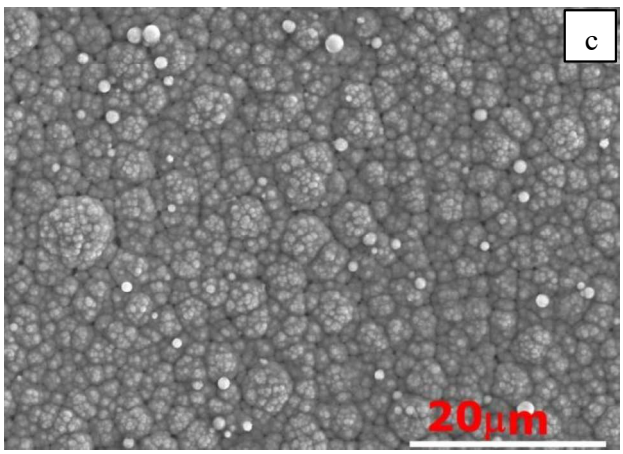
c
20µm

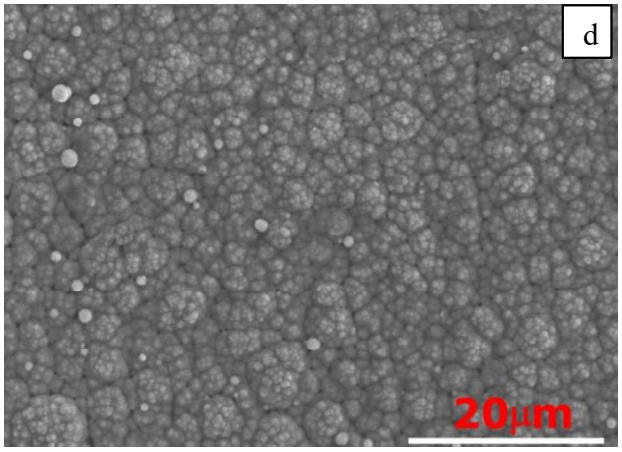

Fig. 5.1: SEM image of (a) as deposited Ni-B, (b) as deposited Ni-B- 5g/l ZrO_2, (c) as deposited Ni-B- 10g/l ZrO_2 and (d) as deposited Ni-B- 15g/l ZrO_2

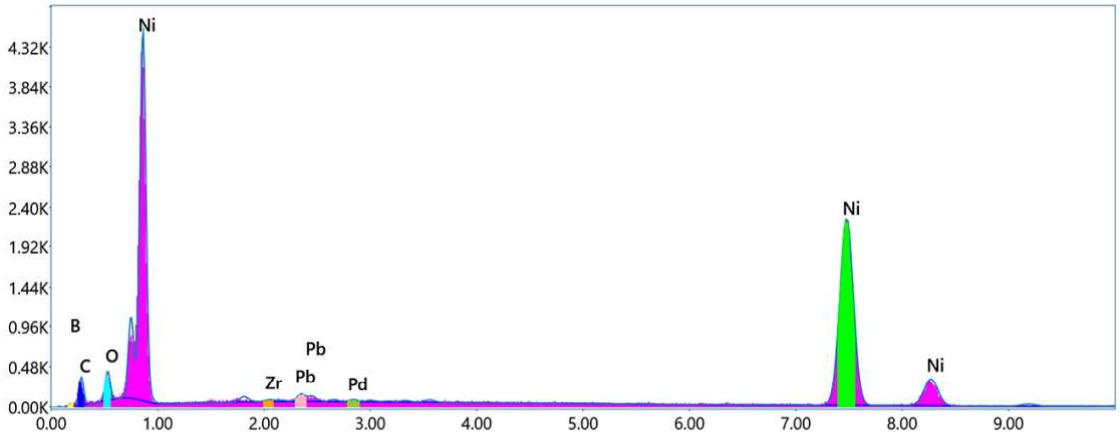

Fig. 5.2 EDAX spectrum peaks of Ni-B-10 g/l ZrO_2

The EDAX (Energy-dispersive X-Ray analysis) spectra in Fig.5.2 shows the presence of Boron, Oxygen, Zirconia, Lead, Palladium and Nickel at their respective energy spectra. Palladium has been used as a surface activator as evidenced by the presence of the same in the EDAX scan. The EDAX scan shown in Fig. 5.3 shows a uniform distribution of nano zirconia as observed from the distribution pattern of elemental Zr. The uniform distribution of nano Zirconia is a result of ultrasonication. Ultrasonication facilitated the formation of a colloidal solution which in turn allowed the zirconia particles to remain in the solution throughout the coating without sedimenting. One of the primary requirements of a sound coating with reinforced nanoparticles is the homogenous

distribution of the nanoparticles. As evident from the SEM images, the same has been achieved in the present study.

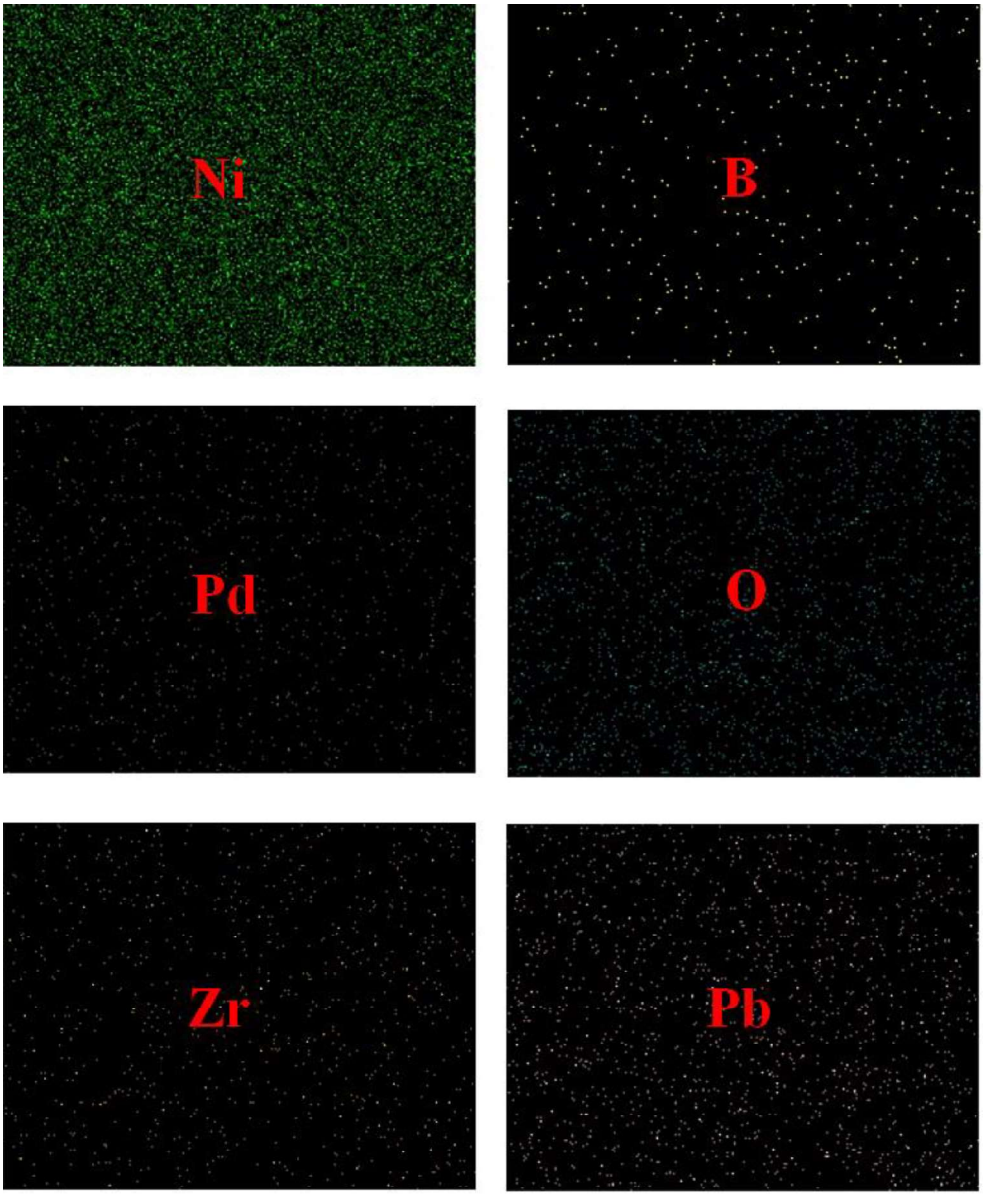

Fig.5.3: EDAX area scan of the surface of Ni-B-10 g/l ZrO_2

5.3.2 Micro Vicker's hardness and elastic modulus

Fig. 5.4 shows the microhardness of the specimen under study. The expected increase in hardness occurs after the addition of nano-sized ZrO_2 particles. This can be attributed to the inclusion of the hard nanoparticles, which, when embedded in the more

pliable Ni-B matrix, helps in sharing the load that is being applied normally during the indentation hardness test. In addition, these nanoparticles impede the flow of material when a vertical load is applied during the test. This helps to restrict the size of the indentation, which ultimately leads to a higher value for the material's hardness. Even though the addition of nanoparticles results in an increase in the coating's hardness, at high concentrations of nanoparticles the property deteriorates. This variation in hardness values is due to the inhomogeneous distribution of nano-ZrO_2 powders in the Ni-B-15 g/l ZrO_2 coatings, which is caused by a higher degree of agglomeration of alumina beyond a concentration of 10 g/l.

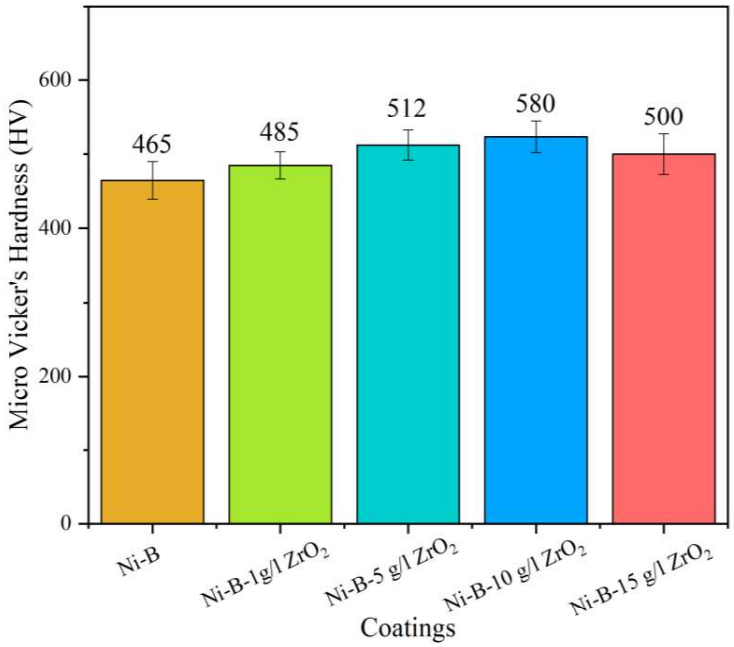

Fig. 5.4: Micro Vicker's hardness of coatings

This agglomeration of alumina is what causes this deviation from the trend in hardness values. The elastic modulus of the as-deposited coatings is shown in Figure 5.5. The incorporation of nanoparticles results in an increase in the material's elastic modulus which is more or less gradual. The elastic modulus (E) of the reinforced Ni-B-10g/l ZrO_2 coating is higher than that of the binary Ni-B coating, coming in at 83 GPa as opposed to

75.9 GPa. On further addition of nanoparticles, there is a drastic decrease in the modulus value to 75 GPa. This may be due to the higher degree of agglomeration which tends to decrease the adsorption of the nanoparticles in the coating as a result their effectiveness in improving the overall elastic modulus decreases.

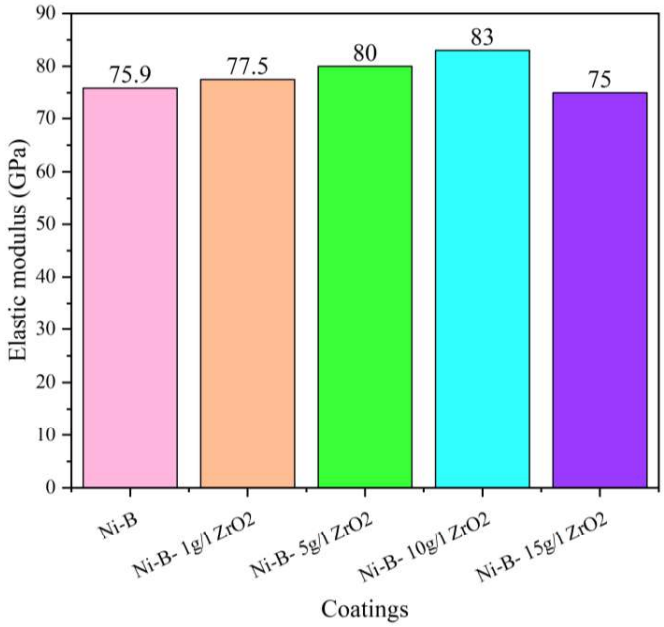

Fig. 5.5. Elastic modulus of the coatings under study

5.3.3 Wear and friction behaviour

Fig. 5.6 shows the wear rate of specimens under study. Fig. 5.7 shows the coefficient of friction values. It is observed that with the addition of ZrO_2 nanoparticles, the specific wear rate of the samples increased initially up to a nanopowder concentration of 10 g/l but with a further increase, the wear resistance decreases, as a result, the wear rate increased. The specific wear rate for Ni-B, Ni-B- 1 g/l ZrO_2, Ni-B- 5 g/l ZrO_2, Ni-B- 10 g/l ZrO_2 and Ni-B- 15 g/l ZrO_2 are 8.8 x 10^{-5} mm^3/Nm, 7.3 x 10-5 mm^3/Nm, 6.7 x 10^{-5} mm^3/Nm, 3.9 x 10^{-5} mm^3/Nm and 5.2 x 10^{-5} mm^3/Nm, respectively. This is due to the fact that the nanoparticles perform multiple functions which affect the wear resistance of the coating.

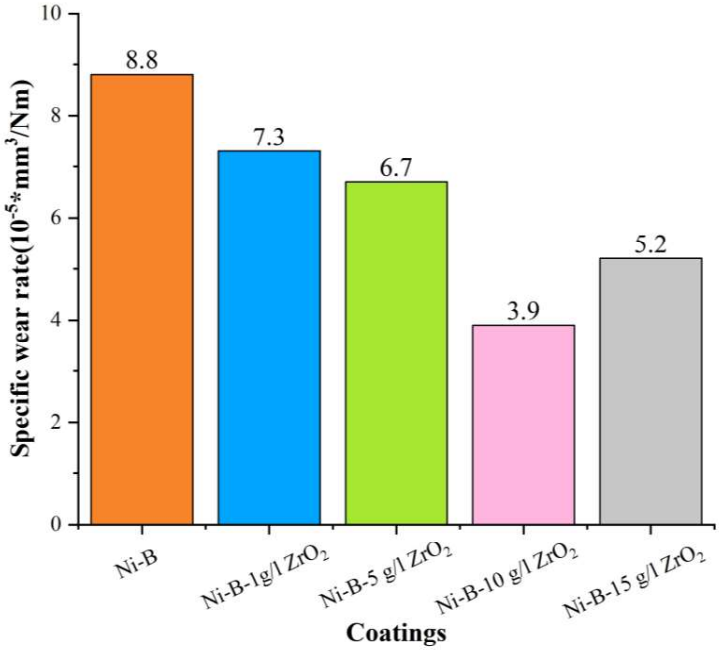

Fig. 5.6: The specific wear rate of the as-deposited binary Ni-B coating and reinforced coatings

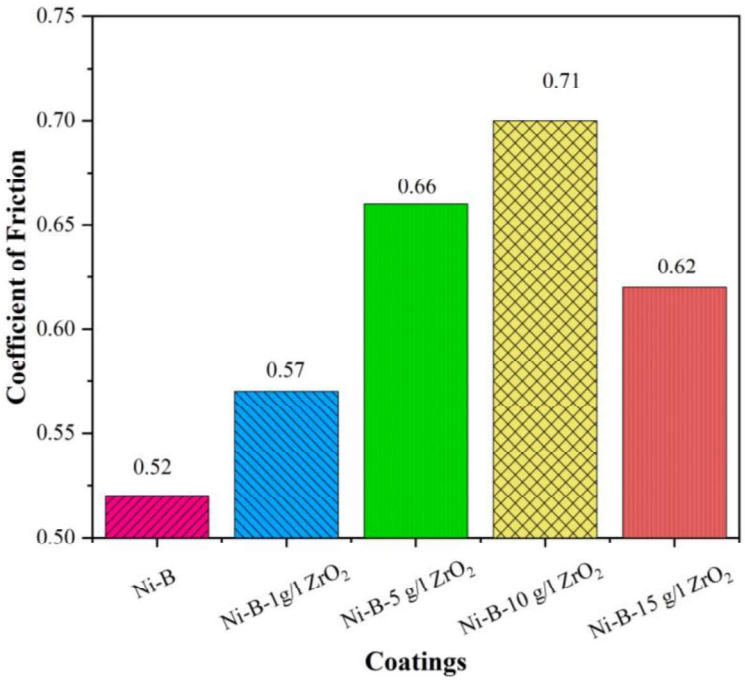

Fig. 5.7: The coefficient of friction of the as-deposited binary Ni-B coating and reinforced coatings

Firstly, these embedded nanoparticles obstruct the dislocation motion and do not easily allow the dislocation to flow through the coating. This slows down the process of deformation and finally material failure. Secondly, these particles increase the frictional force hence more load is required to remove the material (coating). Finally, they act as load-bearing members and help distribute the applied throughout the coating and thus do not allow the stress to concentrate at a place that may be detrimental to the wear resistance behaviour of the coating. This may be attributed to the fact that higher concentrations of nanoparticles which inherently exhibit high surface energy, contribute to a high agglomeration rate. This causes the nanoparticles to accumulate in large volumes and sediment to the bottom of the beaker during the coating. The adsorption of the nanoparticles into the coating decreases and makes the addition of nanoparticles less effective as compared to coatings with lower concentrations of nanoparticles. As the addition of nanoparticles increases the friction coefficient also increases as shown in Fig.5.7. Overall, it may be said that with the addition of nanoparticles up to a certain concentration (10 g/l) the wear resistance and friction coefficient both increases.

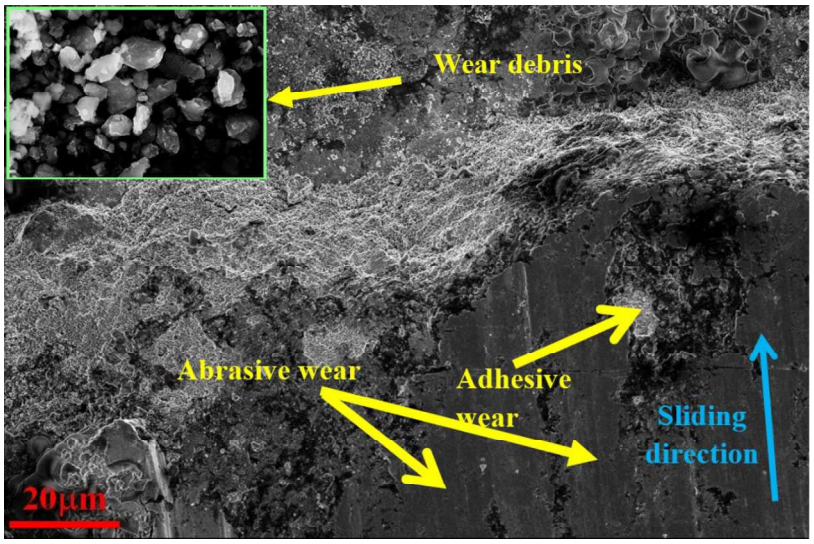

Fig. 5.8: SEM image showing the wear morphology of Ni-B-10 g/l ZrO_2

Fig. 5.8 shows the SEM image of the worn surface of Ni-B-10 g/l ZrO_2 coating. The wear morphology shows both adhesive and abrasive wear. The worn surface shows

coating pluck-out which is typical of adhesive wear, where due to localized welding, the top surface of the specimen attaches to the counter face. This welded protrusion, at a later stage, due to the continuous sliding motion between the specimen and the counter face, breaks. This creates a crater as seen in Fig. 5.8, indicating adhesive wear. On the other there is also evidence of abrasive wear due to three body abrasions, this is brought about by the presence of ploughing marks. Hence, it may be observed that the wear phenomenon is a combination of both abrasive and adhesive wear.

5.3.4 Scratch resistance

Fig. 5.9 (a) and (b) show the scratches on the Ni-B and Ni-B-ZrO_2 coatings, respectively. Fig. 5.9 (c) shows the scratch width values of the specimen. The scratch hardness for a set of applied loads (20 N, 30 N, and 40 N) increases with the addition of ZrO_2 in the coatings. The best results are obtained for higher Ni-B-10 g/l ZrO_2 coating. This can be attributed to the inclusion of hard ZrO_2 nanoparticles which are found to be embedded in the as-deposited Nickel-Boron matrix. Also, at a very high concentration of 15 g/l, the hardness decreased as the amount of adsorption of ZrO_2 decreased due to a high degree of agglomeration. These hard particles act as an obstruction to penetration resulting in a lower scratch width.

From Fig. 5.9 (c) it is observed that the minimum scratch width is obtained for the Ni-B-10 g/l ZrO_2 for all the applied loads. The trend of decreasing scratch width is observed with the addition of ZrO_2 up to a concentration of 10 g/l, thereafter the scratch width increases, for all applied loads, for the coating Ni-B-15 g/l ZrO_2. This is because at higher concentrations the nanoparticles agglomerate and do not contribute to the improvement of the coating properties.

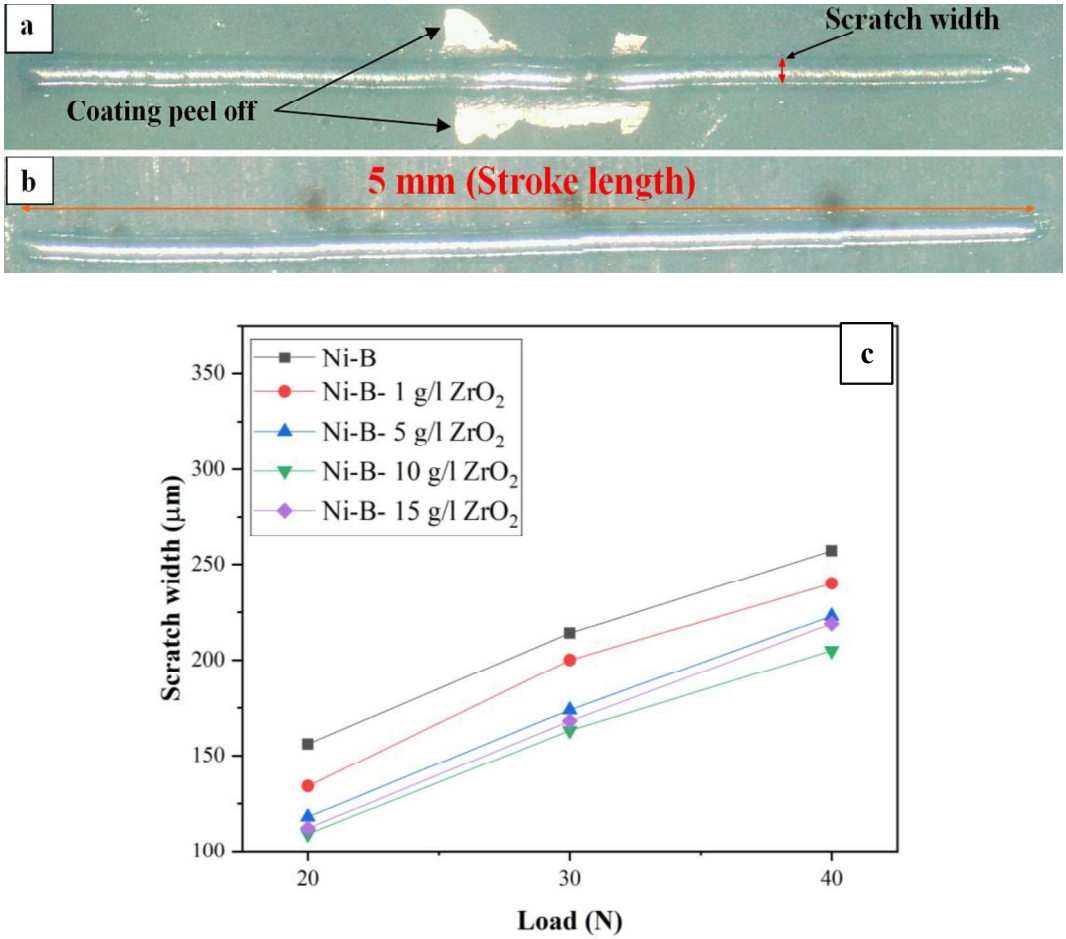

Fig.5.9: Optical image of (a) as deposited Ni-B, (b) Ni-B- 10 g/l ZrO_2 and (c) Scratch width obtained at varying loads of 20 N, 30 N and 40 N

5.3.5 Corrosion

Fig. 5.10 shows the Tafel curves and Fig. 5.11 shows the Nyquist plots for all the coatings under study. The slope of the anodic and cathodic parts is shown in Table 5.3. The electrochemical corrosion test is done by the commonly used three electrode method. In the case of Ni-B and Ni-B-5 g/l ZrO_2, the anodic corrosion is more dominant over the cathodic corrosion as indicated by a much higher value of β_a (anodic slope) as compared to β_c (cathodic slope). The rest of the coatings show more balanced anodic and cathodic corrosion. The E_{corr} also shifts to a nobler value for the coatings with higher concentrations of nanoparticles.

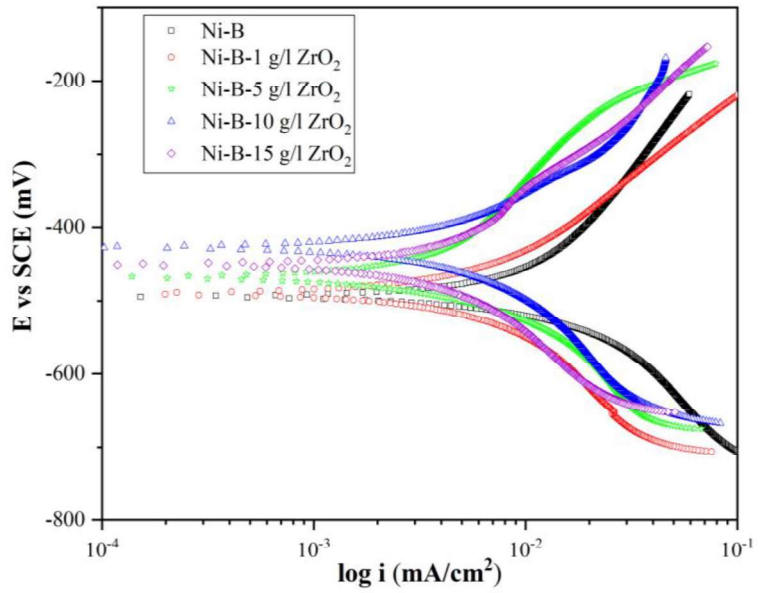

Fig. 5.10: Tafel curves of the as-deposited coatings

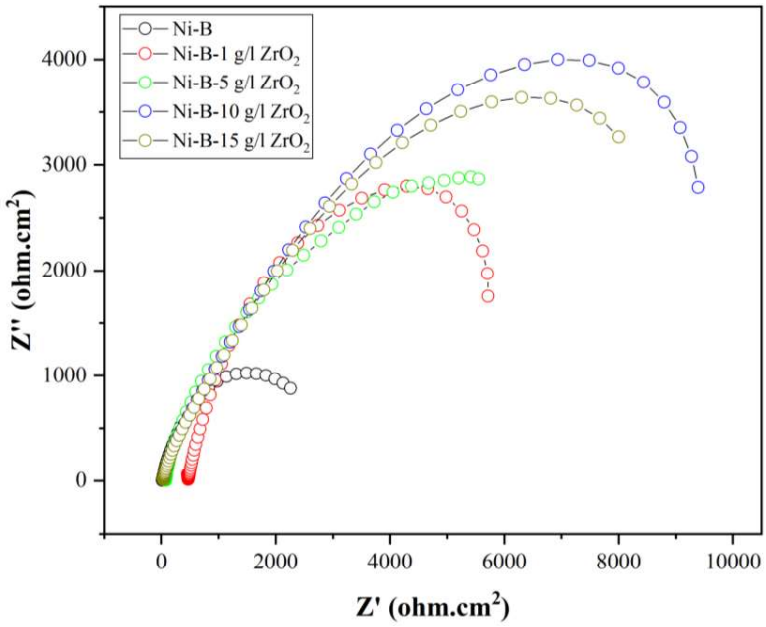

Fig.5.11: Nyquist plot for the coatings under study

The best corrosion potential value is obtained for Ni-B-10 g/l ZrO_2 at -428.31 mV. As compared to the binary Ni-B coating which has a value of -494 mV the Ni-B-10 g/l ZrO_2 coating showed an improvement of around 13 %. Although it should be noted that the corrosion current density and not the corrosion potential is the determining factor in the

corrosion resistance property of a material. In the present study, the corrosion current density I_{corr} for the Ni-B-10 g/l ZrO_2 is the least, hence this coating has the highest corrosion resistance to the standard corrosion environment of 3.5 % NaCl. The R_{ct} value increases with the addition of nanoparticles.

The R_{ct} value is calculated from a semicircle fit into the EIS plot shown in Fig. 3.13. The values of Ecorr, Icorr and Rct are shown in Table 3. The R_{ct} value of Ni-B-10 g/l ZrO_2 is 5 times that of the binary as deposited Ni-B. The coating Ni-B-15 g/l ZrO_2 does not follow the trend and shows an R_{ct} value of 1.1 x 10^4 which shows a lower corrosion resistance as compared to Ni-B-10 g/l ZrO_2. This may be due to the lower degree of adsorption of ZrO2 in the Ni-B-15 g/l ZrO_2 coating owing to high agglomeration.

Table 5.3: Corrosion data obtained from the Tafel plot and the Nyquist plot

Coating	E_{corr} (mV)	I_{corr} (mA/cm^2)	β_a (mV/dec)	β_c (mV/dec)	R_{ct} ($ohms.cm^2$)
Ni-B	-494	0.011	365.8	196.5	$0.3x10^4$
Ni-B- 1 g/l ZrO_2	-491.6	0.004	152.2	151.7	$0.8x10^4$
Ni-B- 5 g/l ZrO_2	-468.1	0.0031	188.3	105	$1.04x10^4$
Ni-B- 10 g/l ZrO_2	-428.3	0.0028	98	95	$1.5x10^4$
Ni-B- 15 g/l ZrO_2	-451	0.003	209.6	207.6	$1.1x10^4$

In recent times, there is an enhanced interest among researchers for using electroless nickel variants in corrosion protection of construction steel rebars (Mukhopadhyay and Sahoo, 2022b;Mukhopadhyay and Sahoo, 2022a;Mukhopadhyay and Sahoo, 2022c;Mukhopadhyay and Sahoo, 2021b;Mukhopadhyay and Sahoo, 2021a;Mukhopadhyay and Sahoo, 2019) and high temperature applications (Kundu, Das and Sahoo, 2021;Sahoo, 2021) Evaluation of the present coating variant in such applications defines a future scope of work.

5.4 Closure

The present chapter dealt with the study of zirconia-reinforced electroless Ni-B coatings deposited on mild steel substrates. The addition of ZrO_2 nanoparticles is assisted

by ultrasonication which helps in forming a uniform colloidal solution, which is then added to the coating bath. The coatings are deposited varying the zirconia concentrations (1 g/l, 5g/l, 10 g/l and 15 g/l). The deposited coatings are investigated for Vicker's microhardness, elastic modulus, friction, wear, scratch width and corrosion resistance. The results of the deposited coatings are also compared with binary Ni-B coatings. The coating with a zirconia concentration of 10 g/l in the bath shows the most promising result. This coating shows a decreased specific wear rate of nearly 1/3rd as compared to the binary Ni-B coating. The coating with a zirconia concentration of 10g/l also shows an improvement in corrosion resistance. The E_{corr} of the coating shows an increase of approximately 13% towards a nobler value as compared to the unreinforced coating (binary Ni-B coating). The same coating also shows an increase in the elastic modulus to nearly 14 % as compared to the binary Ni-B coating. The scratch width of the coating with 10 g/l zirconia concentration is minimum among the coatings under study. It is also observed that the above-mentioned properties deteriorated upon increasing the concentration of the nano-zirconia in the bath beyond 10 g/l.

This page is intentionally blank

Chapter 6: Comparison between Nano-Alumina reinforced electroless Ni-B and Ni-P coatings

Outline: *6.1. Introduction, 6.2 Experimental details, 6.3 Results and discussion, 6.3.1 Coating morphology and Micro Vicker's hardness 6.3.2 X-Ray Diffraction, 6.3.3 Scratch resistance, 6.3.4 Wear behaviour, 6.3.5 Corrosion, 4.4 Closure*

6.1 Introduction

This chapter provides an overview of the fundamental aspects that form the basis of electroless nickel-phosphorus (Ni-P) coatings. Subsequently, the chapter subsequently the chapter compares the effect of nano-alumina reinforcement in Ni-P coating and Ni-B coatings. The results from the previous chapters established Ni-B-10 g/l Al_2O_3 as the best Ni-B reinforced coating among the three Ni-B reinforced (Alumina, Titania, Zirconia) coatings. Hence, the present chapter compares Ni-B-10 g/l Al_2O_3 with Ni-P-10 g/l Al_2O_3 coating.

6.2 Experimental details

Table 6.1 lists the composition of coating bath for Ni-P coating. The deposition was done on mild steel samples. Flat ground samples dimension 15 mm X 15 mm X 2 mm were used for scratch testing and coating characterizations. Cylindrical ground samples of length 30 mm and diameter 6 mm were used for the tribo testing. These samples were characterized using Scanning Electron Microscopy & X-Ray Diffractometry. These samples were further subjected to hardness, scratch test and wear test. The tests mentioned above are explained in detail in Chapter 2.

Table 6.1: Composition of the coating bath for Ni-P deposition

Chemicals	Amount in the bath	Use
Nickel Chloride (II) hexahydrate	20g/l	Source of Ni
Nickel (II) Sulphate hexahydrate	20g/l	Source of Ni
Sodium succinate	12g/l	Complexing agent
Sodium hypophosphite	12g/l	Reducing agent
Nano alumina	10 g/l	Reinforcement

6.3 Results and discussion

6.3.1 Coating morphology and micro Vicker's hardness

Fig. 6.1 shows the as deposited electroless microstructure replete with typical cauliflower like nodular structures. The cross-section revealed the columnar structure of the Nickel-Phosphorus coatings. The deposition kinetics of the coatings highly depends on the temperature of the bath as well as the duration of the coating. The presence of alumina particles is observed in the Fig. 6.1 and the agglomerated particles can be observed to be embedded in the porosities and voids. These particles being hard tend to improve the wear resistance and average hardness of the material of the coating. Fig. 6.2 shows the Vicker's micro hardness values for the specimen under study. Hardness for Ni-P-Al_2O_3 increased by approximately 18 % on addition of the nano particles as compared to Ni-P binary coatings. This could be attributed to the high hardness of the alumina particles which is effective in restricting the dislocation flow. Ni-B-Al_2O_3, shows better hardness as compared to Ni-P-Al_2O_3, this is obvious as the Ni-B matrix is harder than Ni-P due to the presence of boron. This is extensively reported in literature.

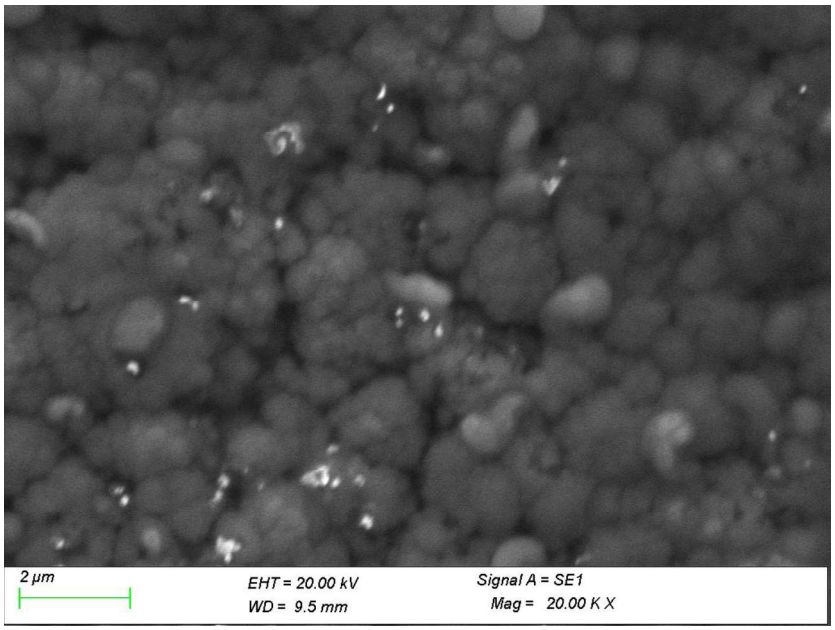

Fig. 6.1: SEM micrograph of the Nickel-Phosphorus-nano Al_2O_3

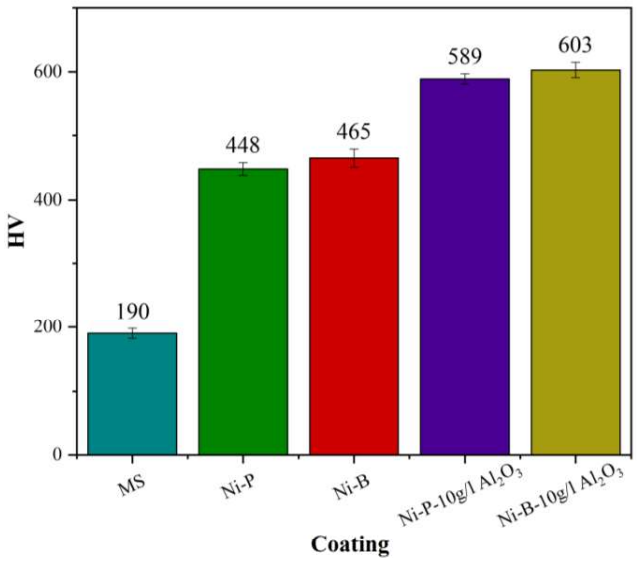

Fig. 6.2: Vickers's micro hardness comparison

6.3.2 X-Ray Diffraction

Fig. 6.3 shows the XRD (X-Ray Diffraction) pattern of the Nickel-Phosporus-nano Al_2O_3 coatings.

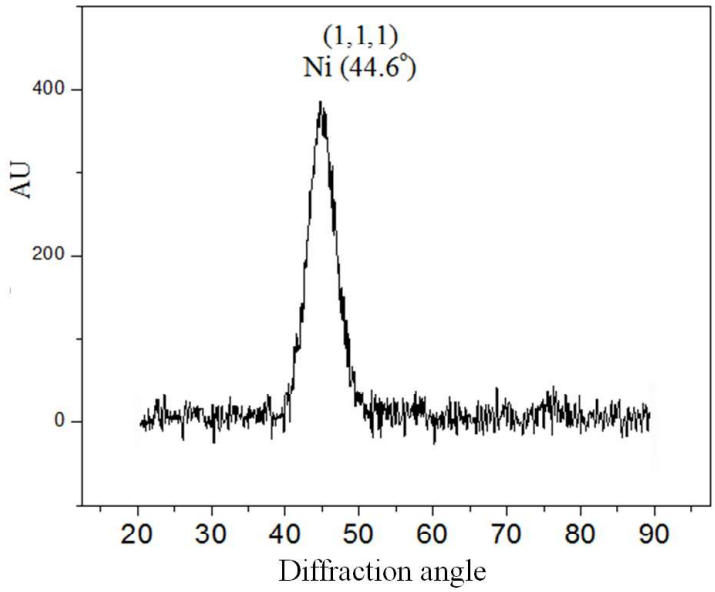

Fig. 6.3: XRD of electorless Ni-P-nano-Al_2O_3 coating

X'Pert Highscore plus software was used to analyze the diffraction data and to identify the phases corresponding to the peaks obtained, on the basis of JCPDS data. The as-deposited nickel peak shows an amorphous nature. It is observed that by adding nano alumina particles to the coating the nature of the coating does not change ie: no transition from amorphous to crystalline is seen in XRD pattern. The nodules changed from coarser to finer structure, same was reported for Ni-B electroless coatings reinforced with nano alumina particles. At a diffraction angle (2θ) of 44.6° Nickel peak was identified.

6.3.3 Scratch resistance

The scratch width values of the specimen are shown in Fig. 6.4. The scratch hardness of the alumina reinforced coating is the highest among the three. This can be a result of the hard alumina nanoparticles embedded in the coatings. These particles tend to provide resistance to penetration as well as the travel of the diamond indenter resulting in high scratch hardness. Fig. 6.5 shows the scratches taken on mild steel, as deposited Nickel-Phosphorus and as deposited Nickel-Phosporus-10 g/l Al_2O_3 (nano).

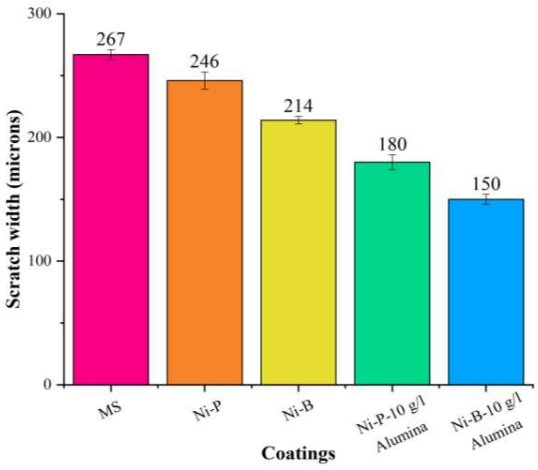

Fig. 6.4: Scratch width comparison among coatings

It is observed that for the Nickel-Phosphorus coating, there is a coating peel-off around the scratch. The same is not observed for the mild steel sample or the Nickel-Phosphorus-10 g/l Al_2O_3 sample. The coating peel-off may be attributed to the brittleness of these coatings. In the case of the Nickel-Phosporus-10 (g/l) Al_2O_3 coating the addition of alumina seems to have made the coating more ductile.

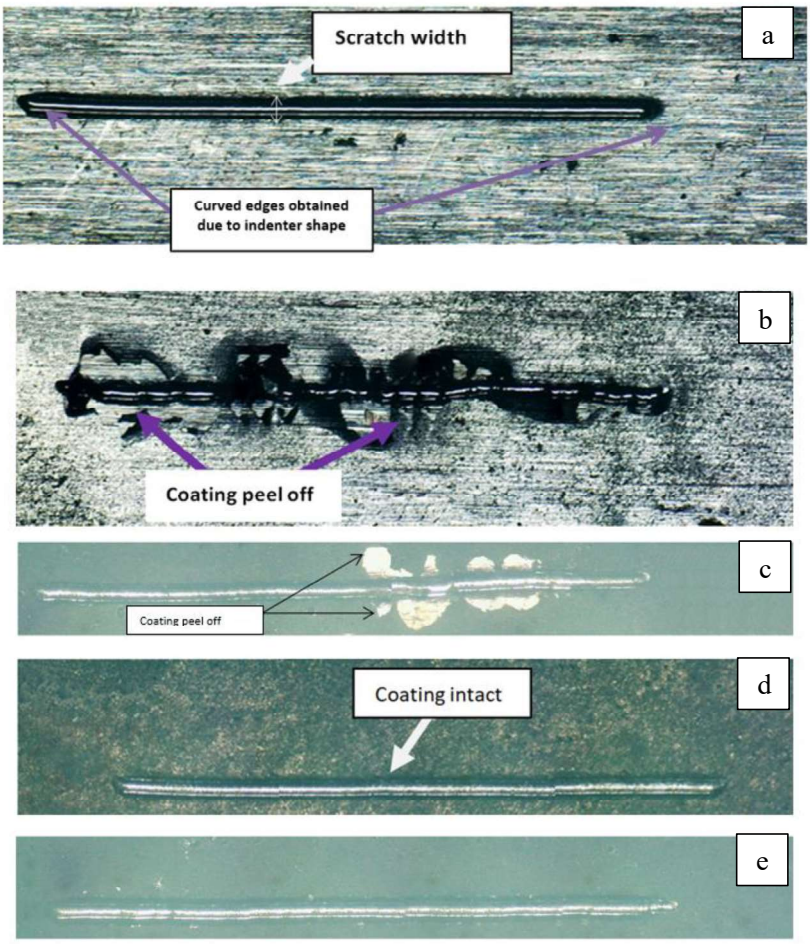

Fig. 6.5: Optical image of scratch on (a) MS (mild steel), (b) as deposited Nickel-Phosphorus, (c) as deposited Nickel-Boron, (d) as deposited Nickel-Phosphorus -10 g/l nano Al_2O_3 and (e) as deposited Nickel-Boron -10 g/l nano Al_2O_3

The average scratch width was found to be approximately 267 µm, 240 µm, 220 and 170 µm for the mild steel, as deposited Nickel-Phosphorus, as deposited Ni-B and as deposited Nickel-Phosphorus-10 (g/l) Al_2O_3 (nano) specimen, respectively for an applied load of 30 N. The alumina reinforced coating shows the least width which can be attributed to its high hardness. As compared to Ni-P-10 (g/l) Al_2O_3 the Ni-B-10 (g/l) Al_2O_3 showed a lower width of approximately 150 µm. This shows that the hardness of Ni-B-10 (g/l) Al_2O_3 is relatively more than the Ni-P-10 (g/l) Al_2O_3. It should be noted here that the semi-circular curves obtained at the edges are due to the shape of the scratch indenter. During

the measurement of the width, these semicircular portions are not considered. The average scratch width is a measure of only the linear portion of the scratch.

6.3.4 Wear behaviour

Fig.6.6 shows the specific wear rate of as deposited Nickel-Phosphorus, MS and as deposited Nickel-Phosporus-10 (g/l) Al_2O_3 (nano). As expected, the wear rate of the uncoated substrate is the highest among the coatings.

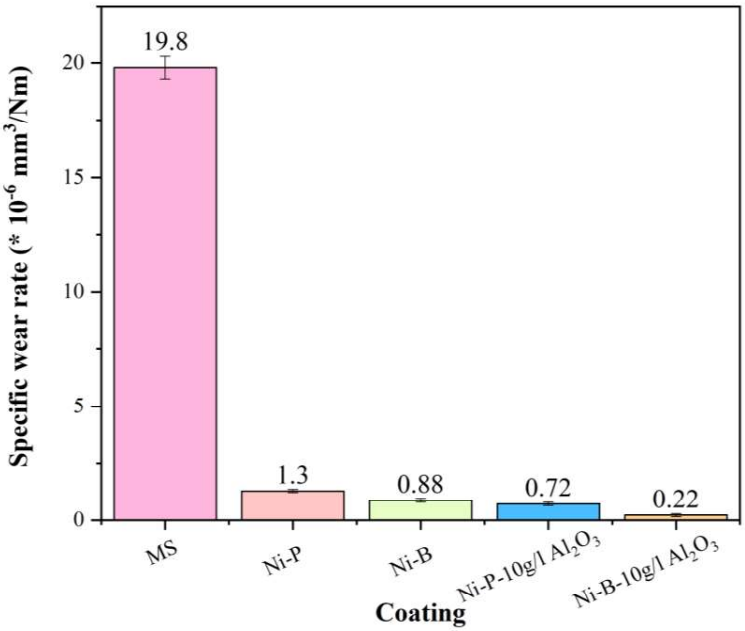

Fig. 6.6: Specific wear rate comparison

The specific wear rate of Nickel-Phosporus -10 (g/l) Al_2O_3 (nano) is very less compared to that of the substrate material (MS). Simultaneously it must be noted that the as deposited Nickel-Boron -10 g/l nano Al_2O_3 is most resistant to wear among all the coatings this is because of the harder Ni-B matrix as compared to the Ni-P matrix. The wear mechanism of the as deposited Ni-P coatings follows the same phenomena as the other coated samples. They also showed signs of both abrasive and adhesive wear during the pin-on-disk sliding test.

6.3.5 Corrosion

Table 6.2 shows the E_{corr} and I_{corr} values obtained by analyzing the Tafel curve. The method of obtaining the E_{corr} and I_{corr} is shown in detail in chapter 2. As can be seen the best corrosion resistance is obtained for the Ni-P coatings. Both E_{corr} and I_{corr} for the binary Ni-P and Ni-P reinforced are more corrosion resistant as compared to binary Ni-B and Ni-B reinforced, respectively. The E_{corr} value improves by nearly 5% and 10% for Ni-P and Ni-P reinforced as compared to binary Ni-B and Ni-B reinforced, respectively. Similarly, the I_{corr} values decreases from 0.001126 mA/cm^2 for Ni-B to 0.00732 mA/cm^2. The correspond values for the reinforced coatings are 0.0026 mA/cm^2 and 0.0018 mA/cm^2 for Ni-B-10 g/l TiO_2 and Ni-P-10 g/l TiO_2. Respectively.

The presence of phosphorus content in Ni-P coatings is considered the primary factor responsible for their superior corrosion resistance compared to Ni-B coatings. This can be attributed to the unique properties imparted by phosphorus, which enhances the protective characteristics of the coating. The higher concentration of phosphorus in the Ni-P coating forms a stable and dense amorphous phase, which acts as a barrier against corrosive agents. This barrier effectively inhibits the diffusion of corrosive species, such as oxygen and moisture, into the underlying metal substrate.

Furthermore, the higher crystallite sizes observed in Ni-P coatings contribute to their enhanced corrosion resistance. The larger crystallite sizes provide a more continuous and homogeneous structure, reducing the number of defects and discontinuities in the coating. Consequently, the diffusion pathways for corrosive species are impeded, limiting their ability to penetrate the coating and reach the underlying metal.

Additionally, the lower micro strains exhibited by Ni-P coatings play a significant role in their improved corrosion resistance. Lower micro strains indicate a reduced presence of internal stresses within the coating, which can lead to crack formation and corrosion initiation. The decreased occurrence of micro strains in Ni-P coatings helps maintain the structural integrity of the coating, preventing the formation of corrosion sites and subsequent degradation.

Table 6.2: E_{corr} and I_{corr} obtained from Tafel curve

Sl.No.	Specimen	E_{corr} (mV)	I_{corr} (mA/cm^2)
1	MS	- 722.51	0.008
2	Ni-P	- 473.60	0.00732
3	Ni-B	- 494.54	0.01126
4	Ni-P-10	- 411.24	0.0018
5	Ni-B-10	- 421.02	0.0026

6.4 Closure

In this chapter, an effort has been made to study the tribological behavior of the Nickel-Phosphorus coatings reinforced with nano alumina powders. The study includes the incorporation of 10 g/l of nano alumina power into the Nickel-Phosphorus coatings. Prior to the introduction of the alumina powder into the coating bath, it was ultrasonicated in a wet media (deionized water). After preparing a sound reinforced as-deposited coating of Nickel-Phosphorus-Alumina (nano), it was compared to a binary Nickel-Phosphorus coating and an uncoated mild steel specimen. These were subjected to a sliding wear test on a pin-on-disk setup and the wear rate was evaluated from the difference in weight (before and after the test). The reinforced (Nickel-Boron-Alumina) coating was found to be the most resistant to wear amongst the three. Besides this, the present chapter also compares the coating with respect to their scratch width, micro Vicker's hardness and corrosion resistance. This chapter also includes a characterization study of the as-deposited reinforced coating surface via X-Ray diffraction (XRD) and Scanning electron microscopy (SEM).

Chapter 7: Conclusion and future scope

Outline: *7.1. Conclusions, 7.2 Future scope*

7.1 Conclusions

This study envisages the effect of the addition of nano alumina, nano titania and nano zirconia on the tribomechanical behaviour of the Ni-B coatings. Samples were coated with varying concentrations of these nanoparticles. These coatings were then characterized and tested. The major conclusions from this investigation are given below.

Ni-B-Alumina

- The addition of alumina nanoparticles increased the microhardness of the coatings. The maximum microhardness of 614 HV was observed for the coating Ni-B-12.5. The hardness shown is the average hardness of the coatings.

- As compared to Ni-B coating, the elastic modulus is observed to increase by approximately 62% and 48% for Ni-B-10 and Ni-B-12.5 coatings, respectively. This shows that the elastic modulus of the Ni-B-12.5 decreased by around 9 % as compared to Ni-B-10.

- The wear resistance of the coatings is found to increase with the increase in alumina reinforcement up to Ni-B-10. However, when the concentration of nanoparticles in the coating bath is increased to 12.5 g/l. the wear resistance decreases as compared to Ni-B-10, due to the increase in the agglomeration of the nanoparticles as well as decrease in elastic modulus. The Ni-B-10 shows a 4 fold decrease in the specific wear rate as compared to Ni-B coating. The Ni-B-12.5 coating as compared to Ni-B-10 shows an increase in the specific wear rate of nearly 2 times. Ni-B-10 coating displayed the least specific wear rate, i.e., the highest wear resistance amongst all the alumina reinforced coatings under study.

- Ni-B-10 coating shows a decrease of 77 % in the I_{corr} values and an increase of around 15% in the Ecorr value as compared to the binary Ni-B coating. Ni-B-12.5 coating showed a decrease of E_{corr} by nearly 8 % as compared to the Ni-B-10 coating also, the corrosion current density decreased increased from 0.0026 to 0.0092 mA/cm^2.

Ni-B-Titania

- Sound coatings reinforced with TiO_2 are developed. Ultrasonication helped develop a colloidal solution of nanoparticles and deionized water which was later used in the coating bath to prepare the reinforced coatings.

- SEM images showed the presence of nanoparticles which was also corroborated by the EDAX.

- XRD peaks indicate a mixed nature of the amorphous and crystalline structure.

- The hardness is found to increase from 465 HV for the as-deposited Ni-B coating to 480 HV for Ni-B-10 g/l TiO_2 coating.

- The elastic modulus of Ni-B-10 g/l TiO_2 also increased to nearly 1.5 times that of the Ni-B coating. But for the coating Ni-B-15 g/l TiO_2 the elastic modulus decreased to 110 GPa as compared to 118 GPa for Ni-B-10 g/l TiO_2 coating.

- The scratch hardness of Ni-B-10 g/l TiO_2 increased to more than 2 times as compared to Ni-B coating for the applied load condition of 20N.

- The wear resistance of the Ni-B-10 g/l TiO_2 coating was found to be the best. The specific wear rate of Ni-B-10 g/l TiO_2 decreased to a value of 3.2 * 10-5 mm^3/Nm as compared to 8.8 * 10^{-5} mm^3/Nm for Ni-B coating.

- The E_{corr} value of Ni-B-10 g/l TiO_2 increased by 7 % as compared to Ni-B. Also,

the I_{corr} value of Ni-B-10 g/l TiO_2 decreased to 0.003 mA/cm^2 as compared to 0.0113 mA/cm^2 for Ni-B.

Ni-B-Zirconia

- The Vickers microhardness value for Ni-B- 10 g/l ZrO_2 was found to be 580 HV as compared to the 465 HV for as-deposited binary Ni-B. With a further increase of ZrO_2 concentration to 15 g/l the hardness decreased to 500 HV.

- The elastic modulus gradually increased from 73 GPa for as-deposited Ni-B to 83 GPa for Ni-B- 10 g/l ZrO_2.

- The specific wear rate of the Ni-B-10 g/l ZrO_2 decreased by nearly 1/3rd to 3.2 * 10^{-5} mm^3/ Nm as compared to 8.8 * 10^{-5} mm^3/ Nm for Ni-B coating. An increase in the friction coefficient was also observed with the addition of zirconia nanoparticles up to a concentration of 10 g/l but with further addition, the friction coefficient decreases ie. for the coating Ni-B-15 g/l ZrO_2.

- The scratch width decreases with the addition of the zirconia nanoparticles. The decrease in width for the Ni-B-10 g/l ZrO_2 coating is found to be around 34 %, 28 % and 23 % for the applied load of 20 N, 30 N and 40 N, respectively, as compared to the binary Ni-B coating.

- The corrosion resistance of Ni-B-10 g/l ZrO_2 is the best among the coatings under study. The E_{corr} decreases from a value of – 494 mV for Ni-B to a nobler value of – 428 mV Ni-B-10 g/l ZrO_2. The R_{ct} decreases from 0.3 * 10^4 ohms.cm^2 for Ni-B to 1.5 * 10^4 ohms.cm^2 for Ni-B-10 g/l ZrO_2. The I_{corr} decreases to 0.0028 mA/cm^2 for Ni-B-10 g/l ZrO_2 as compared to the unreinforced Ni-B coating which has a high corrosion current density of 0.011 mA/cm^2.

Overall, the best wear resistance was obtained for the Ni-B-10 (Al_2O_3) coating although the hardest coating was the Ni-B-12.5 (Al_2O_3). The best corrosion resistance and the best elastic modulus was obtained for alumina reinforced Ni-B-10 coating among the Ni-B reinforced coatings but as compared to the Ni-P-10 (g/l) the corrosion resistance of Ni-B-10 coating falls short.

7.2 Future scope

While promising results have been obtained with the use of surfactants, it is crucial to ensure that those utilized in industrial applications are as benign as possible. Additionally, there is still much exploration to be done to make electroless Ni-B coating more eco-friendly. The use of organic and sustainable stabilizers in electroless nickel plating is still in its early stages. Additionally, the high temperature and pH of the plating baths used with sodium borohydride require a significant amount of energy. The next hurdle in the field may involve exploring alternatives to the widespread use of ethylene diamine. The industrial use of of electroless Ni-B coating is a significant challenge. There have been limited investigations into the recycling, retreatment, and replenishment of coating baths to streamline their integration into industrial processes. These investigations are imperative to ensure the practicality and longevity of the technology, as well as enable the complete assessment of the economic and environmental implications of applying EN-B coatings. Lifecycle assessment is one such method, but its efficacy is contingent upon a comprehensive understanding of the aging behavior of electroless nickel-boron plating baths. Thus, conducting further research on these aspects is crucial to address the challenges and maximize the potential of this technology. In addition to its well-established use in enhancing resistance to wear and corrosion, there is great potential for electroless nickel-boron coatings to find new applications in a variety of fields. For example, a deeper understanding of the impact of the stabilizing agent on the microstructure and morphology of the coatings could allow for the engineering of very smooth and shiny deposits, making them suitable for decorative applications. Additionally, textured surfaces with hydrophobic properties could be created, which could be useful in fields like self-cleaning coatings or biomedical devices.

Moreover, the conductivity and catalytic activity of electroless nickel-boron coatings in both film and powder form have been under investigated. They could potentially be utilized in areas such as water splitting, supercapacitors, and catalysis, where their properties could provide unique advantages over other materials. For instance, the high conductivity of electroless nickel-boron coatings could make them ideal for use in high-performance supercapacitors, while their catalytic activity could be harnessed for a variety of applications, such as hydrogen generation via water splitting. By exploring these new applications, the full potential of electroless nickel-boron coatings can be realized, making them an even more versatile and valuable material in a range of industries.

This page is intentionally left blank

References

Aal, A.A., Hassan, H.B. and Rahim, M.A.A. (2008) 'Nanostructured Ni-P-TiO_2 composite coatings for electrocatalytic oxidation of small organic molecules', 620, pp. 17–25. Available at: https://doi.org/10.1016/j.jelechem.2008.03.004.

Afroukhteh, S., Dehghanian, C. and Emamy, M. (2012a) 'Applied Surface Science Preparation of the Ni – P composite coating co-deposited by nano TiC particles and evaluation of it' s corrosion property', Applied Surface Science, 258(7), pp. 2597–2601. Available at: https://doi.org/10.1016/j.apsusc.2011.10.101.

Afroukhteh, S., Dehghanian, C. and Emamy, M. (2012b) 'Progress in Natural Science: Materials International Preparation of electroless Ni-P composite coatings containing nano-scattered alumina in presence of polymeric surfactant', Progress in Natural Science: Materials International, 22(4), pp. 318–325. Available at: https://doi.org/10.1016/j.pnsc.2012.06.006.

Alirezaei, S. et al. (2004) 'Effect of alumina content on surface morphology and hardness of Ni-P-Al_2O_3 (a) electroless composite coatings', 184, pp. 170–175. Available at: https://doi.org/10.1016/j.surfcoat.2003.11.013.

Alirezaei, S. et al. (2005) 'Effect of alumina content on wear behaviour of Ni-P-Al_2O_3 (α) electroless composite coatings', Surface Engineering, 21(1), pp. 60–66. Available at: https://doi.org/10.1179/174329305X23272.

Anik, M., Körpe, E. and Şen, E. (2008) 'Effect of coating bath composition on the properties of electroless nickel-boron films', Surface and Coatings Technology, 202(9), pp. 1718–1727. Available at: https://doi.org/10.1016/j.surfcoat.2007.07.031.

Araghi, A. and Paydar, M.H. (2010) 'Electroless deposition of Ni–P–B4C composite coating on AZ91D magnesium alloy and investigation on its wear and corrosion resistance', Materials & Design, 31(6), pp. 3095–3099. Available at: https://doi.org/10.1016/j.matdes.2009.12.042.

Ardakani, S.R. et al. (2016) 'Characterization of Ni-P-SiO_2-Al_2O_3 nano-composite coatings on aluminum substrate', Materials Chemistry and Physics. Available at: https://doi.org/10.1016/j.matchemphys.2016.12.023.

Ashassi-sorkhabi, H. and Es, M. (2013) 'Corrosion resistance enhancement of electroless Ni – P coating by incorporation of ultrasonically dispersed diamond nanoparticles', Corrosion Science, 77, pp. 185–193. Available at: https://doi.org/10.1016/j.corsci.2013.07.046.

Baldwin, C. and Such, T.E. (1968) 'The Plating Rates and Physical Properties of Electroless Nickel/Phosphorus Alloy Deposits', Transactions of the IMF, 46(1), pp. 73–80. Available at: https://doi.org/10.1080/00202967.1968.11870052.

Barker, D. (1993) ‘Electroless deposition of metals’, Transactions of the IMF, 71(3), pp. 121–124, Available at: https://doi.org/10.1016/0376-4583(81)90138-2

Baudrand, D. and Bengston, J. (1995) ‘Electroless plating processes: developing technologies for electroless nickel, palladium, and gold’, Metal finishing, 93(9), pp. 55–57, Available at: https://doi.org/10.1016/0026-0576(95)99502-2

Berkh, O., Eskin, S. and Zahavi, J. (1996) ‘Properties of electrodeposited NiP-SiC composite coatings’, Metal Finishing, 94(3), pp. 35–40, Available at: https://doi.org/10.1016/0026-0576(96)84169-9

Bhattacharyya, S. et al. (2023) ‘A corrosion and tribo-failure analysis of Ni-P-Cu coated mild steel (AISI-1040) at varied copper concentration’, Engineering Failure Analysis, 146, p. 107063. Available at: https://doi.org/10.1016/j.engfailanal.2023.107063.

Bigdeli, F. and Allahkaram, S.R. (2009) ‘An investigation on corrosion resistance of as-applied and heat treated Ni – P / nanoSiC coatings’, Materials and Design, 30(10), pp. 4450–4453. Available at: https://doi.org/10.1016/j.matdes.2009.04.020.

Biswas, A., Das, S.K. and Sahoo, P. (2017) ‘Correlating tribological performance with phase transformation behavior for electroless Ni-(high) P coating’, Surface and Coatings Technology, 328, pp. 102–114. Available at: https://doi.org/10.1016/j.surfcoat.2017.08.043.

Bonin, L. et al. (2018) ‘Optimization of electroless NiB deposition without stabilizer, based on surface roughness and plating rate’, Journal of Alloys and Compounds, 767, pp. 276–284. Available at: https://doi.org/10.1016/j.jallcom.2018.06.330.

Bonin, L., Vitry, V. and Delaunois, F. (2019) ‘The tin stabilization effect on the microstructure, corrosion and wear resistance of electroless NiB coatings’, Surface and Coatings Technology, 357, pp. 353–363. Available at: https://doi.org/10.1016/j.surfcoat.2018.10.011.

Brenner, A. and Riddell, G.E. (1946) ‘Nickel plating on steel by chemical reduction’, Journal of Research of the National Bureau of Standards, 37(1), p. 31. Available at: https://doi.org/10.6028/jres.037.019.

Breteau, P. (1911) ‘Nickel deposited by reduction with hypophosphite’, Bull Soc Chem, 9, p. 515.

Budinski, K.G. (1988) Surface engineering for wear resistance. Englewood Cliffs, N.J.: Prentice Hall.

Bülbül, F. et al. (2012) ‘Tribological and corrosion behaviour of electroless Ni-B coating possessing a blackberry like structure’, Metals and Materials International, 18(4), pp. 631–637. Available at: https://doi.org/10.1007/s12540-012-4011-1.

Çelik, I., Karakan, M. and Bülbül, F. (2016) 'Investigation of structural and tribological properties of electroless Ni-B coated pure titanium', Proceedings of the Institution of Mechanical Engineers, Part J: Journal of Engineering Tribology, 230(1), pp. 57–63. Available at: https://doi.org/10.1177/1350650115588568.

Chen, W., Gao, W. and He, Y. (2010) 'Surface & Coatings Technology A novel electroless plating of Ni – P – TiO 2 nano-composite coatings', Surface & Coatings Technology, 204(15), pp. 2493–2498. Available at: https://doi.org/10.1016/j.surfcoat.2010.01.032.

Chen, X.M., Li, G.Y. and Lian, J.S. (2008) 'Deposition of electroless Ni-P/Ni-W-P duplex coatings on AZ91D magnesium alloy', Transactions of Nonferrous Metals Society of China (English Edition), 18(SPEC. ISSUE 1), pp. s323–s328. Available at: https://doi.org/10.1016/S1003-6326(10)60225-7.

Correa, E. et al. (2012) 'Nickel–boron plating on magnesium and AZ91D alloy by a chromium-free electroless process', Surface and Coatings Technology, 206(13), pp. 3088–3093. Available at: https://doi.org/10.1016/j.surfcoat.2011.12.023.

Correa, E. et al. (2013) 'Tribological behavior of electroless Ni–B coatings on magnesium and AZ91D alloy', Wear, 305(1–2), pp. 115–123. Available at: https://doi.org/10.1016/j.wear.2013.06.004.

Cullity, B.D. (1956) Elements of X-ray Diffraction. Addison-Wesley Publishing.

Czagány, M., Baumli, P. and Kaptay, G. (2017) 'The influence of the phosphorous content and heat treatment on the nano-micro-structure, thickness and micro-hardness of electroless Ni-P coatings on steel', Applied Surface Science, 423, pp. 160–169. Available at: https://doi.org/10.1016/j.apsusc.2017.06.168.

Dadkhah, M. and Ansari, F. (2016) 'Thermal treatment synthesis of SnO_2 nanoparticles and investigation of its light harvesting application', Applied Physics A [Preprint]. Available at: https://doi.org/10.1007/s00339-016-0233-2.

Das, S.K. and Sahoo, P. (2011) 'Tribological characteristics of electroless Ni-B coating and optimization of coating parameters using Taguchi based grey relational analysis', Materials and Design, 32(4), pp. 2228–2238. Available at: https://doi.org/10.1016/j.matdes.2010.11.028.

Delaunois, F. and Lienard, P. (2002) 'Heat treatments for electroless nickel – boron plating on aluminium alloys', 160, pp. 239–248. Available at: https://doi.org/10.1016/S0257-8972(02)00415-2

Delaunois, F., Petitjean, J.P. and Lienard, P. (2000) 'Autocatalytic electroless nickel-boron plating on light alloys', 124, pp. 201–209. Available at: https://doi.org/10.1016/S0257-8972(99)00621-0

Dervos, C.T., Novakovic, J. and Vassiliou, P. (2004) 'Vacuum heat treatment of electroless Ni-B coatings', Materials Letters, 58(5), pp. 619–623. Available at: https://doi.org/10.1016/S0167-577X(03)00581-0.

Doğan, F. et al. (2020) 'Optimization of pulsed electro co-deposition for Ni-B-TiN composites and the variation of tribological and corrosion behaviors', Surface and Coatings Technology, 400, p. 126209. Available at: https://doi.org/10.1016/j.surfcoat.2020.126209.

Domínguez-Ríos, C. et al. (2012) 'Measurement of mechanical properties of an electroless Ni-B coating using nanoindentation', Industrial and Engineering Chemistry Research, 51(22), pp. 7762–7768. Available at: https://doi.org/10.1021/ie201760g.

Duncan, R.N. (1996) 'The metallurgical structure of electroless nickel deposits: Effect on coating properties', Plating and Surface Finishing, 83(11), pp. 65–69.

Ebrahimian-Hosseinabadi, M., Azari-Dorcheh, K. and Moonir Vaghefi, S.M. (2006) 'Wear behavior of electroless Ni–P–B_4C composite coatings', Wear, 260(1–2), pp. 123–127. Available at: https://doi.org/10.1016/j.wear.2005.01.020.

Ekmekci, D. and Bulbul, F. (2015) 'Preparation and characterization of electroless Ni–B/nano-SiO_2, Al_2O_3, TiO_2 and CuO composite coatings', Bulletin of Materials Science, 38(3), pp. 761–768. Available at: https://doi.org/10.1007/s12034-015-0912-1.

Ernest, T., Sorensen, R. and Guilinger, T. (1998) 'Effectiveness of nickel plating in inhibiting atmospheric corrosion of copper alloy contacts'. Available at: https://doi.org/10.2172/674975.

Ernst, P., Wadsworth, L.P. and Marshall, G.W. (1997) 'Porosity of electroless nickel coatings investigated using different porosity tests and their application', Transactions of the Institute of Metal Finishing, 75(5), pp. 194–198. Available at: https://doi.org/10.1080/00202967.1997.11871171.

Fan, X. et al. (2012) 'Improving stability of thermal barrier coatings on magnesium alloy with electroless plated Ni-P interlayer', Surface and Coatings Technology, 206(21), pp. 4471–4480. Available at: https://doi.org/10.1016/j.surfcoat.2012.05.004.

Farrokhzad, M.A. (2017) 'Surface & Coatings Technology High temperature oxidation behaviour of autocatalytic Ni-P-BN (h) coatings', SCT, 309, pp. 390–400. Available at: https://doi.org/10.1016/j.surfcoat.2016.11.089.

Fetohi, A.E., Hameed, R.M.A. and El-Khatib, K.M. (2015) 'Development of electroless Ni-P modified aluminum substrates in a simulated fuel cell environment', Journal of Industrial and Engineering Chemistry, 30, pp. 239–248. Available at: https://doi.org/10.1016/j.jiec.2015.05.028.

Freitas, C. and Müller, R.H. (1998) 'Effect of light and temperature on zeta potential and physical stability in solid lipid nanoparticle (SLNTM) dispersions', International Journal of Pharmaceutics, 168(2), pp. 221–229. Available at: https://doi.org/10.1016/S0378-5173(98)00092-1.

Gadhari, P. and Sahoo, P. (2016) 'Electroless Nickel-Phosphorus Composite Coatings: A Review', International Journal of Manufacturing, Materials, and Mechanical Engineering, 6(1), pp. 14-50. Available at: https://doi.org/10.4018/IJMMME.2016010102.

Gaevskaya, T. V, Novotortseva, I.G. and Tsybulskaya, L.S. (1996) 'The Effect of Boron on the Microstructure and Properties of Electrodeposited Nickel Films.', Metal finishing, (June), pp. 100–103. Available at: https://doi.org/10.1016/0026-0576(96)83649-X.

Gawne, D.T. and Ma, U. (1987) 'Wear mechanisms in electroless nickel coatings', Wear, 120(2), pp. 125–149. Available at: https://doi.org/10.1016/0043-1648(87)90063-9.

Gawne, D.T. and Ma, U. (1988) 'Engineering properties of chromium plating and electroless and electroplated nickel', Surface engineering, 4(3), pp. 239–249.

Gay, P.A. et al. (2007) 'Characterisation and mechanical properties of electroless NiP–ZrO_2 coatings', Surface and Coatings Technology, 202(4–7), pp. 1167–1171. Available at: https://doi.org/10.1016/j.surfcoat.2007.05.081.

Georgiza, E., Gouda, V. and Vassiliou, P. (2017) 'Production and properties of composite electroless Ni-B-SiC coatings', Surface and Coatings Technology, 325, pp. 46–51. Available at: https://doi.org/10.1016/j.surfcoat.2017.06.019.

Ghaderi, M. et al. (2016) 'Investigation of High Temperature Wear Resistance of Electroless Nickel Coating with Different Contents of Phosphorous', Prot Met Phys Chem Surf, 52(3), pp. 538–542. Available at: https://doi.org/10.1134/S2070205116030126.

Gilley, K.L. et al. (2012) 'Heat Treatments Modify the Tribological Properties of Nickel Boron Coatings', Acs Applied Materials & Interfaces, 8, pp. 3069–76. Available at: https://doi.org/10.1021/am3004297.

Goettems, F.S. et al. (2017) 'Wear Behaviour of Electroless heat Treated Ni-P Coatings as Alternative to Electroplated hard Chromium Deposits', 20(5), pp. 1300–1308, Available at: https://doi.org/10.1590/1980-5373-MR-2017-0347.

Goldenstein, A.W. et al. (1957) 'Structure of Chemically Deposited Nickel', Journal of The Electrochemical Society, pp. 104–110, Available at: https://doi.org/10.1149/1.2428503.

Gorbunova, K.M., Ivanov, M. V and Moiseev, V.P. (1973) 'Electroless Deposition of Nickel-Boron Alloys', Journal of The Electrochemical Society, 120(5), pp. 613–618. Available at: https://doi.org/10.1149/1.2403514

Gould, A.J., Boden, P.J. and Harris, S.J. (1981) 'Phosphorus distribution in electroless nickel deposits', Surface Technology, 12(1), pp. 93–102. Available at: https://doi.org/10.1016/0376-4583(81)90140-0.

Grosjean, A. et al. (2001) 'Hardness, friction and wear characteristics of nickel-SiC electroless composite deposits', Surface and Coatings Technology, 137(1) pp. 92–96, Available at: https://doi.org/10.1016/S0257-8972(00)01088-4.

Gül, H. et al. (2009) 'Characteristics of electro-co-deposited Ni–Al_2O_3 nano-particle reinforced metal matrix composite (MMC) coatings', Wear, 267(5–8), pp. 976–990. Available at: https://doi.org/10.1016/j.wear.2008.12.022.

Gültekin, D., Duru, E. and Akbulut, H. (2021) 'Improved wear behaviors of lead-free electroless Ni B and Ni-B/CeO2 composite coatings', Surface and Coatings Technology, 422, p. 127525. Available at: https://doi.org/10.1016/j.surfcoat.2021.127525.

Gutzeit, G. (1955) 'Industrial Nickel Coating by Chemical Catalytic Reduction', Transactions of the IMF, 33(1), pp. 383–423. Available at: https://doi.org/10.1080/00202967.1955.11869708.

Gutzeit, G. (1959) 'Catalytic Nickel Deposition from Aqueous Solution.', Plating and surface finishing, 46, pp. 1158–1164.

Gutzeit, G. and Mapp, E.T. (1954) 'Chemical Nickel Plating', Anti-Corrosion Methods and Materials, 3(10), pp. 331–336. Available at: https://doi.org/doi.org/10.1108/eb019232.

Hamid, Z Abdel, Hassan, H.B. and Attyia, A.M. (2010) 'Surface & Coatings Technology Influence of deposition temperature and heat treatment on the performance of electroless Ni-B films', 205, pp. 2348–2354. Available at: https://doi.org/10.1016/j.surfcoat.2010.09.025.

Hsu, C. et al. (2015) 'Applied Surface Science The effect of incorporated self-lubricated BN (h) particles on the tribological properties of Ni – P / BN (h) composite coatings', Applied Surface Science, 357, pp. 1727–1735. Available at: https://doi.org/10.1016/j.apsusc.2015.09.207.

Hu, R. et al. (2018) 'Deposition Process and Properties of Electroless Ni-P-Al_2O_3 Composite Coatings on Magnesium Alloy', Nanoscale Research Letters, 13(1), p. 198. Available at: https://doi.org/10.1186/s11671-018-2608-0.

Hu, X.G. et al. (2009) 'coatings and their corrosion properties', 25(5), pp. 361–366. Available at: https://doi.org/10.1179/174329408X282532.

Hunter, R.J. (2013) Zeta potential in colloid science: principles and applications. Academic press.

International Standardization Organization (2012) 'Colloidal systems - Methods for zeta-potential determination — Part 1: Electroacoustic and electrokinetic phenomena', \ISO 13099-1:2012(E).

Islam, M. et al. (2015) ‘Electroless Ni-P / SiC nanocomposite coatings with small amounts of SiC nanoparticles for superior corrosion resistance and hardness’, Journal of Materials Engineering and Performance, 24(12), pp. 4835–4843. Available at: https://doi.org/10.1007/s11665-015-1801-x.

Islam, M. and Shehbaz, T. (2011) ‘Effect of synthesis conditions and post-deposition treatments on composition and structural morphology of medium-phosphorus electroless Ni-P films’, Surface and Coatings Technology, 205(19), pp. 4397–4400. Available at: https://doi.org/10.1016/j.surfcoat.2011.03.042.

Jiang, J., Oberdörster, G. and Biswas, P. (2009) ‘Characterization of size, surface charge, and agglomeration state of nanoparticle dispersions for toxicological studies’, Journal of Nanoparticle Research, 11(1), pp. 77–89. Available at: https://doi.org/10.1007/s11051-008-9446-4.

Kanta, A.-F. et al. (2010) ‘Nickel–boron electrochemical properties investigations’, Journal of Alloys and Compounds, 505(1), pp. 151–156. Available at: https://doi.org/10.1016/j.jallcom.2010.05.168.

Kanta, A.-F., Vitry, V. and Delaunois, F. (2009) ‘Effect of thermochemical and heat treatments on electroless nickel–boron’, Materials Letters, 63(30), pp. 2662–2665. Available at: https://doi.org/10.1016/j.matlet.2009.09.031.

Karthikeyan, S. and Ramamoorthy, B. (2014) ‘Applied Surface Science Effect of reducing agent and nano Al_2O_3 particles on the properties of electroless Ni – P coating’, Applied Surface Science, 307, pp. 654–660. Available at: https://doi.org/10.1016/j.apsusc.2014.04.092.

Kaya, B. et al. (2008) ‘Preparation and Properties of Electroless Ni-B and Ni-B Nanocomposite Coatings’, Proceedings of the World Congress on Engineering and Computer Science (WCECS 2008).

Kreye, H., Muller, H.-H. and Petzel, T.H. (1986) ‘Structure and Thermal Stability of Chemically Deposited Nickel--Phosphorus Coatings’, Galvanotechnik, 77(3), pp. 561–567.

Krishnan, K.H. et al. (2006) ‘An overall aspect of electroless Ni-P depositions—A review article’, Metallurgical and Materials Transactions A, 37(6), pp. 1917–1926. Available at: https://doi.org/10.1007/s11661-006-0134-7.

Krishnaveni, K., Narayanan, T.S.N.S. and Seshadri, S.K. (2008) ‘Electrodeposited Ni – B – Si 3 N 4 composite coating: Preparation and evaluation of its characteristic properties’, Journal of Alloys and Compounds, 466, pp. 412–420. Available at: https://doi.org/10.1016/j.jallcom.2007.11.104.

Krishnaveni, K., Sankara Narayanan, T.S.N. and Seshadri, S.K. (2005) 'Electroless Ni–B coatings: preparation and evaluation of hardness and wear resistance', Surface and Coatings Technology, 190(1), pp. 115–121. Available at: https://doi.org/10.1016/j.surfcoat.2004.01.038.

Krishnaveni, K., Sankara Narayanan, T.S.N. and Seshadri, S.K. (2012) 'Electroless Ni-B-Si3N4 Composite Coating: Deposition and Evaluation of Its Characteristic Properties', Synthesis and Reactivity in Inorganic, Metal-Organic, and Nano-Metal Chemistry, 42(7), pp. 920–927. Available at: https://doi.org/10.1080/15533174.2011.618475.

Kumar, A. and Dixit, C.K. (2017) 'Methods for characterization of nanoparticles', in Advances in Nanomedicine for the Delivery of Therapeutic Nucleic Acids. Elsevier Inc., pp. 44–58. Available at: https://doi.org/10.1016/B978-0-08-100557-6.00003-1.

Kundu, S., Das, S.K. and Sahoo, P. (2018) 'A parametric investigation of high temperature friction performance of electroless Ni-P deposits', Materials Today: Proceedings, 5(2), pp. 8547–8556. Available at: https://doi.org/10.1016/j.matpr.2017.11.552.

Kundu, S., Das, S.K. and Sahoo, P. (2021) 'Influence of Alumina Particles on Tribology of Autocatalytic Ni-P Coatings at High Temperature', International Journal of Surface Engineering and Interdisciplinary Materials Science, 9(1), pp. 1–25. Available at: https://doi.org/10.4018/IJSEIMS.2021010101.

Laha, T. et al. (2005) 'Synthesis of nanostructured spherical aluminum oxide powders by plasma engineering', Metallurgical and Materials Transactions A: Physical Metallurgy and Materials Science, 36 A (2), pp. 301–309. Available at: https://doi.org/10.1007/s11661-005-0303-0.

Lee, J.Y. and Lee, H.K. (2018) 'Electroless Ni-P metallization on palladium activated polyacrylonitrile (PAN) fiber by using a drying process', Materials Chemistry and Physics, 204, pp. 257–261. Available at: https://doi.org/10.1016/j.matchemphys.2017.10.048.

Leo, O.A., Staia, M.H. and Hintermann, H.E. (2005) 'Wear mechanism of Ni-P-BN (h) composite autocatalytic coatings', 200, pp. 1825–1829. Available at: https://doi.org/10.1016/j.surfcoat.2005.08.061.

Li, B. et al. (2018) 'Influence of alumina nanoparticles on microstructure and properties of Ni-B composite coating', Journal of Alloys and Compounds, 762, pp. 133–142. Available at: https://doi.org/10.1016/j.jallcom.2018.05.227.

Li, D. et al. (2017) 'Enhancing structure integrity and corrosion resistance of Mg alloy by a two-step deposition to avoid F ions etching to nano-SiO_2 reinforcement', Journal of Alloys and Compounds, 705, pp. 70–78. Available at: https://doi.org/10.1016/j.jallcom.2017.01.204.

Li, J. et al. (2006) ‘Studies of the porosity in electroless nickel deposits on magnesium alloy’, Applied Surface Science, 252(8), pp. 2839–2846. Available at: https://doi.org/10.1016/j.apsusc.2005.04.028.

Liu, Y.Y. et al. (2007) ‘Synthesis and tribological behavior of electroless Ni – P – WC nanocomposite coatings’, 201, pp. 7246–7251. Available at: https://doi.org/10.1016/j.surfcoat.2007.01.035.

Loto, C.A. (2016) ‘Electroless Nickel Plating – A Review’, Silicon, 8, pp. 177–186. Available at: https://doi.org/10.1007/s12633-015-9367-7.

Lu, G.W. and Gao, P. (2010) ‘Emulsions and Microemulsions for Topical and Transdermal Drug Delivery’, in Handbook of Non-Invasive Drug Delivery Systems. Elsevier, pp. 59–94. Available at: https://doi.org/10.1016/b978-0-8155-2025-2.10003-4.

Luo, H. et al. (2015) ‘Surface & Coatings Technology Development of electroless Ni – P / nano-WC composite coatings and investigation on its properties’, Surface & Coatings Technology, 277, pp. 99–106. Available at: https://doi.org/10.1016/j.surfcoat.2015.07.011.

Ma, C. et al. (2014) ‘Effect of heat treatment on structures and corrosion characteristics of electroless Ni-P-SiC nanocomposite coatings’, Ceramics International, 40(7 PART A), pp. 9279–9284. Available at: https://doi.org/10.1016/j.ceramint.2014.01.150.

Maclean, J.D. and Karten, S.M. (1954) ‘A practical application of electroless nickel plating’, Plating, 41(11), pp. 1284–1287.

Maestro, A. et al. (2015) ‘Particle and Particle-Surfactant Mixtures at Fluid Interfaces: Assembly, Morphology, and Rheological Description’, Advances in Condensed Matter Physics. Edited by C. Rosenblatt, 2015. Available at: https://doi.org/10.1155/2015/917516.

Mahdavi, S., Asghari-Alamdari, A. and Zolola-Meibodi, M. (2020) ‘Effect of alumina particle size on characteristics, corrosion, and tribological behavior of Co/Al_2O_3 composite coatings’, Ceramics International, 46(4), pp. 5351–5359. Available at: https://doi.org/10.1016/j.ceramint.2019.10.289.

De Minjer, C.H. and Brenner, A. (1957) ‘Studies on electroless nickel plating’, Plating, 44(12), pp. 1297–1305.

Makkar, P., Agarwala, R.C. and Agarwala, V. (2014) ‘Wear characteristics of mechanically milled TiO 2 nanoparticles incorporated in electroless Ni – P coatings’, Advanced Powder Technology, 25(5), pp. 1653–1660. Available at: https://doi.org/10.1016/j.apt.2014.05.018.

Mallory, G. (1991) ‘The fundamental aspects of electroless nickel plating’, electroless plating: fundamentals and applications, pp. 1–56.

Mallory, G.O. and Altura, D. (1983) 'The effect of stress on the properties of electroless nickel-phosphorus deposits', SAE Technical Papers, pp. 1-9. Available at: https://doi.org/10.4271/830693.

Mandal, D., Sharma, L.K. and Mukherjee, S. (2016) 'Defect-induced weak ferromagnetism in transition metal-doped ZnO nanoparticles', Applied Physics A: Materials Science and Processing, 122(12), pp. 1–10. Available at: https://doi.org/10.1007/s00339-016-0573-y.

Manning, P.E. (1980) 'The effect of scan rate on pitting potentials of high performance alloys in acidic chloride solution', Corrosion, 36(9), pp. 468–474.

Matsubara, H. et al. (2007) 'Co-deposition mechanism of nanodiamond with electrolessly plated nickel films', 52, pp. 3047–3052. Available at: https://doi.org/10.1016/j.electacta.2006.09.043.

Mukhopadhyay, A., Barman, T.K. and Sahoo, P. (2018) 'Effect of Heat Treatment on the Characteristics of Electroless Ni-B, Ni-B-W and Ni-B-Mo Coatings', Materials Today: Proceedings, 5(2), pp. 3306–3315. Available at: https://doi.org/10.1016/j.matpr.2017.11.573.

Mukhopadhyay, A. and Sahoo, S. (2019) 'Corrosion protection of reinforcement steel rebars by the application of electroless nickel coatings', Engineering Research Express, 1(1), p. 015021. Available at: https://doi.org/10.1088/2631-8695/ab35f0.

Mukhopadhyay, A. and Sahoo, S. (2021a) 'Corrosion performance of steel rebars by application of electroless Ni-P-W coating: An optimization approach using grey relational analysis', FME Transactions, 49(2), pp. 445–455. Available at: https://doi.org/10.5937/fme2102445M.

Mukhopadhyay, A. and Sahoo, S. (2021b) 'Optimized electroless Ni-Cu-P coatings for corrosion protection of steel rebars from pitting attack of chlorides', Engineering Transactions, 69(3), pp. 315–332. Available at: https://doi.org/10.24423/EngTrans.1367.20210826.

Mukhopadhyay, A. and Sahoo, S. (2022a) 'A Grey-Fuzzy Based Approach for the Optimization of Corrosion Resistance of Rebars Coated with Ternary Electroless Nickel Coatings', Journal of Soft Computing in Civil Engineering, 6(2), pp. 107–127. Available at: https://doi.org/10.22115/SCCE.2022.326903.1401.

Mukhopadhyay, A. and Sahoo, S. (2022b) 'Electroless Nickel Phosphorus Coatings to Mitigate the Corrosion of Construction Steel', International Journal of Surface Engineering and Interdisciplinary Materials Science, 10(1), pp. 1–10. Available at: https://doi.org/10.4018/IJSEIMS.311415.

Mukhopadhyay, A. and Sahoo, S. (2022c) 'Improving corrosion resistance of reinforcement steel rebars exposed to sulphate attack by the use of electroless nickel coatings', European Journal of Environmental and Civil Engineering, 26(11), pp. 5180–5195. Available at: https://doi.org/10.1080/19648189.2021.1886177.

Murty, P.R. et al. (2015) ‘Effect of reinforcement of nano Al_2O_3 on mechanical properties of’, Materials Today: Proceedings, 2(4–5), pp. 3712–3717. Available at: https://doi.org/10.1016/j.matpr.2015.07.152.

Narayanan, R. and Seshadri, S.K. (2001) ‘Chromium-Ceria electrodeposition using nitrate additives’, Metal finishing, 99(2), pp. 84–89. Available at: https://doi.org/10.1016/S0026-0576(01)81009-6

Narayanan, T.S.N.S. and Seshadri, S.K. (2004) ‘Formation and characterization of borohydride reduced electroless nickel deposits’, 365, pp. 197–205. Available at: https://doi.org/10.1016/S0925-8388(03)00680-7.

Novák, M., Vojtěch, D. and Vítů, T. (2010) ‘Influence of heat treatment on tribological properties of electroless Ni–P and Ni–P–Al2O3 coatings on Al–Si casting alloy’, Applied Surface Science, 256(9), pp. 2956–2960. Available at: https://doi.org/10.1016/j.apsusc.2009.11.057.

Oraon, B. (2007) ‘Materials & Design Parametric optimization and prediction of electroless Ni – B deposition’, 28, pp. 2138–2147. Available at: https://doi.org/10.1016/j.matdes.2006.05.017.

Pal, S. and Jayaram, V. (2018) ‘Effect of Microstructure on the Hardness and Dry Sliding Behavior of Electroless Ni-B Coating’, Materialia [Preprint]. Available at: https://doi.org/10.1016/j.mtla.2018.09.004.

Palaniappa, M. and Seshadri, S.K. (2008) ‘Friction and wear behavior of electroless Ni–P and Ni–W–P alloy coatings’, Wear, 265(5–6), pp. 735–740. Available at: https://doi.org/10.1016/j.wear.2008.01.002.

Park, I.C. and Kim, S.J. (2018) ‘Cavitation erosion behavior in seawater of electroless Ni-P coating and process optimization using Taguchi method’, Applied Surface Science [Preprint]. Available at: https://doi.org/10.1016/j.apsusc.2018.02.033.

Parker, K. (2018) ‘Internal Stress Measurements of Electroless Nickel Coatings by the Rigid Strip Method’, in Testing of Metallic and Inorganic Coatings. 100 Barr Harbor Drive, PO Box C700, West Conshohocken, PA 19428-2959: ASTM International, pp. 111-111–12. Available at: https://doi.org/10.1520/STP20032S.

Parker, K. and Shah, H. (1970) ‘The Stress of Electroless Nickel Deposits on Beryllium’, Journal of The Electrochemical Society, 117(8), p. 1091. Available at: https://doi.org/10.1149/1.2407728.

Purohit, P. and Vagge, S.T. (2016) ‘Evaluation of alumina incorporated combined ceramic layer thermal barrier coating’, Surface and Coatings Technology, 307, pp. 871–878. Available at: https://doi.org/10.1016/j.surfcoat.2016.10.022.

Rabizadeh, T. and Allahkaram, S.R. (2011) 'Corrosion resistance enhancement of Ni-P electroless coatings by incorporation', Materials and Design, 32(1), pp. 133–138. Available at: https://doi.org/10.1016/j.matdes.2010.06.021.

Rabizadeh, T., Allahkaram, S.R. and Zarebidaki, A. (2010) 'An investigation on effects of heat treatment on corrosion properties of Ni-P electroless nano-coatings', Materials and Design, 31(7), pp. 3174–3179. Available at: https://doi.org/10.1016/j.matdes.2010.02.027.

Ranganatha, S., Venkatesha, T. V and Vathsala, K. (2012) 'Process and properties of electroless Ni-Cu-P-ZrO_2 nanocomposite coatings', Materials Research Bulletin, 47(3), pp. 635–645. Available at: https://doi.org/10.1016/j.materresbull.2011.12.024.

Rao, Q.L. et al. (2005) 'Microstructure evolution of electroless Ni-B film during its depositing process', Applied Surface Science, 240(1–4), pp. 28–33. Available at: https://doi.org/10.1016/j.apsusc.2004.07.059.

Riedel, W. (1991) Electroless nickel plating. Metals Park, Ohio: ASM International; Stevenage, England: Finishing Publications Ltd.

Ruan, H.D., Frost, R.L. and Kloprogge, J.T. (2001) 'Comparison of Raman spectra in characterizing gibbsite, bayerite, diaspore and boehmite', Journal of Raman Spectroscopy, 32(9), pp. 745–750. Available at: https://doi.org/10.1002/jrs.736.

Sadreddini, S. and Afshar, A. (2014) 'Applied Surface Science Corrosion resistance enhancement of Ni-P-nano SiO_2 composite coatings on aluminum', Applied Surface Science, 303, pp. 125–130. Available at: https://doi.org/10.1016/j.apsusc.2014.02.109.

Sadreddini, S., Ardakani, S.R. and Rassaee, H. (2017) 'Corrosion Behavior and Microhardness of Ni-P-SiO_2-Al_2O_3 Nano-composite Coatings on Magnesium Alloy', Journal of Materials Engineering and Performance [Preprint]. Available at: https://doi.org/10.1007/s11665-017-2632-8.

Sahoo, P. and Das, S.K. (2011) 'Tribology of electroless nickel coatings - A review', Materials and Design, 32(4), pp. 1760–1775. Available at: https://doi.org/10.1016/j.matdes.2010.11.013.

Sahoo, S. (ed.) (2021) Recent Advances in Layered Materials and Structures. Singapore: Springer Singapore (Materials Horizons: From Nature to Nanomaterials). Available at: https://doi.org/10.1007/978-981-33-4550-8.

Sarbishei, S., Faghihi Sani, M.A. and Mohammadi, M.R. (2016) 'Effects of alumina nanoparticles concentration on microstructure and corrosion behavior of coatings formed on titanium substrate via PEO process', Ceramics International, 42(7), pp. 8789–8797. Available at: https://doi.org/10.1016/j.ceramint.2016.02.120.

Sarret, M., Müller, C. and Amell, A. (2006) 'Electroless NiP micro- and nano-composite coatings', Surface and Coatings Technology, 201(1–2), pp. 389–395. Available at: https://doi.org/10.1016/j.surfcoat.2005.11.127.

Sha, W., Wu, X. and Keong, K.G. (2011) 'Introduction to electroless copper and nickel–phosphorus (Ni–P) depositions', in Electroless Copper and Nickel–Phosphorus Plating. Elsevier.

Shah, R. et al. (2014) 'Anticonvulsant hypersensitivity syndrome associated with carbamazepine administration: Case series', Journal of Pharmacology and Pharmacotherapeutics, 5(1), p. 59. Available at: https://doi.org/10.4103/0976-500X.124428.

Shakoor, R.A. et al. (2014) 'Properties of electrodeposited Ni–B–Al2O3 composite coatings', Materials & Design, 64, pp. 127–135. Available at: https://doi.org/10.1016/j.matdes.2014.07.026.

Sharma, A. and Singh, A.K. (2011) 'Corrosion and Wear Resistance Study of Ni-P and Ni-P-PTFE Nanocomposite Coatings', 1(3). Available at: https://doi.org/10.2478/s13531-011-0023-8.

Sharma, A. and Singh, A.K. (2013) 'Electroless Ni-P and Ni-P-Al2O3 Nanocomposite Coatings and Their Corrosion and Wear Resistance', 22(January), pp. 176–183. Available at: https://doi.org/10.1007/s11665-012-0224-1.

Sharma, Sarika and Sharma, Sulaxna (2016) 'Co-deposition of Synthesized ZnO Nanoparticles into Ni-P Matrix Using Electroless Technique and Their Corrosion Study', Journal of Materials Engineering and Performance, 25(10), pp. 4383–4393. Available at: https://doi.org/10.1007/s11665-016-2292-0.

Shi, L.T. et al. (2016) 'Effects of cobalt content on mechanical and corrosion properties of electroless Ni-Co-P / TiN nanocomposite coatings', 67(10), pp. 1–8. Available at: https://doi.org/10.1002/maco.201608844.

Soleimani, R. et al. (2015) 'Journal of Industrial and Engineering Chemistry Development of mathematical model to evaluate microstructure and corrosion behavior of electroless Ni – P / nano-SiC coating deposited on 6061 aluminum alloy', Journal of Industrial and Engineering Chemistry, 23, pp. 328–337. Available at: https://doi.org/10.1016/j.jiec.2014.09.002.

Sosa Domínguez, A. et al. (2017) 'Characterization and corrosion resistance of electroless black Ni-P coatings of double black layer on carbon steel', Surface and Coatings Technology, 326, pp. 192–199. Available at: https://doi.org/10.1016/j.surfcoat.2017.07.044.

Sribalaji, M. et al. (2016) 'Nanoindentation and nanoscratch behavior of electroless deposited nickel-phosphorous coating', Materials Chemistry and Physics, 177, pp. 220–228. Available at: https://doi.org/10.1016/j.matchemphys.2016.04.022.

Srinivasan, K.N. et al. (2010a) ‘Studies on development of electroless Ni–B bath for corrosion resistance and wear resistance applications’, Surface Engineering, 26(3), pp. 153–158. Available at: https://doi.org/10.1179/174329409X409468.

Srinivasan, K.N. et al. (2010b) ‘Studies on development of electroless Ni–B bath for corrosion resistance and wear resistance applications’, Surface Engineering, 26(3), pp. 153–158. Available at: https://doi.org/10.1179/174329409X409468.

Srivastava, A. et al. (1992) ‘Factors Influencing the Deposition Rate of Ni--B Electroless Films’, Zeitschrift fur Metallkunde(Germany), 83(4), pp. 251–253.

Sudagar, J., Lian, J. and Sha, W. (2013) ‘Electroless nickel, alloy, composite and nano coatings – A critical review’, Journal of Alloys and Compounds, 571, pp. 183–204. Available at: https://doi.org/10.1016/j.jallcom.2013.03.107.

Szunerits, S. and Thouin, L. (2007) ‘Microelectrode Arrays’, in Handbook of Electrochemistry. Elsevier, pp. 391–428. Available at: https://doi.org/10.1016/B978-044451958-0.50023-9.

Thomas Evans, W. and Schlesinger, M. (1994) ‘The Effect of Solution pH and Heat-Treatment on the Properties of Electroless Nickel Boron Films’, Journal of the Electrochemical Society, 141(1), pp. 78–82. Available at: https://doi.org/10.1149/1.2054713.

Tomlinson, W.J. and Carroll, M.W. (1990) ‘Substrate roughness, deposit thickness and the corrosion of electroless nickel coatings’, Journal of materials science, 25(12), pp. 4972–4976.

Townsend, H.E. (1994) ASM Handbook: Vol 05 Surface Engineering, ASM Handbook. Available at: https://doi.org/10.1361/asmhba000.

Tsujikawa, M. et al. (2005) ‘Friction and Wear Behavior of Laser Irradiated Amorphous Metal’, Journal of Metastable and Nanocrystalline Materials, 24–25, pp. 375–378. Available at: https://doi.org/10.4028/www.scientific.net/JMNM.24-25.375.

Vijayanand, M. et al. (2021) ‘Modelling and optimisation of hardness in citrate stabilised electroless nickel boron (ENi-B) coatings using back propagation neural network – Box Behnken design and simulated annealing – genetic algorithm’, Transactions of the IMF, 99(5), pp. 253–264. Available at: https://doi.org/10.1080/00202967.2021.1898172.

Vitry,V., Delaunois, F. and Dumortier, C. (2008) ‘Mechanical properties and scratch test resistance of nickel–boron coated aluminium alloy after heat treatments’, Surface and Coatings Technology, 202(14), pp. 3316–3324. Available at: https://doi.org/10.1016/j.surfcoat.2007.12.001.

Vitry, V. et al. (2012) ‘Applied Surface Science Experimental study on the formation and growth of electroless nickel – boron coatings from borohydride-reduced bath on mild steel’, 263, pp. 640–647.

Vitry, V. et al. (2012a) ‘Structural state of electroless nickel-boron deposits (5wt.% B): Characterization by XRD and TEM’, Surface and Coatings Technology, 206(16), pp. 3444–3449. Available at: https://doi.org/10.1016/j.surfcoat.2012.02.003.

Vitry, V. et al. (2012b) ‘Structural state of electroless nickel-boron deposits (5wt.% B): Characterization by XRD and TEM’, Surface and Coatings Technology, 206(16), pp. 3444–3449. Available at: https://doi.org/10.1016/j.surfcoat.2012.02.003.

Vitry, V. et al. (2022) ‘Recent advances in electroless nickel-boron coatings’, Surface and Coatings Technology, 429, p. 127937. Available at: https://doi.org/10.1016/j.surfcoat.2021.127937.

Vitry, V., Kanta, A.F. and Delaunois, F. (2011) ‘Mechanical and wear characterization of electroless nickel-boron coatings’, Surface and Coatings Technology, 206(7), pp. 1879–1885. Available at: https://doi.org/10.1016/j.surfcoat.2011.08.008.

Wang, H.L., Liu, L.Y. and Jiang, W.F. (2014) ‘Effect of novel ternary ligand system on acidic electroless Ni-P plating on AZ91D magnesium alloy’, Transactions of Nonferrous Metals Society of China (English Edition), 24(9), pp. 3014–3022. Available at: https://doi.org/10.1016/S1003-6326(14)63439-7.

Wang, S. et al. (2015) ‘Applied Surface Science Microstructure and mechanical properties of Ni-P-Si3N4 nanowire electroless composite coatings’, 357, pp. 328–332, Available at: https://doi.org/10.1016/j.apsusc.2015.09.011.

Wang, W. et al. (2016) ‘Ductile electroless Ni-P coating onto flexible printed circuit board’, Applied Surface Science, 367, pp. 528–532. Available at: https://doi.org/10.1016/j.apsusc.2016.01.254.

Wang, Y. et al. (2015) ‘Duplex Ni – P – ZrO_2 / Ni – P electroless coating on stainless steel’, Journal of Alloys and Compounds, 630, pp. 189–194. Available at: https://doi.org/10.1016/j.jallcom.2015.01.064.

Wang, Y. et al. (2015) ‘Microstructure and properties of sol-enhanced Ni-Co-TiO_2 nano-composite coatings on mild steel’, Journal of Alloys and Compounds, 649, pp. 222–228. Available at: https://doi.org/10.1016/j.jallcom.2015.07.147.

Watanabe, T. and Tanabe, Y. (1983) ‘The Lattice Images of Amorphous-like Ni-B Alloy Films Prepared by Electroless Plating Method’, Transactions of the Japan Institute of Metals, 24(6) pp. 396–404, Available at: https://doi.org/10.2320/matertrans1960.24.396.

Wu, X. et al. (2015) ‘Surface & Coatings Technology Improving the properties of 211Z Al alloy by enhanced electroless Ni – P – TiO_2 nanocomposite coatings with TiO_2 sol’, 270, pp. 170–174. Available at: https://doi.org/10.1016/j.surfcoat.2015.03.006.

Xie, Z. and Shan, S. (2017) 'Nanocontainers-enhanced self-healing Ni coating for corrosion protection of Mg alloy', Journal of Materials Science. 53(5), pp. 3744-3755. Available at: https://doi.org/10.1007/s10853-017-1774-2.

Xu, H. et al. (2005) 'Synthesis and properties of electroless Ni -P-Nanometer Diamond composite coatings', 191, pp. 161–165. Available at: https://doi.org/10.1016/j.surfcoat.2004.03.045.

Xu, M. et al. (2017) 'CO_2/N_2 triggered switchable Pickering emulsions stabilized by alumina nanoparticles in combination with a conventional anionic surfactant', RSC Advances, 7(47), pp. 29742–29751. Available at: https://doi.org/10.1039/c7ra03722h.

Yang, H. et al. (2017) 'Reinforcement Size Dependence of Load Bearing Capacity in Ultrafine-Grained Metal Matrix Composites', Metallurgical and Materials Transactions A, 48(9), pp. 4385–4392. Available at: https://doi.org/10.1007/s11661-017-4186-7.

Yang, Y., Chen, W. and Zhou, C. (2011) 'Fabrication and characterization of electroless Ni – P – ZrO_2 nano-composite coatings', pp. 19–26. Available at: https://doi.org/10.1007/s13204-011-0003-6.

Yazdani, S, Tima, R. and Mahboubi, F. (2018) 'Applied Surface Science Investigation of wear behavior of as-plated and plasma-nitrided Ni-B-CNT electroless having di ff erent CNTs concentration', Applied Surface Science, 457(July), pp. 942–955. Available at: https://doi.org/10.1016/j.apsusc.2018.07.020.

Yazdani, S., Tima, R. and Mahboubi, F. (2018) 'Investigation of wear behavior of as-plated and plasma-nitrided Ni-B-CNT electroless having different CNTs concentration', Applied Surface Science, 457, pp. 942–955. Available at: https://doi.org/10.1016/j.apsusc.2018.07.020.

Yu, L., Huang, W. and Zhao, X. (2011) 'Preparation and characterization of Ni – P – nanoTiN electroless composite coatings', Journal of Alloys and Compounds, 509(10), pp. 4154–4159. Available at: https://doi.org/10.1016/j.jallcom.2011.01.025.

Ziyuan, S., Deqing, W. and Zhimin, D. (2006) 'Nanocrystalline Ni-B coating surface strengthening pure copper', Applied Surface Science, 253(3), pp. 1051–1054. Available at: https://doi.org/10.1016/j.apsusc.2005.12.169.

Publications from the thesis

J. Inst. Eng. India Ser. D
https://doi.org/10.1007/s40033-023-00508-4

ORIGINAL CONTRIBUTION

Tribological Behavior, Mechanical Properties and Electrochemical Corrosion Response of Ultrasonically Assisted TiO_2 Reinforced Electroless Ni–B Coatings

Deviprasanna Mohanty[1] · Tapan Kumar Barman[1] · Prasanta Sahoo[1]

Received: 19 May 2023 / Accepted: 18 June 2023

Abstract This study involves the investigation into the effect of nano-TiO_2 (Titania) reinforced into electroless Ni–B coating. The electroless coating method used in the study involves the addition of an ultrasonicated colloidal solution of nano-Titania into the electroless coating bath during deposition. Four sets of coating are prepared for the study with 0 g/l, 5 g/l, 10 g/l and 15 g/l concentrations of Titania. These as-deposited coatings are characterized using energy-dispersive X-ray analysis, X-ray diffractometry and scanning electron microscopy. The samples are also subjected to mechanical property evaluation using microhardness test, scratch test and nanoindentation test. Tribological behaviour and corrosion resistance of the coatings are evaluated in pin-on-disk tribometer and electrochemical corrosion test, respectively. The titania concentration of 10 g/l performs best among the coatings under study. The coating with titania concentration of 10 g/l shows an improvement in scratch hardness of nearly 2 times as compared to the binary Ni–B coating. The same coating when compared to the unreinforced coating also shows an increase of elastic modulus by nearly 1.5 times. The electrochemical corrosion resistance as well as the wear resistance of the same coating with a titania concentration of 10 g/l also show improvement over unreinforced Ni–B coating. This study provides a detailed analysis of the TiO_2 reinforced Ni–B coating based on their tribo-mechanical properties. Also, a saturation concentration of TiO_2 is established beyond which the coating properties start to deteriorate.

✉ Prasanta Sahoo
psjume@gmail.com

[1] Department of Mechanical Engineering, Jadavpur University, Kolkata, India

Published online: 29 June 2023

Keywords Electroless · Ni–B · TiO_2 · Mechanical properties · Wear · Corrosion

Introduction

The process of electroless coating deposition is characterized as an autocatalytic process. In this type of deposition process, a source of metal ion is reduced by a reducing agent in a chemical bath. These metallic ions then get deposited on an activated substrate surface. Electroless nickel (EN) coatings are known for their excellent thickness homogeneity and ability to conform to complex geometries. The two predominant types of EN coatings are electroless nickel phosphorus (ENP) and electroless nickel boron (ENB). The discovery of ENP dates back to 1946 when Brenner and Riddell [1] first observed its properties. Warf and Schaltegger [2] in 1955 developed the first ENB coating. ENP coatings are generally known for their corrosion protection ability and ENB coatings are more popular for their wear resistance and hardness properties. Besides, as-deposited Ni–B binary and composite coatings also show good electrical properties and solderability [3–12]. The electroless plating process is relied upon by numerous industries, including those involved in electromagnetic shielding, decorative platings, chemical production, automotive manufacturing, and aerospace technology. Additionally, various other sectors, such as computer manufacturing, food and beverage industry, plastic, printing and petrochemical industries, utilize electroless plating as well [13–16].

Compared to pure EN coatings, Ni–B coatings exhibit higher chemical stability [17]. The incorporation of nanoparticles such as alumina, silica, silicon carbide, and others has the potential to enhance both the tribo-mechanical properties as well as the electrochemical corrosion response of

This page is intentionally left blank

ARTICLE IN PRESS

Materials Today: Proceedings xxx (xxxx) xxx

Contents lists available at ScienceDirect

Materials Today: Proceedings

journal homepage: www.elsevier.com/locate/matpr

Scratch and corrosion behaviour study of electroless Ni-B reinforced with ultrasonicated nano TiO_2

Deviprasanna Mohanty *, Ajoy Kumar Bhowmick, Tapan Kumar Barman, Prasanta Sahoo

Department of Mechanical Engineering, Jadavpur University, Kolkata 70003, India

ARTICLE INFO

Article history:
Available online xxxx

Keywords:
electroless Ni-B
Nanoparticles
Titania
Scratch
Corrosion

ABSTRACT

The present investigation is a study into the scratch and corrosion response of as-coated Ni-B-TiO_2 as compared to the as-deposited Ni-B coatings. Ultrasonicated nano TiO_2 particles were used to reinforce electroless Ni-B coatings. The presence of hard nano TiO_2 particles improved the scratch hardness of the Nickel-Boron-TiO_2 coatings. During the scratch test for an applied load of 20 N, the Nickel-Boron-TiO_2 coating showed a decrease of 42 % in scratch width as compared to the Ni-B coatings. Corrosion behavior also showed remarkable improvement with the addition of nanoparticles. As compared to the Nickel-Boron coatings, the corrosion potential E_{corr} improved by 5 % while the corrosion current density I_{corr} showed a 1.5-fold decrease for Ni-B- TiO_2 coatings. The double-layer capacitance C_{dl} which is a qualitative indicator of the porosities present in the coatings was nearly halved with the addition of TiO_2 nanoparticles. The specimen underwent SEM analysis for the morphological study and scratch testing to determine the scratch hardness and corrosion behaviour to identify the electrochemical response to a corrosive environment.

Selection and peer-review under responsibility of the scientific committee of the International Conference on Advances in Materials, Sensors and Microelectronic Devices.

1. Introduction

Electroless coatings are versatile coatings. The process involves an autocatalytic reaction with the deposition of electroless nickel/copper/nickel-phosphorus/nickel-boron, etc on an activated substrate. The application of electroless coatings varies from use in small gears to large cylinders used in printing machines. The varied applications may be attributed to a range of properties that the coatings possess such as high surface hardness, high elastic modulus, excellent resistance to a corrosive environment, and high wear resistance. To further improve the properties of these coatings several nanoparticles in the form of inorganic and organic inclusions have been embedded into the electroless nickel coatings. Nano-Diamond [1,2], Alumina [3–5], TiN [6], WO_3 [7], SiO_2 [8] are a few such examples. Maclean et al. [9] have observed the nano NiTi particles embedded in an electroless Ni-P matrix help to arrest crack growth.

The primary issue with the addition of any nanoparticles is the agglomeration of these particles due to their high surface energy. To avoid deagglomeration, methods such as magnetic stirring, ultrasonication, and rapid expansions from supercritical suspensions (RESS) have been used [10]. Ultrasonication is one of the cheapest and most effective options available to modern researchers [10,11]. Wang et al. [12] have shown a novel use of zirconia fibers in dentures. Novacovic et al. [13] incorporated TiO_2 in an electroless Ni-P bath and achieved a corrosion potential of -0.41 V. They reported a corrosion rate of 0.015 mm/year. The literature shows extensive studies into the electroless Ni-P-Titania (TiO_2) coatings but, Ni-B-nano Titania coatings have not been explored in detail for their mechanical and electrochemical behaviour. Ekmekci and Bulbul [8] have characterized the electroless Ni-B-TiO_2 (2.5 g/l) by the X-Ray diffraction method and found a predominately amorphous nature of the coating.

This research aims to successfully incorporate crystalline nano TiO_2 as hard particle inclusion to improve the mechanical properties of electroless Ni-B coatings. The presence of nano titania particles is expected to also improve the electrochemical properties simultaneously.

* Corresponding author.
E-mail address: deviprasannamohanty.me@gmail.com (D. Mohanty).

https://doi.org/10.1016/j.matpr.2023.03.353

Selection and peer-review under responsibility of the scientific committee of the International Conference on Advances in Materials, Sensors and Microelectronic Devices.

Please cite this article as: D. Mohanty, A.K. Bhowmick, T.K. Barman et al., Scratch and corrosion behaviour study of electroless Ni-B reinforced with ultrasonicated nano TiO_2, Materials Today: Proceedings, https://doi.org/10.1016/j.matpr.2023.03.353

This page is intentionally left blank

Jurnal Tribologi 30 (2021) 24-43

MYTRIBOS Malaysian Tribology Society

Jurnal Tribologi

Website : jurnaltribologi.mytribos.org e-issn: 2289-7232

Effect of incorporation of nano-alumina on tribo-mechanical behavior of electroless Ni-B coatings

Deviprasanna Mohanty, Tapan Kumar Barman, Prasanta Sahoo *

Department of Mechanical Engineering, Jadavpur University, 700032 Kolkata, INDIA.
*Corresponding author: psjume@gmail.com

KEYWORDS

Corrosion
Electroless Ni-B
Friction
Nano- alumina
Nano-indentation
Wear

ABSTRACT

Electroless Ni-B coatings find versatile use due to high hardness and wear resistance that gets enhanced due to incorporation of hard nanoparticles. However, incorporation of nanoparticles suffers from high degree of agglomeration owing to small size and high surface energy. The present investigation aims at the deposition of electroless Ni-B-nano Al_2O_3 coatings using Sodium Dodecyl Sulphate (SDS) as surfactant and attempts to find the optimum amount of nano-alumina powder for superior tribo-mechanical characteristics. Thus, electroless Ni-B-nano Al_2O_3 coatings were prepared with varying concentrations of nano-Al_2O_3 (0 g/l, 2.5 g/l, 5 g/l, 7.5 g/l, 10 g/l, 12.5 g/l) in a chemical bath. To minimize agglomeration of alumina nanoparticles, ultrasonication technique was used. Coatings were characterized by Scanning electron microscopy (SEM), X-Ray diffraction (XRD) and Raman spectroscopy. Hardness, elastic modulus, wear resistance and corrosion resistance of the coatings were evaluated. Wear resistance and corrosion properties of the coatings show an improvement with the increase in the concentration of nanoparticles (Al_2O_3) in the bath up to 10 g/l but on further increasing the concentration to 12.5 g/l deterioration in wear resistance and corrosion resistance is observed. As compared to binary Ni-B coating, the coating prepared with 10 g/l concentration of nanoparticles shows an increase of around 30% and 60% for Vicker's microhardness and elastic modulus, respectively. The optimum amount of alumina nano-powder in the coating bath is thus found as 10 g/l considering superior elastic modulus, corrosion resistance and wear resistance.

Received 21 May 2021; received in revised form 25 June 2021; accepted 2 August 2021.
To cite this article: Mohanty et al. (2021). Effect of incorporation of nano-alumina on tribo-mechanical behavior of electroless Ni-B coatings. Jurnal Tribologi 30, pp.24-43.

This page is intentionally left blank

Materials Today: Proceedings 19 (2019) 317–321

Contents lists available at ScienceDirect

Materials Today: Proceedings

journal homepage: www.elsevier.com/locate/matpr

Characterisation and corrosion study of electroless Nickel-Boron coating reinforced with alumina nanoparticles

Deviprasanna Mohanty *, Tapan Kumar Barman, Prasanta Sahoo

Department of Mechanical Engineering, Jadavpur University, Kolkata 700032, India

ARTICLE INFO

Article history:
Received 24 June 2019
Accepted 3 July 2019
Available online 6 August 2019

Keywords:
Electroless coatings
Nickel-Boron
Corrosion
Nano-particles
Micro hardness

ABSTRACT

This investigation deals with the study of 1 g/l alumina reinforced electroless Ni-B coatings on a low carbon steel substrate. Reinforced coatings were prepared from the as-received nano powders. The alumina nano particles were ultra-sonicated before being introduced into the coating bath. The reinforced coatings exhibited an improvement in hardness, and corrosion resistance. A significant increase of nearly 10%, was observed in case of the hardness of the reinforced coatings. Corrosion potential increased by about 6% with the addition of alumina nano particles. The agglomerated nano particles seem to embed in the nodular boundaries of the cauliflower like Ni-B morphology and in inter nodular porosities. This, in turn, improved the corrosion resistance by forming an intimate sacrificial layer on the vulnerable substrate material.

Selection and peer-review under responsibility of the scientific committee of the 1st International Conference on Manufacturing, Material Science and Engineering.

1. Introduction

A number of coating methods have been prevalent in the last few decades. Each has its pros and cons. Thermal spray coatings, thin film coatings such as PVD (physical vapour deposition) and CVD (chemical vapour deposition), surface hardening processes such as flame hardening and induction hardening, diffusion processes such as carborising and nitriding and plating processes such as electro deposition and electroless deposition are examples of some coating methods [1]. The advantage of electroless coating is its simplicity, cost effectiveness and the ability to coat any surface, metals, non metals and ceramics. Electroless plating is a versatile autocatalytic coating process which enhances the properties of engineering components [2–8]. In this plating process, a reducing agent reacts with a metallic salt in a liquid solution which results in a uniform coating of metal atoms onto the substrate. In contrast to electroplating, electroless plating can generate uniform coating even on intricate shapes and non-conducting surfaces. The uses of electroless plating process include VLSI (Very large scale integrated) technology, electromagnetic shielding, decorative platings, functional coatings for oil and gas, automotive, chemical and aerospace industries, petrochemical, food, plastics, computer and printing industries [9–14]. Second phase particle deposition onto a binary electroless Ni-B or Ni-P coating opens a plethora of new possibilities. Higher hardness, improved corrosion and wear resistance, higher abrasion resistance [2–8,15,16]. A high hardness and wear resistance may be achieved by heat treatment also, but with temperature, the corrosion resistance of the coatings deteriorates [17]. There are two types of secondary particle reinforcement. The first category includes particles which are used for improving the properties such as wear, abrasion resistance and corrosion resistance of the base material. These are necessarily metal oxides, carbides and nitrides [18–20]. The second category includes particles which are soft and lubricious in nature, such as, polytetrafluoroethylene (PTFE), boron nitride and molybdenum sulphide etc [21–23].

In case of the present study, it is expected that the addition of alumina will result in an increased hardness, refined nodular grain size as well as a better corrosion resistant coating. The need to use alumina as the reinforcement in the coating spans from the fact that alumina is relatively cheaper as compared to other ceramic particles. This is due to the abundant presence of aluminium in the earth's crust. The bulk hardness of alumina is around 15–19 GPa, this may help improve the hardness of the resulting composite coatings. Also, owing to their size, these alumina nano particles are expected to penetrate into the porosities and nodular gaps of the Nickel-Boron coatings thus rendering the coatings

* Corresponding author.
E-mail address: deviprasannamohanty.me@gmail.com (D. Mohanty).

https://doi.org/10.1016/j.matpr.2019.07.216
2214-7853/
Selection and peer-review under responsibility of the scientific committee of the 1st International Conference on Manufacturing, Material Science and Engineering.

This page is intentionally left blank

Effect of Nano Alumina Reinforcements on the Tribological Behavior of Electroless Nickel-Phosphorus Coatings

D. Mohanty, T. K. Barman, and P. Sahoo

Abstract Nickel-Phosphorus electroless coatings are of versatile nature. In the present research, an effort has been made to study the tribological behavior of the Nickel-Phosphorus coatings reinforced with nano alumina powders. The study includes the incorporation of 1 g/l of nano alumina power into the Nickel-Phosphorus coatings. Prior to the introduction of the alumina powder into the coating bath, it was ultrasonicated in a wet media (deionized water). After preparing a sound reinforced as-deposited coating of Nickel-Phosphorus-Alumina (nano), it was compared to a binary Nickel-Phosphorus coating and an uncoated mild steel specimen. These were subjected to a sliding wear test on a pin-on-disk setup and the wear rate was evaluated from the difference in weight (before and after the test). The reinforced (Nickel-Phosphorus-Alumina) coating was found to be the most resistant to wear amongst the three. Besides this, the present research also compares the coating with respect to their scratch hardness and micro-Vicker hardness. This research also includes a characterization study of the as-deposited reinforced coating surface via X-ray diffractometry and Scanning electron microscopy (SEM).

Keywords Electroless coating · Nano-particles · Nickel-Phosphorus · Scratch hardness · Wear behavior

1 Introduction

Coatings are surface modification methods used to impart specific properties to the material while leaving the bulk property of the material intact. Electroless nickel coating is one such surface modification method which provides enhanced mechanical as well as corrosion protection to the substrate materials. These coatings have operational simplicity, need low investment and form very thin coating [1]. Besides, electroless coatings have an added advantage as they can be deposited on non-metallic substrates. Such a property paves the path for the use of these coatings in the computer

D. Mohanty (✉) · T. K. Barman · P. Sahoo
Department of Mechanical Engineering, Jadavpur University, Kolkata, WB 700032, India
e-mail: deviprasannamohanty.me@gmail.com

T. S. Sudarshan et al. (eds.), *Recent Advancements in Mechanical Engineering*,
Lecture Notes in Mechanical Engineering,
https://doi.org/10.1007/978-981-19-3266-3_17